

Stony Brook University



OFFICIAL COPY

The official electronic file of this thesis or dissertation is maintained by the University Libraries on behalf of The Graduate School at Stony Brook University.

© All Rights Reserved by Author.

Dilation Behavior of Thermal Spray Coatings

A Dissertation Presented

By

Miryan Lorena Bejarano López

to

The Graduate School

in Partial Fulfillment of the

Requirements

for the Degree of

Doctor of Philosophy

In

Material Science and Engineering

Stony Brook University

May 2016

Stony Brook University

The Graduate School

Miryan Lorena Bejarano López

We, the dissertation committee for the above candidate for the
Doctor of Philosophy degree, hereby recommend
acceptance of this dissertation.

Dr. Sanjay Sampath (Dissertation Advisor)
Distinguished Professor, Materials Science and Engineering Department

Dr. David Welch
Adjunct Professor, Materials Science and Engineering Department

Dr. Curt Johnson
Adjunct Professor, Materials Science and Engineering Department

Dr. Edgar Lara-Curzio
Research Scientist at Oak Ridge National Laboratory (ORNL)-
Leader of the Mechanical Properties and Mechanics Group in the Materials Science and
Technology Division (MSTD)

This dissertation is accepted by the Graduate School

Charles Taber
Dean of the Graduate School

Abstract of the Dissertation

Dilation Behavior of Thermal Spray Coatings

by

Miryan Lorena Bejarano López

Doctor of Philosophy

in

Materials Science and Engineering

Stony Brook University

2016

Thermal Spray (TS) is a very versatile manufacturing process to deposit thick coatings on a variety of substrates. Coatings are used in protective (i.e. wear, chemical attack, high temperature, etc.) and functional (i.e. sensors) applications. TS coatings have a unique lamellar microstructure as a result of the overlapping of millions of molten and partially-molten particles. During processing, high deformation by impact, high temperature, and rapid solidification lead to a complex hierarchical material system that contains a high amount of microstructural defects. The presence of defects in the microstructure contribute to differences in property values in comparison to bulk materials.

Thermal stresses and residual strains arise from processing, thermal gradients and thermal exposure. Evaluation of thermal properties, in this case, the coefficient of thermal expansion (CTE) is of vital importance to enhance coating performance. In this dissertation, expansion measurements of various metals, alloys, ceramics, and cermet coatings; were carried out using various techniques (push rod dilatometry, x-ray diffraction XRD, digital image correlation DIC, and curvature method) to determine the dilation behavior at the atomic, micro- and macro-scale levels. The main results were.

1) Mathematical models (Turner and Kerner) used for composite materials, successfully predicted the CTE property of a TS coating where the primary phase is the coating material and the secondary phases can be oxides, precipitates, etc. (formed as a byproduct of the spraying process). CTE was found not to be affected by porosity

- 2) Despite the anisotropic behavior characteristic of TS coatings, the experimental results shown that CTE results to be reasonable isotropic within the scope of this study.
- 3) The curvature method was found to be an alternative technique to obtain the CTE, as well as the Young's modulus of coating in a bi-material strip, with good approximation
- 4) An anomalous expansion behavior during the first heating exposure was exhibited by all coatings. The effect was named here, as "thermal shakedown", and is magnified in metals and alloys
- 5) Non-isothermal rapid annealing of defects was correlated to this first irreversible contraction or expansion behavior. Although observed in most thermal spray materials, two material systems, pure Al and Ni-5Al were evaluated in-depth to quantify the mechanisms contributing to this behavior: vacancy formation, dislocation annealing, grain boundaries annihilation, residual stress relief, inelastic mechanical effects, etc.

Correct determination of CTE values are important for design to assure integrity and functionality of coatings. Considerations of appropriate measurements are described in this dissertation.

Dedication

To the three that are the inspiration and motor of my life, my dear husband Alfredo and my lovely kids Alfredo and Antonio.

Frontispiece

“Nobody ever figures out what life is all about, and it doesn't matter. Explore the world. Nearly everything is really interesting if you go into it deeply enough.”

Richard Feynman

Acknowledgments

The process to earn a doctorate degree has been very long and many people have contribute with me on this route. I would like to thank all the people who contributed to make this thesis possible.

Foremost, I thank my college and husband Dr. Alfredo Valarezo and our kids Alfredo and Antonio for their support and understanding during this process. My credit to my husband for being my partner with whom I share not only the knowledge of the field of study but a life full of happiness, efforts and sacrifices that allow us to reach together our goals. Without their constant encouragement and support it had not been possible for me to achieve this educational goal. My love for ever to you.

Thanks to my professor advisor Prof. Sanjay Sampath for giving me the opportunity to enrich my knowledge as well as to grow professionally in an environment full of challenges and experiences at the Center for Thermal Spray Research, CTSR.

Thank you to my committee members Prof. David Welch, Dr. Lara-Curzio, and Prof. Curtis Jhonson. Thank you Prof. David Welch, for being one of the best professors I had, I greatly appreciate the discussion and suggestions where you shared your knowledge with me. My profound thanks to Dr. Edgar Lara-Curzio for giving me the opportunity to access the research facilities at the High Temperature Materials Laboratory HTML in Oak Ridge National Laboratory ORNL. Working with very knowledgeable people at ORNL was an enriching experience, I thank all their contributions to conduct this research. Thank you Prof. Curtis Jhonson, your insightful comments and suggestions widened my research from various perspectives.

I thank my parents, I have always felt their blessings from heaven. My entire family, my brother and sisters, my aunt, nieces, nephews and family in law have helped me with their kindness, love and support. Thank you all for your help. Also thanks to my friends, colleagues, lab mates, with whom I have worked before and work now with me for being always supportive and encouraging to continue this research.

Table of Contents

Chapter 1: Introduction	1
1.1 Fundamentals of thermal expansion	5
1.1.1 Energy versus Interatomic Distance	5
1.1.2 Linear and Volumetric Coefficient of Thermal Expansion (CTE)	8
1.2 Techniques to Measure Thermal Expansion	9
1.2.1 Study of Defects by Dilatometry	10
1.3 Organization of the Dissertation	11
Chapter 2: Statement of the Problem	14
2.1 Thermal Expansion Property of TS Coatings	14
2.2 Anomalous Dilation Behavior of TS Coatings: Thermal Shakedown	15
Chapter 3: Coefficient of Thermal Expansion of Thermal Spray Coatings	17
3.1 Introduction	17
3.2 Measured Values of CTE for Thermal Spray Coatings	18
3.3 Coefficient of Thermal Expansion Bulk vs. Coating Material	22
3.3.1 Analysis of TS Coating as Composite Material	22
3.3.2 Anisotropy of Thermal Expansion in TS coatings	28
3.4 Experimental Methods for CTE measurement	30
3.4.1 Push rod Dilatometer	30
3.4.2 Process Induced Effects on Thermal Expansion: Materials and Processes	34
3.5 Results and Discussion	34
3.5.1 Cyclic Heat Treatment	36
3.5.2 Anisotropy in Coatings	47
3.5.3 Process Induced Effects	49
3.6 Coefficient of Thermal Expansion-CTE by the Curvature Method	51
3.7 Conclusions	55
Chapter 4: Thermal Shakedown: Anomalous Expansion Behavior of Thermal Spray Coatings during Non-Isothermal Annealing	57
4.1 Introduction	57
4.1.1 Research Problem Statement	59
4.2 Experimental Methods for Shakedown Magnitude Analysis	61

4.2.1 Materials and Processes	61
4.2.2 Elemental Mapping by SEM	63
4.2.3 X-Ray Diffraction (XRD) at Temperature	66
4.2.4 Push rod (and Dual Push rod) Dilatometers	68
4.2.5 Differential Scanning Calorimetry (DSC) and Thermal Gravimetry (TG) Measurements	68
4.2.6 Digital Image Correlation (DIC) Technique for strain field monitoring	69
4.3 Results and Discussion	69
4.3.1 Microstructure Characterization:	74
4.3.2 Differential Thermal Analysis and Thermal Gravimetry	76
4.3.3 D-spacing, shift of the peak	77
4.3.4 X-ray Diffraction Analysis and Mechanisms Contributing to the Shakedown Effect	81
4.3.5 Digital Image Correlation (DIC) of unconstrained splat	85
4.3.6 Analysis of Results	86
4.4. Conclusions	88
Chapter 5: Future Work	90
5.1 Introduction	90
5.2 Thermal stresses in TS coatings: analysis of thermo-mechanical behavior of coatings via dilatometry	90
5.2.1 Considerations	94
5.2.2 Suggestions	94
5.3 Shakedown Behavior at Elevated Temperatures	95
5.3.1 Considerations	96
5.3.2 Suggestions	97
5.4 Kinetics: Heating Rate Effect on Shakedown	98
5.4.1 Considerations	99
5.4.2 Suggestions	100
5.5 Shakedown Effect under Vacuum Conditions	100
5.5.1 Considerations	101
5.5.2 Suggestions	102
References	103

List of Figures

Figure 1. Illustration of TS coatings applications at medium and high temperatures (Siemens)	2
Figure 2. a) Potential energy of atoms as a function of atomic distance (actual), b) Potential energy (hypothetic parabolic approximation).....	6
Figure 3 Thermal strain versus temperature. a) Linear thermal strain vs temperature, b) Secant and tangent to obtain coefficient of thermal expansion.	8
Figure 4 CTE dependence on composition of a) Ni-20%Cr coatings with precipitation of Cr ₂ O ₃ and b) Ni-5Al coatings with precipitation of Al ₂ O ₃ . Two analytical models are presented for bulk materials, Kerner model for lower bound and Turner model for upper bound.....	24
Figure 5 Cross-sectional SEM micrographs of various Ni 20 wt% Cr coatings sprayed by HVOF Gas Fuel and HVOF Liquid Fuel; and Plasma Low and Medium energy (Triplex) (Alfredo Valarezo and Sampath 2011)	26
Figure 6 Cross-sectional micrographs of Ni 5 wt% Al Arc Spray and HVOF (S. Sampath et al. 2004) .	27
Figure 7. Coefficient of Thermal Expansion (CTE) of various Al coatings sprayed by different techniques, including: Cold Spray, Combustion Wire Flame Spray- FS-1, another sample of Combustion Wire Flame Spray- FS-2, sprayed at a different time, and atmospheric plasma spray APS process. Differences are minimum and approach to the bulk property.....	28
Figure 8. Schematic of Horizontal Dilatometer by NETZSCH model DIL402C (Netzsch 2006)	31
Figure 9. Analysis of temperature stabilization for the push-rod dilatometer at a heating/cooling rate of 1°C/min. Cycles reach a maximum of 300°C. The heating/cooling rate is stable after 100°C when heat transfer stabilization with the surroundings has been reached.....	33
Figure 10. Typical time-temperature sequence for a heat cycling experiment to study thermal shakedown effect and the CTE in TS coatings.....	36
Figure 11. Linear expansion of an Al-sample deposited by flame spraying, as a function of temperature. Three heating/cooling cycles are presented: a) Raw data and b) Tared data (at 100°C) for comparison of relative expansion.	37
Figure 12. Coefficient of thermal expansion CTE of an Al-sample deposited by flame spraying as a function of temperature. Three heating/cooling cycles are presented. First heating cycle deviated from the nominal behavior which was achieved by all the following heating/cooling cycles.....	38
Figure 13. Comparison of the linear expansion during the first heating cycle –thick line-, and one after it (steady state behavior) -thin line- of various pure metals deposited by different processes. The thermal shakedown makes the linear expansion different in the first heating cycle than in the subsequent cycles.	41
Figure 14. Comparison of the CTE during the first heating of Al-sample coatings sprayed by three different processes (atmospheric plasma spray, cold spray, FS-1 combustion wire flame spray. Shakedown is positive in all cases. First heating cycle –thick line-, and after it (steady state behavior) -thin line. The behavior reduces to the behavior of the bulk Al. FS-2 is another sample sprayed by combustion wire flame spray at a different time.....	42
Figure 15. Comparison of the CTE during the first heating of YSZ coatings sprayed by APS- atmospheric plasma spray. Two feed stock materials were used: F&C fused and crushed, and HOSP hollowed spheres under three different spraying conditions, namely of low, medium, and high energy. The first	

heating cycle is presented for the four coating types. The behavior reduces to the one of the bulk YSZ -dashed line- after the first heating cycle.	44
Figure 16 Analysis of shakedown repeatability, two samples from the same Ni-20%Cr HVOF coating were evaluated during three heating and cooling cycles up to 500°C.	46
Figure 17 CTE of Al flame sprayed coatings using specimens oriented in the through-thickness and in-plane orientations for the shakedown cycle and after it. The line of reference bulk overlaps the behavior of the coating sample (in both orientations) after the first heating cycle.	48
Figure 18. The CTE of various Yttria Stabilized Zirconia-YSZ coatings sprayed by APS- atmospheric plasma spray. The CTE is reported from the second heating cycle (after shakedown). Two feed stock materials were used: F&C fused and crushed, and HOSP hollowed spheres under three different spraying conditions, namely of low, medium, and high energy. The behavior of all samples is comparable to the behavior of the bulk YSZ.	50
Figure 19 Curvature-temperature evolution of two coated plates subjected to heating/cooling cycles. One is the combination of a Ni-20%Cr coating onto Al-6061 T6 substrate, the other one is the combination of a Ni-20%Cr coating onto stainless steel 316 (SS316). Processing assures the coatings have the same properties in both substrates. The behavior is linear elastic. Two heating/cooling cycles are presented for each sample.	54
Figure 20. Calculated CTE and Young's modulus of a Ni-20%Cr coating based on the curvature method, data presented in Figure 19.	54
Figure 21. Linear expansion of an a) Al-sample coating by flame spray in the in-plane orientation, b) Al-sample coating by flame spray in the through-thickness and c) Linear expansion of a Ni-5Al sample coating by arc spray in the in-plane orientation.	61
Figure 22 Elemental mapping of nickel, aluminum, oxygen and carbon, in Ni-5Al-sample by arc spraying.	64
Figure 23. Elemental distribution of Ni5%Al Arc-spray coating. Percentage of constituents	65
Figure 24. Elemental mapping of aluminum coating, Aluminum and Oxygen together with some Carbon as a contaminant on the process	65
Figure 25. Elemental distribution of Al Flame Spray coating. Percentage of constituents	66
Figure 26. Shakedown strain gradients of Al-sample FS-1, in the in-plane (IP) and through-thickness (TT) orientation (FS1 refers to the process: flame spray-FS, and 1 to the first batch of samples), Al-sample FS-2 in the in-plane orientation from batch 2, and Ni-5Al-sample by arc spraying in the in-plane orientation only.	73
Figure 27. Cross-sectional micrographs of Ni-5Al-samples obtained from three different positions by SEM	75
Figure 28. Cross-sectional SEM micrographs of Al-samples FS-2 for three different regions of the sample.	76
Figure 29. DTA-TG curves at a specified heating rate of 5°C/min in air with a flow of Ar, for Al-sample FS-2 and Ni-5Al-sample.	77
Figure 30. In situ monitoring of a) the (111) peak of Al-sample flame sprayed and b) and (111) peak Ni-5Al-sample arc sprayed coating by XRD while heating and cooling. Procedure is described in section 4.2.3. Two-heating cycles are presented. The average peak position shifts with temperature in response to the increased interatomic separation to reach equilibrium.	78

Figure 31. The lattice cell parameter- a (d -spacing) as a function of temperature for a) an Al-sample flame sprayed coating, and b) a Ni-5Al-sample arc sprayed coating. Both coatings relieve stress during first heat cycle.	80
Figure 32. Narrowing of a (111) peak of Al-sample at a fixed temperature of 50°C during a heating/cooling cycle. XRD is carried out using Cu-K α 1, and K α 2 radiation.	83
Figure 33. Dislocation density (ρ) and grain size (d) evolution during a heating cycle. Measurements of XRD are carried out at various temperatures 50°C, 100°C, 200°C, 300°C and 350°C. Williamson Hall method is used to analyze the XRD pattern and determine ρ and d	84
Figure 34. Analysis of deformation of splats of Al-FS2 samples by the Digital Image Correlation (DIC) Technique– Heating and Cooling Cycles up to 325°C. On the right hand side, the change in thermal strain as a function of temperature. On the left hand side, an image of two analyzed splats at temperature (280°C), the colors reflect the strain change with respect to the first image at room temperature.	86
Figure 35. Schematic of sandwich composite sample. Al-6061 substrate of 3.2 mm thickness is coated in both sides with YSZ coating by APS of 0.5 mm thickness	91
Figure 36. Illustration of sandwich composite sample subjected to an increase in temperature (positive temperature gradient). ϵ_{tc} is the thermal strain of YSZ coatings (free standing), ϵ_{ts} is the thermal strain of Al substrate (free standing), and ϵ_o is the resultant strain of the composite.....	92
Figure 37. Linear expansion (thermal strain) of free standing coating (YSZ), substrate material (Al-6061-T6) and sandwich composite coating (YSZ on both sides of Al substrate)	92
Figure 38. Coating modulus of YSZ coating obtained from uniaxial monitoring of sandwich composite expansion	94
Figure 39. Shakedown behavior of Ni-20Cr sample tested in a cyclic manner: heating-cooling. Low-temperature regime reached up to 500°C, and high-temperature regime reached up to 900°C. There are three subsequent cycles for each regime (data of shakedown linear expansion is tared to the reference behavior.....	96
Figure 40. Linear expansion dL/L_o of an Aluminum-flame sprayed coating (Al-FS2) tested in a push-rod dilatometer at three different heating rates: 3°C/min, 10°C/min, 20°C/min. Only the shakedown first heating cycle is considered, and compared to the steady state behavior. For 10°C/min, two different samples were tested.....	99
Figure 41. Linear expansion dL/L_o of an Aluminum-flame sprayed coating (Al-FS2) tested in a push-rod dilatometer under vacuum conditions and under purging-Ar-environment. Only the shakedown first heating cycle is considered, and compared to the steady state behavior.....	101

List of Tables

Table 1. Coating materials for typical applications at low and medium-temperatures (200°C- 600°C). The most common TS process used for each application is also indicated.	3
Table 2. Coating materials used in typical applications at high-temperature (600°C- 1300°C). The most common TS process used for each application is also indicated.	4
Table 3. Compendium of Coefficients of Thermal Expansion (CTE) for Thermal Spray Coatings	21
Table 4. Summary of property values used to model analytically the CTE dependence on composition for two coatings Ni-20%Cr, and Ni-5%Al.	25
Table 5. YSZ-APS coatings within a Process Map, average particle temperature and velocity by DPV, and porosity measurement by image analysis (Vaidya et al. 2008)(Chi 2008)	50
Table 6. Experimental data used to obtain the CTE and Young's modulus of the coating based on the curvature method, and equation 5.	53
Table 7. Thermal spraying parameter for Al-sample: flame spraying	62
Table 8. Thermal spraying parameter for Ni-5Al-sample: wire arc spraying	62
Table 9. Mechanisms that alter the dilation behavior of TS Al- and Ni-5Al-samples during a heating/cooling cycle.	71
Table 10. Proposed experiments and experimental techniques to investigate the mechanisms responsible of <i>shakedown</i> at high-temperature regimes.	97

Chapter 1: Introduction

Thermal Spray (TS) is a versatile manufacturing process to deposit thick coatings. In TS deposition process, ceramics, metals, and alloy materials in the form of particles, wires, or rods can be fed into an energy source system (a torch) that heats up the material and projects it towards a substrate surface to form a coating. Fully-molten or partially-molten particles are successively sprayed to build up a lamellar microstructure. Each individual particle flattens on a pancake like shape, forming a structure called “splat”. The coating is the result of the overlapping of millions of rapidly quenched splats. Throughout the process, the coating material is subjected to high deformation by impact, high temperature, and rapid solidification which leads to a complex system that contains a high amount of microstructural defects, including not only atomic defects, such as: dislocations, vacancies, oxides, non-equilibrium phases; but also, microscale defects, such as: globular pores, interlamellar pores, microcracks, oxide layers, etc. In addition, phase change (liquid to solid) and large temperature change from deposition to cooling results in a complex state of stresses in these coatings.

Despite the microstructural defects, TS techniques are broadly used in diverse applications. In many cases, the defects such as porosity can engender unique functionalities such as providing compliance to thermo-structural coatings. In general, these coatings allow protection of underlying base material, lowering degradation due to wear or chemical attack, thus allowing higher operational temperatures of turbines, incinerators, etc., and extending the lifetime of components (S et al Sampath 2012; Pawlowski 1995; D. Clarke and Phillpot 2005; Brindley 1997). Many examples of protective coatings at temperature can be cited, including TBC’s in aero and gas engines (D. R. Clarke, Oechsner, and Padture 2012; Evans et al. 2001; “Usmani_Sampath_Effect of Carbide Grain Size on the Sliding and Abrasive Wear Behavior of TS WC-Co Coatings.pdf,” n.d.; S et al Sampath 2012; Usmani and Sampath 1999; Rajendran 2012), piston heads, cylinder bores in lightweight alloyed blocks (Rabiei et al. 1999), boiler tubes (Shidu S. Prakasf S. 2006), etc. Some of these applications are illustrated in Figure 1. Applications of dense coatings for wear and friction protection at temperature are also present and increasing, such as piston rings (Rastegar, F. Craft 1993; Hwang et al. 2006), extrusion screws, abrasives, pumps, etc (Davis 2004).



Figure 1. Illustration of TS coatings applications at medium and high temperatures (Siemens)

Since the thermal mismatch in any coating-substrate system is ubiquitous during deposition, heat treatment, and all applications that involve a thermal gradient, accurate analysis of thermal stresses requires determination of correct values of, for instance, linear expansion, and the coefficient of thermal expansion (CTE). Concomitant occurrence of thermal strains, mechanical and thermal fatigue, and contaminants are known to trigger adverse effects that drive the coating failure (Li 2010). Therefore, it is of high interest to monitor the behavior of coatings under circumstances of heat cycles and applied thermal mismatch strains to produce coatings of enhanced performance.

For instance, in the aero-engine and power generation turbines, bond coats and top coats in TBC's are designed to reduce the thermal expansion mismatch (T. a. Taylor and Walsh 2004; Tsipas et al. 2004; Evans, Clarke, and Levi 2008) between the substrate material and the ceramic top coat. YSZ is preferred from other ceramic materials due to its large CTE, and high toughness (Evans, Clarke, and Levi 2008). Moreover, low stiffness achieved through strain tolerance design by control of the deposition process e.g. EB-PVD or segmented vertically cracked coatings (Vassen et al. 2009) reduces the thermal stress in the system. So, not only it is necessary to reduce the thermal strain mismatch but also consider the stiffness of the coatings to minimize loading of interfaces that can result in micro and macro cracking, or delamination. However, often high

thermal stresses are inevitable especially in applications where dense coatings are required, for example in wear, corrosion or friction resistance. Some applications of TS coatings at temperature are cited in Table 1 and 2. Table 1, low and medium (200°C- 600°C) temperature applications are listed and in table2, applications that usually work under high temperatures range (600°C- 1300°C) are include:

Coating Material	Application	Process	Source
Mo, Mo-CrC-NiCr	Coatings for piston rings	APS (atmospheric plasma spray)	(Rastegar, F. Craft 1993)
High strength steels	Cylinder bores	Arc Spray	(Rabiei et al. 1999; Edrisy, Perry, and Alpas 2005)
Inconel 718, 625 (Ni-corrosion and heat resistant alloys)	Reclamation of the same parent material	HVOF	(Lypfout et al. 2008)
CrC-NiCr	Sliding wear and corrosion protection in gas turbines	Arc Spray, HVOF	(Lih et al. 2000)
NiCr, NiCrBSi,	Waste to energy boilers	Arc Spray, HVOF	(Shidu S. Prakash S. 2006; Yuuzou Kawahara 2007)
Abradables, Al reinforced with SiC	Flow sealing in gas turbines	APS	(Johnston and Evans 2007)
WC-Co, WC-CoCr, CrC-NiCr	Extrusion screws, mud rotors, pump impellers, others.	HVOF	(Lima et al 2014)
Mg, Al, Cu	Especial reclamation applications in Aero-engines, nuclear reactors, others.	Cold Spray	(AL-Mangour et al. 2013)

Table 1. Coating materials for typical applications at low and medium-temperatures (200°C- 600°C). The most common TS process used for each application is also indicated.

Coating Material	Application	Process	Source
Ytria stabilized zirconia (YSZ), La ₂ Zr ₂ O ₇ , Ga ₂ Zr ₂ O ₇	Thermal barrier coatings (TBC's), and environmental barrier coatings (EBC's): for turbine blades, vanes, and combustors in aero and gas turbines	APS (atmospheric plasma spray)	((Vassen et al. 2009)
NiAl alloys, MCrAlY (M=Ni, CoNi) of different compositions	Bond coats for TBCs:	APS, VPS (vacuum plasma spraying), HVOF	(T. a. Taylor and Walsh 2004; Pollock et al 2012)

Ni-20Cr	High temperature boilers, meso-scale sensors, others	APS, HVOF	(Shidu S. Prakash S. 2006)
---------	--	-----------	----------------------------

Table 2. Coating materials used in typical applications at high-temperature (600°C- 1300°C). The most common TS process used for each application is also indicated.

Although materials of enhanced characteristics (i.e. super alloys, single crystals) are used in high performance applications, they are sometimes not able to meet multifunctional requirements of for instance thermal shock resistance and at same time adequate mechanical properties. For this reason industry has introduced broad usage of TS coatings into the manufacturing area (Sanjay Sampath et al. 2013). Coatings contribute to improve efficiency in the operational conditions of equipment as described above for wear, corrosion and temperature resistance. A wide range of variety of coatings can be deposited with TS processes, and for every case, it is of importance to analyze the thermal strains and stresses that gets magnified when the coatings work under temperature environments. Thermal expansion of coatings that work under different temperature regimes (table 1 and 2) is evaluated in this study.

Over the years, use of bulk expansion properties has been of common practice for TS coatings. One reason has been the limitations in applying the techniques for expansion measurements on relatively thin coatings where sample preparation may compromise the results. Nowadays, these restrictions can be overcome with different techniques (high precision Dilatometry method, Digital-Image-Correlation; X-Rays Diffraction with temperature or Curvature Method). All these methods are applied in this study. Accurate coefficients of thermal expansion (CTE) values are of vital importance for evaluation of coating integrity and performance.

As discussed above, correct determination of CTE is essential to fully understand thermal strain and stresses in coatings under temperature conditions. Since TS coatings exhibit singular microstructural architecture which depends on the spraying techniques and parameters, it is expected to have influences of these microstructural features on the thermal expansion property. Therefore, influence of spraying process and parameters on thermal expansion is also of interest in the present dissertation. To address these differences the approach is to evaluate pure metals and alloys coatings deposited by different processes and also ceramic YSZ deposited under the framework of process maps (Valarezo et al. 2007; Vaidya et al. 2008). Lamellar structure of

coatings produces anisotropy of properties (Sharma et al. 2006), anisotropy of thermal expansion is also of intriguing to be evaluated. Examination of thermal expansion anisotropy is evaluated using very thick Aluminum and Ni5%Al coatings. Since a principal outcome in TS coatings is the microstructural defects (i.e. dislocations, grain boundaries) that result from deposition process, presence of these defects leads to accumulation of energy in the coating. This energy is prompted to be released by annealing when the coating is exposed to temperature (Raabe 2014). This effect is evident on the expansion behavior of coatings when they are subjected to temperature cycles.

For further understanding fundamentals of natural expansion exhibit by most of the engineering materials is described in this chapter. Brief definitions of the linear and volumetric coefficient of thermal expansion CTE are presented together with explanation on some of the available techniques to obtain the expansion property of materials. Organization and structure of the document is also described.

1.1 Fundamentals of thermal expansion

Most materials that experience an increment in temperature will expand; implying thereby that atomic vibrations are anharmonic (Duane C. Wallace 1965). Anharmonicity is supported by the asymmetry of the potential energy versus interatomic separation curve which is discussed as follows.

1.1.1 Energy versus Interatomic Distance

Expansion is the result of an increment in the average atomic distance between atoms due to an increase in temperature. This phenomenon is best understood by considering intermolecular forces of a solid material (Kittel 2004). These forces are attractive and repulsive in nature. Their effect is canceled out at certain inter-atomic separation, where the potential energy is minimized. This potential energy is the integral of the forces over the inter-atomic spacing. In Figure 2a, the potential energy of a pair of atoms is plotted as a function of the inter-atomic spacing. The minimum potential energy possible E_0 corresponds to the equilibrium inter-atomic separation r_0 at the absolute zero temperature (0 K). The potential energy (E_1, E_2, E_3 , etc.) is amplified as temperature rises (T_1, T_2, T_3 , etc). As the average potential energy increases by heating up the

material, increment in temperature ΔT , the mean spacing between atoms becomes larger Δr , thus the material expands.

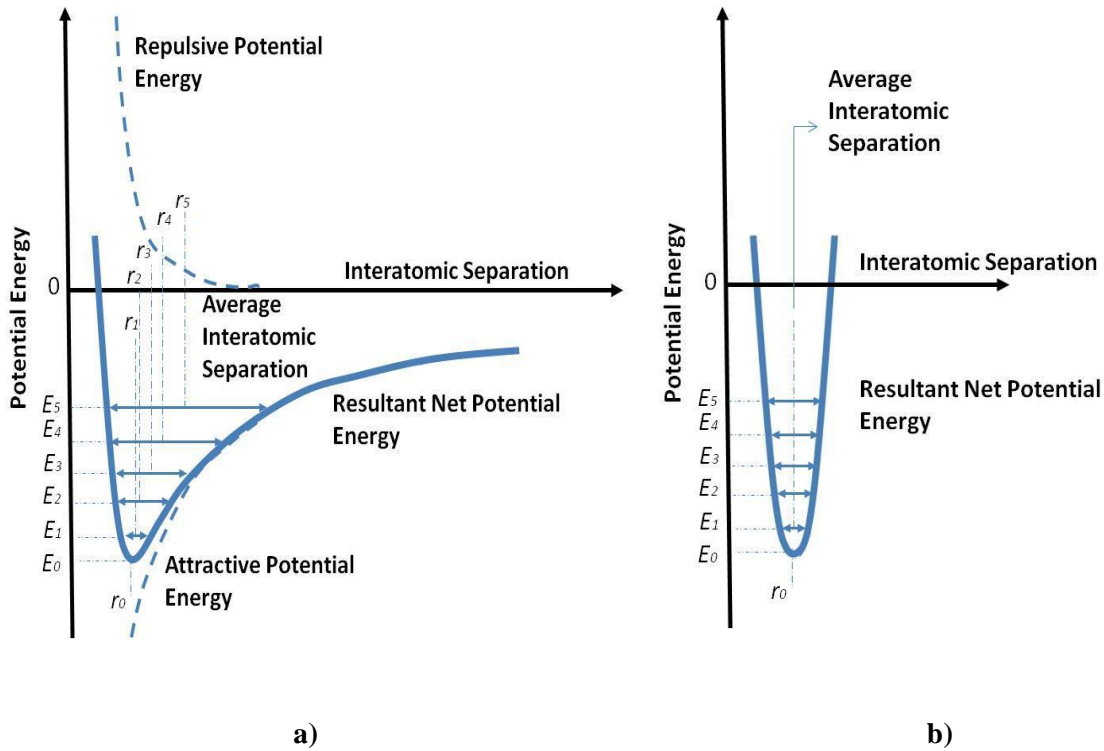


Figure 2. a) Potential energy of atoms as a function of atomic distance (actual), b) Potential energy (hypothetic parabolic approximation).

Asymmetry of the potential energy versus interatomic separation is what makes expansion possible. If the potential energy curve were symmetric, there would be no net change in the interatomic separation, and consequently, no thermal expansion will occur when heating the material. In Figure 2b, which is a representation of a hypothetical symmetric curve, an increment in temperature would not affect the mean position (the oscillation range is symmetric) and hence, the average atomic spacing remains unchanged.

This energy represents the energy required to separate these atoms. The magnitude and shape of the bonding energy versus interatomic separation curve vary from material to material. As the curve appears narrower and deeper, the material has larger atomic bonding energy (e.g. ionic bond in ceramics). Increment in atomic separation will be lower in response to a temperature increase, resulting in lower thermal expansion in these materials. This contributes to the expansion

response of different classes of materials, low for ceramics, large for metals, and larger for polymers.

Most engineering applications, where thermal expansion needs to be considered are above room temperature. In these cases, the behavior shown by the expansion of solid materials is modeled closely as linear with respect to temperature. Nevertheless, there exists also some cases where materials are used in cold environments. At low temperatures, the relationship between the coefficient of thermal expansion CTE (α) and the absolute temperature (T) is proportional to T^3 . The CTE is approximately 0 at 0 [K] but it rises rapidly with temperature until it reaches the Debye temperature. (Kittel 2004; Duane C. Wallace 1965; Dugdale and MacDonald 1954; Zhang, Li, and Li 2013)

Both CTE and the specific heat present similar behavior. The specific heat at constant volume C_v as well as the CTE of a crystalline solid are dependent on the vibrational energy of atoms. According to Grüneisen, a relationship between both, α and C_v , is given by the following mathematical relation:

$$\alpha = \frac{\gamma C_v \rho}{B} \quad \text{Equation 1}$$

Where γ represents the Grüneisen constant, C_v specific heat at constant volume, ρ density and B bulk modulus. Grüneisen constant γ can be obtained by relation of the frequency of atomic vibration with respect to the atomic volume change. Bulk modulus and density are not strongly dependent on temperature. If Grüneisen constant were also independent of temperature (it does not at certain range of temperature), it will indicate thermal expansion will vary with temperature in the same manner as the specific heat and it will be proportional to T^3 at low temperature range (cryogenic range). At around and above room temperature which is important for most engineering applications, the thermal expansion will vary proportionally linear to the temperature (Kittel 2004), as observed in Figure 3a. All the thermal expansion values from literature and from the author presented in this document are above room temperature.

For the cases, where the thermal expansion deviates from a straight line, the thermal expansion property in a range of temperature, can be determined with the secant method as illustrated in Figure 3b (in blue). More commonly, the CTE is obtained using the tangent method

as illustrated also in Figure 3b (in red), obtaining the derivative of the linear expansion, and thus, the CTE in the vicinity of the temperature value.

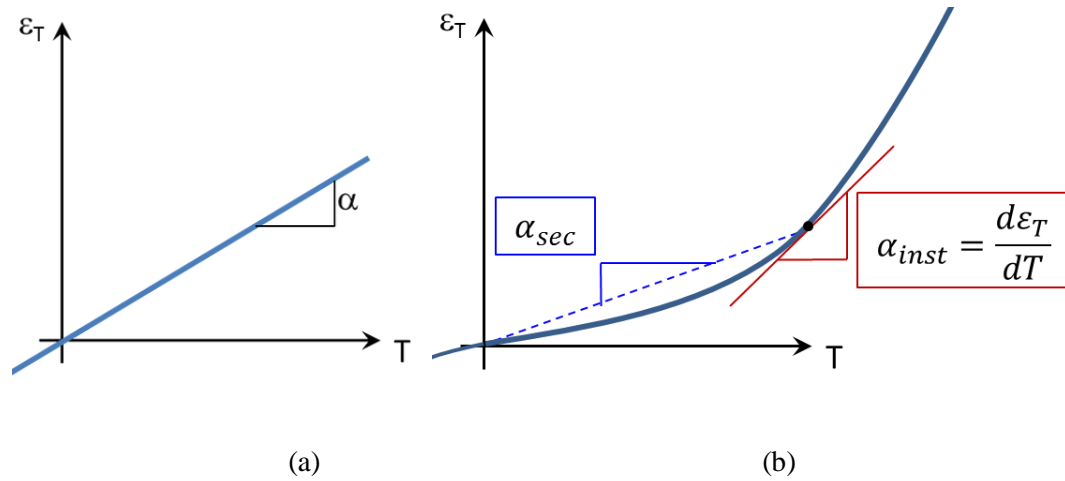


Figure 3 Thermal strain versus temperature. a) Linear thermal strain vs temperature, b) Secant and tangent to obtain coefficient of thermal expansion.

1.1.2 Linear and Volumetric Coefficient of Thermal Expansion (CTE)

Most of the materials will dilate when they are subjected to a temperature increase. Generally the expansion coefficient has two forms: linear (α) and volumetric (β). The coefficient of linear expansion, (CTE or α) is a measure of the fractional change in length per unit of change with temperature ($1/^\circ\text{C}$, $\text{mm}/\text{mm } ^\circ\text{C}$, $1/\text{K}$, etc). Usually it is measured under zero applied stress. The mathematical definition is:

$$\alpha = \frac{1}{L} \left(\frac{\delta L}{\delta T} \right) \quad \text{Equation 2}$$

Where, L is the original length of the material, δL is the longitudinal dilation or contraction of the material, and δT is the temperature gradient responsible for the δL . $\left(\frac{\delta L}{L} \right)$ is also known as the linear expansion, or thermal strain.

The volumetric thermal expansion coefficient is the ratio of the change in volume with respect to a unit change in temperature, while keeping the pressure constant. The mathematical definition is:

$$\beta = \frac{1}{V} \left(\frac{\delta V}{\delta T} \right) \quad \text{Equation 3}$$

Where, V is the original volume of the material, δV is the volumetric change, due to a δT temperature gradient.

The relationship between β , and the specific heat at constant volume C_v is described as follows:

$$\beta = \frac{C_v}{Q_o[1-k(\frac{U}{Q_o})]^2} \quad \text{Equation 4}$$

Where, U is the energy of the lattice vibrations, Q_o and k are constants. If the Debye temperature θ_D is known, both C_v and U may be calculated at any temperature T (Kittel 2004; Graham and Hagy 1971).

On the other hand, if the material is isotropic, the volumetric expansion is approximately three times the corresponding linear expansion.

$$\beta = 3\alpha \quad \text{Equation 5}$$

When this occurs, it is sufficient and common to report the linear expansion (α) only.

1.2 Techniques to Measure Thermal Expansion

There are various methods to examine to coefficient of thermal expansion. All the techniques use a sensor to monitor the relative deformation of a finite portion of a material under temperature change. Dilation/contraction of a material can be measured by high resolution displacement sensors, these sensors can be in-contact or without contact (non-contact) with the sample. The most common methods to measure the CTE include dilatometry with contact push-roads connected to LVDTs (linear variable differential transformer) or non-contact lasers, optical imaging and optical/electron microscopy followed by computer image analysis, DIC (digital image correlation) is also employed. Another less common method is XRD (X-ray diffraction) technique, monitoring of the d-spacing while *in situ* heating the sample. Also the curvature method is a proposed alternative that can be used to extract the expansion property. The results presented in this document are obtained by using all the described techniques but mainly from dilatometry. Explicit discussion is addressed by XRD monitoring with temperature, DIC and curvature method.

Dilatometer systems can have vertical or horizontal configurations with a single or dual push rod. The dilatometer used in most experiments presented in this document had horizontal

configuration with a single push rod. This instrument consists of an insulated furnace chamber with adjustable heating rate, where a sample is fixed against a movable pushing rod. The second end is either in contact to a fixed support, or to a movable pushing rod. Sample is heated up or cooled down with controlled temperature and in some cases purging inert gas or using vacuum atmosphere. The system measures precise dimensional changes of a specimen as the temperature changes. The displacement is registered with the help of a LVDT (Netzsch 2006). This is the most common method to extract linear dimensional changes through a wide temperature range.

The d-spacing as function of temperature can be measured by monitoring lattice expansion using XRD (or other diffraction techniques) while in situ heating the sample. Interatomic distance increases as the material is heated up and it is recorded by the shifting of the pattern peaks. As the peaks shift, they can also get narrow. Narrowing of the peak on TS coatings is analyzed in this document.

Digital image correlation DIC is another technique employed to obtain expansion property. In this method, high magnification images are taken as a function of temperature. These pictures are post-processed with software that tracks displacement of pixels on every picture. Quality and contrast on the images are of vital importance to obtain precise results.

The curvature method consists in monitoring the curvature change with temperature of a bilayer plate, usually a coating of unknown CTE, on a substrate of well-known properties. By testing, the same coating on two different substrate materials, and knowing the thicknesses, and Poisson's ratios of the substrates and coating, and the elastic modulus of the substrates, CTE of the coating can be computed, as well as its in-plane elastic modulus.

In this document all the methods described above are used, and their advantages and disadvantages are discussed.

1.2.1 Study of Defects by Dilatometry

Dilatometry is used to identify changes in the microstructure associated with phase changes, order-disorder, magnetic- paramagnetic transitions, etc. Atomic lattice defects can also be analyzed with dilatometric measurements, in fact atomic lattice defects study through

measurable length change dates back to experiments presented by Feder and Nowick AS (1958). Irreversible macroscopic length change is a manifestation of annealing of these defects as a function of temperature and time. Also sintering effects have been evaluated via dilatometry studies (Tsipas et al. 2004; Cipitria, Golosnoy, and Clyne 2007; Paul et al. 2007).

TS coatings can contain a considerable amount of defects as a consequence of the deposition process. These defects are not only oxides, non-equilibrium phases, globular pores, interlamellar pores, microcracks, oxide layers but also defects of 0-D vacancies, 1-D dislocations and 2-D grain boundaries. The presence of these defects in the microstructure creates accumulation of energy and an excess of volume in the material which is removed when the material is heated up (Steyskal 2012; Oberdorfer et al. 2010; Oberdorfer et al. 2014). Irreversible contribution on length change of the coating materials is presented on results from dilatometer, X-rays diffraction XRD and digital image correlation DIC monitoring with temperature.

1.3 Organization of the Dissertation

Organization of the dissertation is presented in this section. The following chapters described the investigation that summarizes the expansion behavior of thermal spray coatings. Starting synthesis of expansion theory, evaluation of influences of parameters and processes, following with analysis of particular response when they are done in cyclic manner is described.

In chapter 1, background information on the TS coatings process and the resulting coating microstructure is discussed. Thermal expansion theory based on analysis of potential energy versus interatomic separation is examined together with a short analysis of linear and volumetric coefficient of thermal expansion. Experimental techniques to evaluate the thermal expansion property of materials are presented with a description on the benefit of using expansion measurements to identify microstructural and phase changes in the material.

In chapter 2, the “statement of the problem” that motivates thermal expansion investigation on TS coatings is presented. The need and implications of acquiring an accurate expansion property of TS coatings is discussed. During the investigation of the expansion response of several coatings, an unknown behavior was exhibited by all coatings tested for CTE cyclic measurements. Further supplementary questions were placed In order to understand this phenomena exhibit by the coatings.

In chapter 3, outcomes of expansion measurements from different coating materials are described and analyzed. Expansion measurements were done mainly by dilatometry. Application of mathematical models to extract the thermal expansion coefficient of composite materials was employed in correlation with expansion of TS coatings. This approach was taken considering the microstructural characteristic of TS coating are comparable to composites materials since in TS coatings oxides, precipitates or porosity are considered a second phases. In this chapter a compendium of CTE values from a number of various coatings extracted with experiments run by the author and values reported in literature by other authors is presented. Process induced effects on thermal expansion are analyzed to establish relation between sprays processes and parameters to the expansion response. TS Coatings have lamellar structure what makes them anisotropic, therefore anisotropic behavior is also analyzed. Besides the natural expansion of materials when they are exposed to heat, microstructural progressive changes in coatings due to defect annealing occurred. All these studies were done in a cyclic manner, and the unexpected behavior exhibited by all coatings during the first heating cycle is treated in the following chapter.

In chapter 4, the abnormal trend on expansion response of coatings during first heating cycle is evaluated as a rapid annealing of defects. Progressive microstructural changes occur due to rapid defect annealing. This behavior is studied by applications of different techniques that allow quantification of each defect annealing on its contribution in magnitude to the total permanent length change. This anomalous behavior is addressed based on the atomic, micro and macro-scale, for this reason different technique to evaluate the expansion in cyclic manner were employed. XRD with temperature was used to monitor the lattice expansion and also the peak shifting and broadening. The analysis of experimental results was done with fundamental models. Also DIC technique was employed to analyze the behavior of splats from pictures taken as a function of temperature.

As a way of introduction in this chapter, a description of TS process together with a description of the complex microstructural formation of coatings due to process and parameters is presented. Some applications of coating at temperature are listed. The need to correctly evaluate thermal properties of coatings based on the consequences on the thermal stresses and strain that arise when coatings are used in high temperature applications has been described. A synopsis of the fundamental theory behind expansion properties of the materials was presented. A number of available techniques to measure the coefficient of thermal expansion were briefly described, also

a description on why the dilatometry can be used as a technique to identify microstructural changes when the materials (as TS coatings) contain defects. The present dissertation will contain results and discussions to evaluate thermal expansion properties of a number of coatings considering the abnormal behavior they exhibit when they are evaluated in cyclic manner, corresponding to the first heat cycle.

Chapter 2: Statement of the Problem

2.1 Thermal Expansion Property of TS Coatings

Many examples of protective and functional coatings that work at temperature have been cited in Chapter 1. To achieve coatings of enhanced performance in such applications, the study of thermal properties, and specifically, here, the thermal expansion is necessary. In high temperature applications, the associated occurrence of thermal strains and thermal stresses produce adverse effects that compel coating failure. The challenges increase due to microstructural changes that occur during service. Therefore, it is of high interest to monitor the behavior of coatings under heating/cooling circumstances to ensure coating performance.

The never ending interest in the improvement of coating performance and therefore, the subsequent boost of efficiency in design, motivates advances in research and development to understand the unique properties of TS coatings, in this case the thermal expansion. The uniqueness of properties results from the formation of coatings by the individual impingement of molten or partially molten particles. The interaction of particles with hot gases during in-flight, impact, spreading and solidification determine the types of microstructural defects (vacancies, dislocations, grains boundaries); oxides; decomposed, amorphous, and metastable phases; residual strains, porosity, as well as macro and microcracks. This assortment of microstructural features depend on process parameters and they determine differences in coating properties compared to bulk materials. The above mentioned characteristics limit the reliability of TS coatings due to the lack of certainty in coating property values. Therefore, the motivation for this study was to focus on the following questions:

- How is the expansion response of coatings compared to the corresponding bulk material?
- What is the role of intrinsic and extrinsic defects and residual stresses on the expansion behavior
- What is the impact of lamellar structure on the anisotropic expansion behavior?
- How sensitive is the expansion behavior to processing variables?

- Is there influence of spraying parameters in the expansion results of different types of coatings? (special focus on expansion on ceramics materials because of presence of porosity)

The results obtained from the measurements carried out to answer the above questions raised further queries. When dilatometry measurements were done in cyclic manner, results showed an abnormal behavior in the thermal expansion of all coatings tested. The samples expand more or less in the first heating cycle than in the subsequent passes; meaning, there was an overall relative expansion or relative contraction of the sample. The expansion was larger or smaller during first heating cycle. The new questions arising from these results were studied to understand this anomalous expansion behavior of thermal spray coatings, which is described here as “*thermal shakedown*”.

2.2 Anomalous Dilation Behavior of TS Coatings: Thermal Shakedown

Independent of the spraying process or process parameters, all the coatings measured presented in higher or lower magnitude a positive or negative irreversible dimensional change during the first heating cycle. Subsequent thermal cycles exhibited repeatable and reversible dilation/contraction. The overall irreversible increment or reduction of the original length of the sample is manifested during first heating, and named here as “thermal shakedown”. Understanding of this behavior brought attention to correlate the coating microstructural defects with the anomalous expansion response by answering the questions:

- What mechanisms participate during “thermal shakedown”?
- Is there a correlation between the “thermal shakedown” and the microstructural defect annealing in TS coatings? What is the magnitude of such contribution in strain?
- Does the particular structure of TS coating with presence of pores, oxides, cracks, etc., determine the occurrence of the “thermal shakedown”?
- Is the “thermal shakedown” a process-technology dependent phenomenon?
- Is the “thermal shakedown” a process-parameter dependent phenomenon?
- Is the “thermal shakedown” anisotropic?

In this dissertation, these two main statements, about thermal expansion property of TS coatings and anomalous dilation behavior of TS coatings are addressed thoroughly. Theoretical calculation and experimental evidences have been used to address the proposed inquiries. The analysis of the thermal expansion is covered for a number of systems (materials and processes), and for selected material-models (Ni-5%Al and Al), a compelling and systematic experimental approach guided the understanding of the “thermal shakedown” behavior.

Chapter 3: Coefficient of Thermal Expansion of Thermal Spray Coatings

3.1 Introduction

Thermal stresses are inherently present in surface engineering applications due to the mismatch contraction/expansion of the coatings and the substrate material. Therefore, precise determination of the coefficient of thermal expansion (CTE) in coatings is of vital importance for designers. To fully understand thermal strain behavior in coatings, it is necessary to find out the influence of process techniques and parameters into CTE. Process induced characteristics and features in coatings which include: oxides, residual stress, and interfaces, may lead to a deviation from bulk material properties. The correlation of process induced effects to thermal expansion is addressed in this Chapter.

One of the main objectives in this chapter is to evaluate the CTE for several coating-material and process systems. The well-known technique of “push-rod” dilatometry (single and dual) was used to report the expansion property of several pure metals, alloys, cermets, and ceramics. The experimental procedure is discussed in detail for thermal spray (TS) coatings. A large compendium of CTE values are presented from experiments conducted by the author and from literature. It was found that all coatings present irreversible changes in the microstructure during the first heating cycle that alters the CTE value. This behavior is named here as *thermal shakedown*, and its causes and effects are discussed (more in depth discussion is developed in Chapter 4 for Aluminum and Ni-5%Al-samples). All reported values of the CTE are extracted from the second heat cycle.

The possible processing effects of thermal spray on the CTE were explored by 1) depositing the same material by different spraying techniques (cold spray, HVOF, APS, arc spray); and 2) within the same technique, by varying the spray parameters largely in the context of a process map (YSZ via APS). It is concluded that the spraying technique can significantly affect the expansion behavior during the first heating cycle; but after, the CTE depends strictly on the composition (e.g. precipitates, oxides, etc). The CTE of the coating approaches the bulk when the material is not sensitive to oxidation, and otherwise. The CTE was found not to be an anisotropic property despite the anisotropic nature of TS coatings. Finally, in this chapter, an alternative technique to extract the CTE of coating by curvature is presented and validated.

3.2 Measured Values of CTE for Thermal Spray Coatings

There are several specific studies reporting measured values of the CTE of TS coatings. A few of them report:

- 1) Differences between the CTE of the coatings vs. the bulk value (Wang, D. Berndt 1991; Pawlowski 1995)
- 2) Anisotropic behavior of the expansion (comparing in-plane vs. through-thickness measurements (Berndt, C.C Herman 1982); and,
- 3) No significant effect from process parameters on CTE (Chivavibul et al. 2008; Kuroda 1991).

Deviations from the bulk value and anisotropy found only under certain circumstances will be discussed further. Several past results of CTE are summarized in (Pawlowski 1995). In Table 3, a large compendium of these results from literature is reported, together to the results obtained by the experiments carried out by this author from a variety of coatings used in different applications.

Coating Material	CTE (mm/mm)		Temperature (°C)	Spraying Process	Author
	Longitudinal $\times 10^{-6}$	Transversal $\times 10^{-6}$			
CERAMICS					
YSZ	10.53+0.001T		100-1100	APS	Bejarano, et. al
YSZ	10.26+0.001368T		300-1100	APS Med	Bejarano, et. al
YSZ	10.33+0.00135T		300-1100	APS Low	Bejarano, et. al
YSZ	10.52+0.001408T		300-1100	APS High	Bejarano, et. al
YSZ ¹	10.5			APS 3MB	(J Ilavsky and Berndt 1998)
(YSZ) ZrO ₂ +8Y ₂ O ₃	10	2.9-23.5	300-1300		(Berndt, C.C Herman 1982)
ZrO ₂ +20Y ₂ O ₃	10.6				(Rangaswamy, Herman, and Safai 1980)
Zircon ZrO ₂ SiO ₂	5.1		300-1300		(Suzuki 2000)
Zircon ZrO ₂ SiO ₂ Tetragonal	6.4				(Suzuki 2000)
Zircon ZrO ₂ SiO ₂	6.8				(Suzuki 2000)
Gadolinium Zirconate	8.65+0.00285T		80-1100	APS	Bejarano, et. al
Lanthanum Zirconate	8.35+0.0018T		80-1100	APS	Bejarano, et. al
Al ₂ O ₃	6.7596+0.0022T		300-900	WSPS	Bejarano, et. al
Al ₂ O ₃	7	5.2-7.6			(Wang, D. Berndt 1991)
Al ₂ O ₃	7.6				(Rangaswamy, Herman, and Safai 1980)
TiO ₂	9.8				(Rangaswamy, Herman, and Safai 1980)
Cr ₂ O ₃	7.5		300-900		(A. Tronche 1987)
Spinel MgO-Al ₂ O ₃	7.7				Herman 1990
Forsterite 2MgOSiO ₂	11		300-1000		(Wang, D. Berndt 1991)
Cordierite 2MgO2Al ₂ O ₃	1.7		300-1300		Wang- Herman 1990
Indialite	1.2				Weaver 2000
Quartz	2				Weaver 2000
Glass	4.5				Weaver 2000
PURE METALS					
Al	23.19+0.00149T		100-400	Flame Spray	Bejarano, et. Al
Al	23.6+0.0012T	23.6+0.00129T	100-400	Combustion	Bejarano, et. Al
Al	23.16+0.00155T		100-450	CS	Bejarano, et. Al
Al	23.64+0.00823T+0.000025T ²		0-627	BULK	Touloukian, et al
Ni	14.28+0.00418T		120-600	HVOF - DJ	Bejarano, et. Al
Ni	14.1+0.00644T		120-600	CS	Bejarano, et. Al
Ti	9.61+0.0023T		50-600	CS	Bejarano, et. Al
Cu	17.57+0.001T+ 0.00003T ²		50-600	HVOF	Bejarano, et. Al
Cu	16.85+0.0054T+ 0.0000035T ²		0-1027	BULK	Touloukian, et al
Mo	6.8		300-1300	Flame wire	(Rangaswamy, Herman, and Safai 1980)
METALLIC ALLOYS					

Ni20Cr	12.44+0.0089T	150-500	Triplex (low	Bejarano, et. Al
Ni20Cr	12.9+0.0084T	150-500	Triplex (high	Bejarano, et. Al
Ni20Cr	13.82+0.0072T	150-500	HVOF - JP500	Bejarano, et. Al
Ni20Cr	13.36+0.0064T	150-500	HVOF - JK	Bejarano, et. Al
Ni20Cr	13.26+0.008T	150-500	HVOF-DJ	Bejarano, et. Al
Ni5Al	12.66+0.0076T	100-500	HVOF-JK	Bejarano, et. Al
Ni5Al	12,45 + 0.007T	100-800	Arc Spray	Bejarano, et. Al
Ni5Al	14.9	300-1300	APS	(Rangaswamy, Herman, and Safai 1980)
Ni5Al	13.5	300-1300	APS	(Pawlowski 1995)
Ni31.5Al ²	16-0.006T+0.0000093T ²	20-950	VPS	(Raj and Palczcr 2010)
Ni 20Al	12.5	300-1300	Flame wire	(Rangaswamy, Herman, and Safai 1980)
CoNiCrAlY	9.848+0.013T-0.000007T ²	50-600	HVOF - DJ	Bejarano, et. Al
NiCrAl	16.3	200-950	HVOF JK	(J Ilavsky and Berndt 1998)
NiCrAl	16.4	200-950	HVOF JK	(J Ilavsky and Berndt 1998)
Ni5Al+Cr19	15.5		VPS	(Pawlowski 1995)
Ni+19.2Cr+1.1Si+0.4Fe	17.3	300-1200	VPS	(Pawlowski 1995)
Ni+22Cr+10Al+1Y	18.3	300-1470	VPS	Siemers-Mehan
Ni+17Cr+6Al+0.5Y ²	17-0.0172T+0.00003T ²	20-950	VPS	(Raj and Palczcr 2010)
Inconel 718	11.7+0.009T	100-1000	HVOF DJ	Bejarano, et. Al
Cu-8%Cr ²	19-0.0074T+0.0000153T ²	20-950	VPS	(Raj and Palczcr 2010)
Cu-26%Cr ²	16-0.0038T+0.0000114T ²	20-950	VPS	(Raj and Palczcr 2010)
Cu+8Cr+1Al ²	17-0.00032T+0.0000129T ²	20-950	VPS	(Raj and Palczcr 2010)
Stainless Steel A430	10.74+0.035T	50-800	Arc Spray	Bejarano, et. Al
Stainless Steel A316	16.92+0.053T	50-800	CS	Bejarano, et. Al
Stainless Steel A316	16.8	200-950	HVOF JK	(J Ilavsky and Berndt 1998)
Stainless Steel A316	17.9	200-950	APS 3MB	(J Ilavsky and Berndt 1998)
NiCrAlY (61.97%Ni 27.52%Cr	6.5	25-525	APS	(T. a. Taylor and Walsh 2004)
NiCrAlY (60.71%Ni 25.35%Cr	6.74	25-525	APS	(T. a. Taylor and Walsh 2004)
NiCrAlY (58.3%Ni 27%Cr 13.63%Al	6.42	25-525	APS	(T. a. Taylor and Walsh 2004)
Ni-164 (66.9%Ni 21.85%Cr 9.99%Al	7.04	25-525	APS	(T. a. Taylor and Walsh 2004)
LCO-22 (32%Ni 38%Co 21%Cr	7.51	25-525	APS	(T. a. Taylor and Walsh 2004)
LN-33 (69%Ni 20%Cr 11%Al	6.79	25-525	APS	(T. a. Taylor and Walsh 2004)
LN-33 (64%Ni 23%Cr 13%Al	6.67	25-525	APS	(T. a. Taylor and Walsh 2004)
COMPOSITES				
Abradables (TBD)	19.48+0.0321T	50-250	APS	Bejarano, et. Al
75%NiCrAl 25%YSZ	15.4	200-950	HVOF JK	(J Ilavsky and Berndt 1998)
50%NiCrAl 50%YSZ	12.9	200-950	HVOF JK	(J Ilavsky and Berndt 1998)
75%NiCrAl 25%YSZ	15.7	200-950	HVOFJK	(J Ilavsky and Berndt 1998)
50%NiCrAl 50%YSZ	15.3	200-950	HVOFJK	(J Ilavsky and Berndt 1998)
75%Stainless Steel 25%YSZ	16.7	200-950	HVOF JK	(J Ilavsky and Berndt 1998)
50%Stainless Steel 50%YSZ	16.7	200-950	HVOF JK	(J Ilavsky and Berndt 1998)

75%Stainless Steel 25%YSZ	16.5	200-950	APS 3MB	(J Ilavsky and Berndt 1998)
50%Stainless Steel 50%YSZ	14	200-950	APS 3MB	(J Ilavsky and Berndt 1998)
CERMETS				
WC-20Co	7.4	300-900		(A. Tronche 1987)
WC- CoCr	6.4079+0.0069T	100-400	HVOF JK	Bejarano, et. al
WC-12Co	7.2- 7.5	100-500	HVOF JK	Bejarano, et. al
WC-12Co	5.412+.0053T	150-400	Triplex	Bejarano, et. al

¹ Extrapolated value of CTE, taken from extrapolation of three measurements. The variability of the results reported by the author in this table are consequence of resolution of dilatometry technique and mathematical calculations.

² CTE numbers are extracted from the average behavior of three samples, after the first heating cycle. CTE was extracted by derivation of the linear expansion presented by the author.

Table 3. Compendium of Coefficients of Thermal Expansion (CTE) for Thermal Spray Coatings

3.3 Coefficient of Thermal Expansion Bulk vs. Coating Material

As it has been introduced in Chapter 1, the CTE is an intrinsic property of the material; being this, the change of the atomic distance in equilibrium at certain temperature. With this consideration, TS coatings should have the same CTE for any bulk material in its pure condition. Deviations may be expected due to extrinsic factors produced during the processing. Thus, the complex microstructure of TS coatings can be comparable to a composite material in which the phases are the features that form the coating structure (e.g. feedstock of single or multiple phases, pores, and oxides).

3.3.1 Analysis of TS Coating as Composite Material

Several approaches have been proposed to determine the expansion coefficient of composite materials. The most basic one is the rule of mixture (RoM), as in equation 6, which has proven to be effective in composite coatings and graded coatings (Raj and Palczar 2010; Kesler et al. 1997; J Ilavsky and Berndt 1998; Giovanni Bolelli et al. 2012). There are precise analytical models which include the CTE of each phase, affected by the volume percentage and the stiffness of each one. Hsieh and Tuan (C. L. Hsieh and Tuan 2007) in their study of Al₂O₃-Ni5Al sintered composites testing a large range of compositions conclude that the CTE of the composite can be predicted defining an upper and lower bound according to Kerner (Kerner 1956) in equation 7 and Turner (Turner 1946) in equation 8, respectively. Deviations may be produced in large temperature ranges at high temperatures. For a precise analytical model, the reader is referred to (C. L. Hsieh and Tuan 2007; C.-L. L. Hsieh and Tuan 2006). In the case of TS coatings, these models have not been applied other than the RoM, and their efficacy remains unknown.

$$\alpha_c = \alpha_p V_p + \alpha_m V_m \quad \text{Equation 6, (Rule of Mixtures RoM)}$$

$$\alpha_c = \alpha_p V_p + \alpha_m V_m + (\alpha_p - \alpha_m) V_p V_m \frac{K_p - K_m}{K_m V_m + K_p V_p + 3K_m K_p / 4G_m} \quad \text{Equation 7, (Kerner 1956)}$$

$$\alpha_c = \frac{\alpha_m K_m V_m + \alpha_p K_p V_p}{K_m V_m + K_p V_p} \quad \text{Equation 8, (Turner 1946)}$$

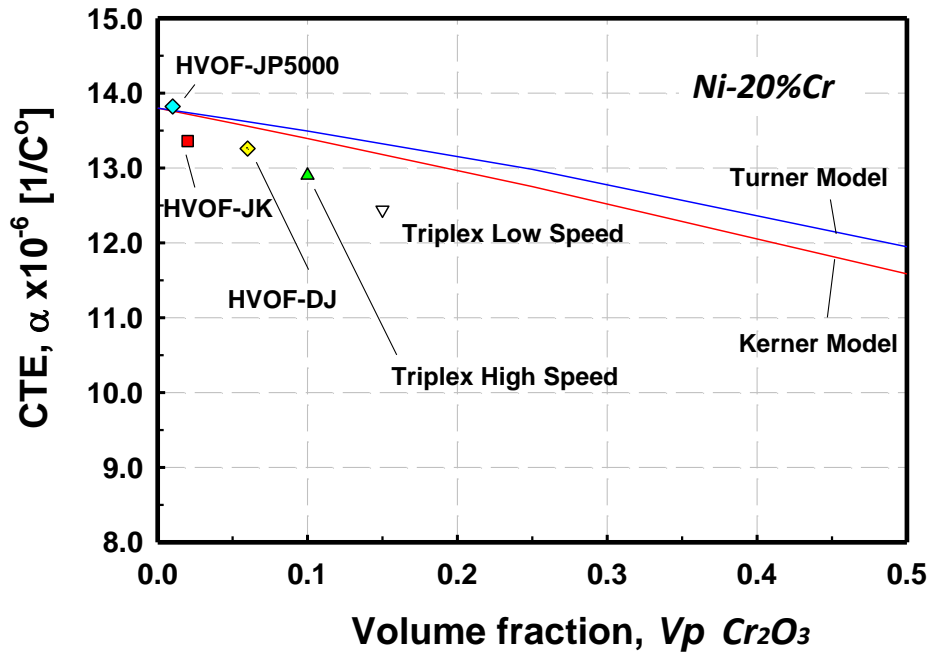
Where the sub-indexes correspond to c=coating (composite) material, m=matrix material, p=second phase (oxides, pores, etc). K corresponds to the bulk modulus, G is the shear modulus, ν = Poisson ratio, and α =coefficient of thermal expansion. Also, $E = 2G(1+\nu)$, $E = 3K(1-2\nu)$, where E is the Young's modulus, and ν is the Poisson ratio.

Three scenarios are illustrated for discussion. One, in which an elemental or alloy material in relatively pure form is in presence of porosity only; another one in which, oxides or in general, multiple phases are present as a by-product of the processing; and the last one in which a blend of powders or wire has been processed to form a composite.

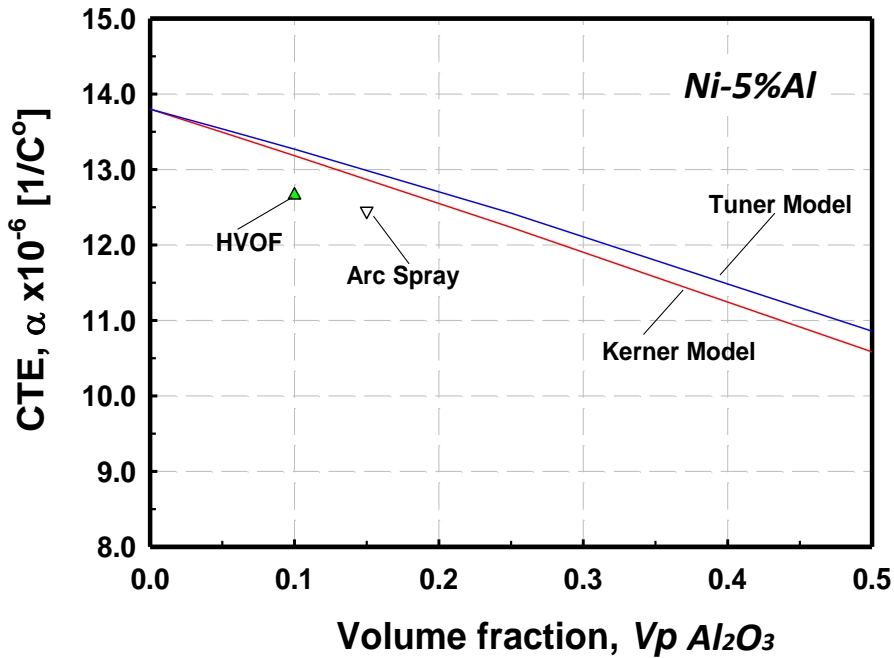
In the first scenario –pure material (m) +porosity (p)-, the CTE of the pure material does not change as the stiffness of the second phase (air in the porosity) is negligible. If considering the analytical models above, by using Kernel and Turner, the CTE of the coating (α_c) results equal to the pure material ($\alpha_c = \alpha_m$), practically neglecting the porosity; whereas using RoM, the CTE for the coating would be deviated resulting in a fraction of property of the pure material due to the porosity content. The RoM analysis is not applicable in this case.

In Table 3, consider the values of CTE for the coatings: YSZ, and Al. Various samples are reported for each material as the processing techniques were varied. The CTE value range between 1.7% to 2.6% compared to the nominal value (bulk). This property range is quite small and can even be considered within the error of the experimental technique. Particularly for YSZ, the microstructures of the various coatings show different porosity levels but the CTE variation is almost negligible. The effect of porosity in CTE can thus be ruled out.

In the second scenario –pure material (m) + oxides (p)-, the CTE of the coating could be predicted by equations 7-8, as long as the type, content, and properties, of oxide are known. The analytical models are represented in Figure 4, for two materials: Ni-5%Al, and Ni-20%Cr.



(a)



(b)

Figure 4 CTE dependence on composition of a) Ni-20%Cr coatings with precipitation of Cr_2O_3 and b) Ni-5Al coatings with precipitation of Al_2O_3 . Two analytical models are presented for bulk materials, Kerner model for lower bound and Turner model for upper bound.

Kerner and Turner models are calculated using data presented in Table 4.

Material	Young Modulus, E, [GPa]	Possion Ratio, ν	Shear Modulus, G, [GPa]	Bulk Modulus, K, [GPa]	CTE, α , [$^{\circ}\text{C}^{-1}$]	Reference
Ni-5%Al	186	0.31	71.2	161.9	14	(C. L. Hsieh and Tuan 2007)
Al ₂ O ₃	401	0.24	162.3	253.5	7.3	(C. L. Hsieh and Tuan 2007)
Ni-20%Cr	113	0.3	43.5	94.2	13.14	(measured by the author)
Cr ₂ O ₃	105	0.20	43.8	58.3	8.95	(Freund & Suresh 2005)

Table 4. Summary of property values used to model analytically the CTE dependence on composition for two coatings Ni-20%Cr, and Ni-5%Al.

Ni-20%Cr coatings were processed according to (Alfredo Valarezo and Sampath 2011) by APS (Triplex low speed, Triplex high speed), and various HVOF techniques (A liquid fuel torch:JP-5000 torch, and two gas fuel torches: DJ-2600 and JK-3000). Further details on these coatings are referred to (Alfredo Valarezo and Sampath 2011). The Cr oxidizes preferential (Brossard et al. 2010; Valarezo & Sampath 2011; Shidu S. Prakash S. 2006) to form Cr₂O₃. The oxide contents are about 15%, 10%, 1%, 6%, 2%, measured by image analysis, respectively in micrographs presented in Figure 5. As the oxide content increases, the CTE decreases provided that the CTE of the oxide (Cr₂O₃) is lower than that of the alloy (Ni-20%Cr). The CTE value decreases in almost 10%.

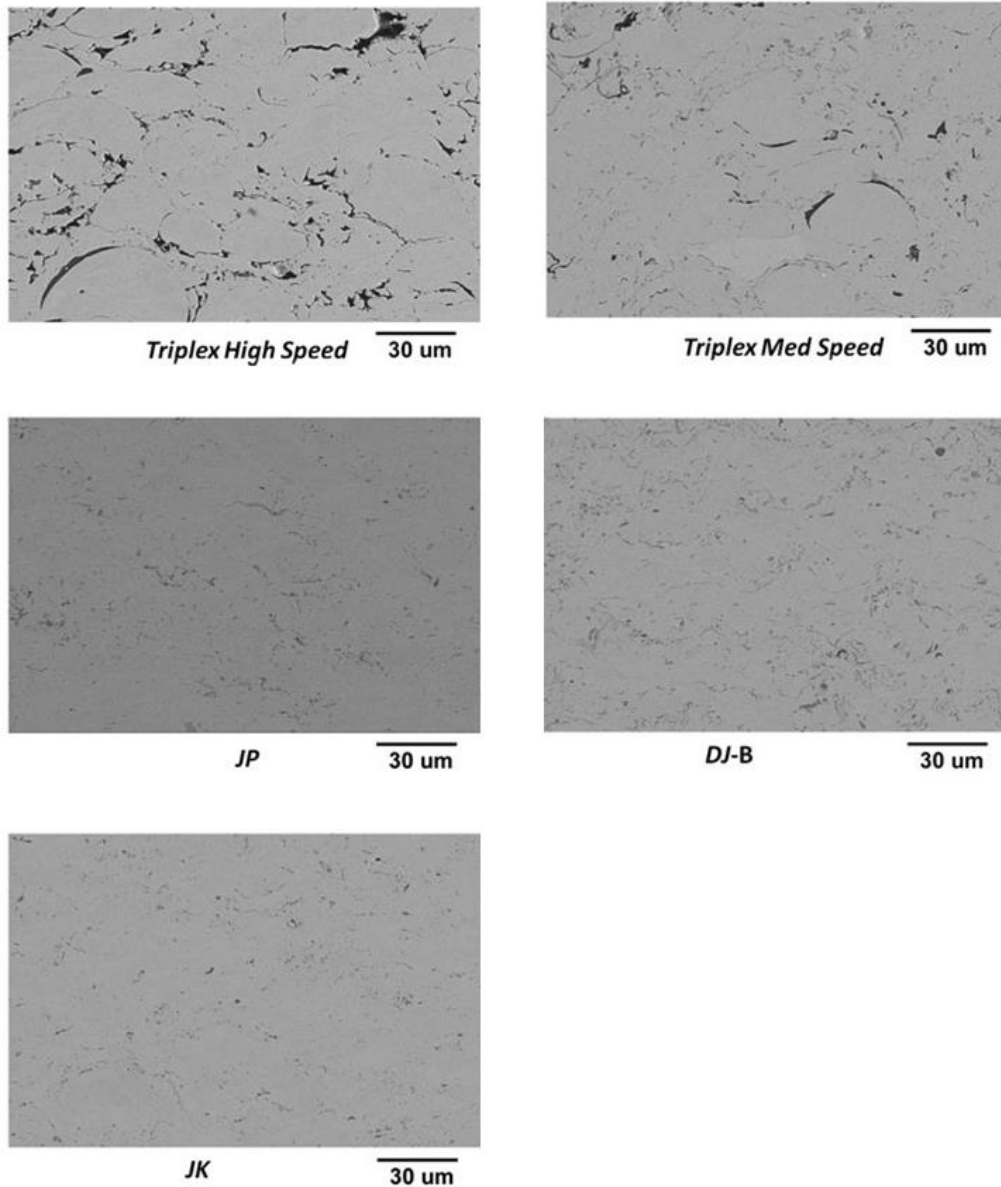


Figure 5 Cross-sectional SEM micrographs of various Ni 20 wt% Cr coatings sprayed by HVOF Gas Fuel and HVOF Liquid Fuel; and Plasma Low and Medium energy (Triplex) (Alfredo Valarezo and Sampath 2011)

For the Ni-5%Al coatings two data points are presented. Coatings were processed by combustion wire flame spray and HVOF techniques (gas fuel torch: JK-3000). In this case, the Al oxidizes preferentially (Deshpande, Sampath, and Zhang 2006) to form Al_2O_3 . Figure 6 shows cross-sectional micrographs of Ni-5Al Arc Spray and HVOF coatings. The oxide contents are

about 5,7%, measured by image analysis in the case of Arc Spray, and 2% for HVOF as reported in (Deshpande, Sampath, and Zhang 2006).

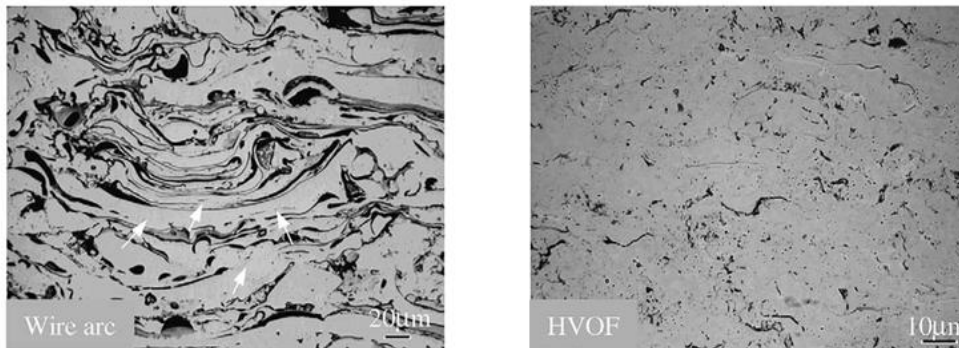


Figure 6 Cross-sectional micrographs of Ni 5 wt% Al Arc Spray and HVOF (S. Sampath et al. 2004)

In Figure 4, the CTE of the two nickel alloys decreases with increasing oxidation, given that the CTE of the second phase is lower than that of the alloy. Similar behavior would be expected to follow other TS coatings. Thus, the CTE can increase or decrease depending upon the expansion behavior and the amount of the secondary phases. The Turner and Kerner models help to define the reference bounds that include most of the scattered data points on a specific zone for bulk materials. The RoM model would fit within the bounds by joining linearly the CTE of the matrix and the second phase. It should be noted that the Turner and Kernel models account not only for the expansion effects but also for the stiffness of each component at the microscale level where bulk properties can be used. Meso- or macro-scale properties of the coatings are not considered since they are often a fraction of the bulk due to the presence of intersplat interfaces and porosity (Leigh 1997; Kroupa and Dubsky 1999). The approach is dependent on a precise definition of composition and properties of the present phases.

For the third scenario, in which a blend of powders or wire is considered to form a composite, the same models could be applied. A first approximation to it, the RoM is presented by (J Ilavsky and Berndt 1998) for a mixture of SS316 and YSZ powders by HOVF and APS. There is no consideration of oxide content of the metallic phase. Three compositions with relatively high metallic compound (above 70%) had a good approximation with RoM. Due to the lack of data along the whole range, the result cannot be generalized. However, the use of the three analytic models is suggested in any case, except when considering the porosity as a second phase, then rule out the RoM model.

In brief, as long as the formation of new phases (e.g. oxides) during processing is low, the CTE property of the bulk can be used as the coating property with good approximation. The effect of porosity is ruled out owing to the lack of stiffness of the air expanding into the open volume. Property range will depend on the sensibility of the feedstock material to be oxidized or precipitate in different phases, and also on the conjugation of properties: CTE, and stiffness of the resultant phases. For instance, for the case of Al sprayed in a wide range of processes shown in Figure 7, the sensitivity of the CTE to change is relatively small, and can be considered with a very good approximation the same as the bulk property. Unfortunately, due to the nature of the material during polishing, it is difficult to determine precisely the amount of oxidation present in the microstructure of each coating, but it is considered low.

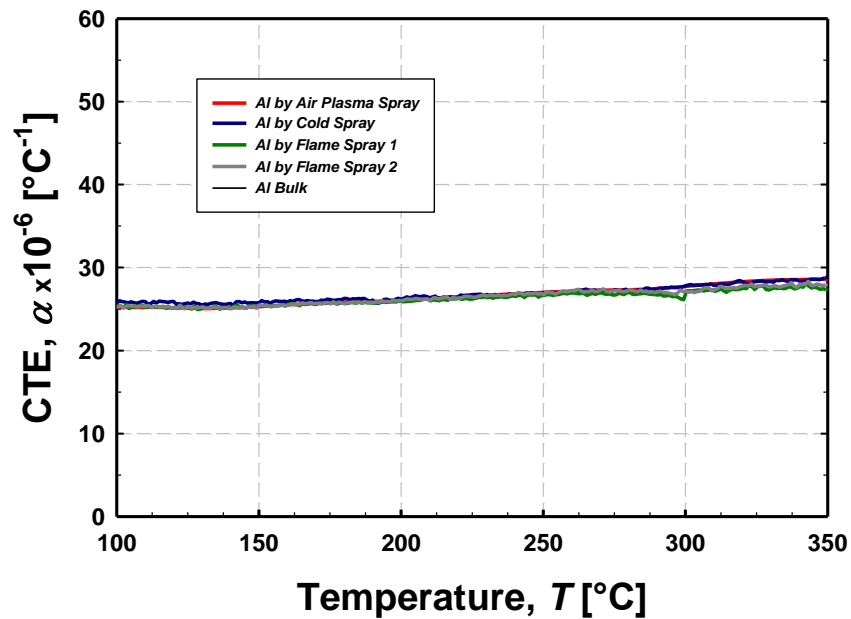


Figure 7. Coefficient of Thermal Expansion (CTE) of various Al coatings sprayed by different techniques, including: Cold Spray, Combustion Wire Flame Spray- FS-1, another sample of Combustion Wire Flame Spray- FS-2, sprayed at a different time, and atmospheric plasma spray APS process. Differences are minimum and approach to the bulk property.

3.3.2 Anisotropy of Thermal Expansion in TS coatings

At the crystalline scale, materials with non-symmetrical lattices experience anisotropic thermal expansion depending on the orientation of the lattice. It is also possible that the material is allotropic and its phases show slightly different CTE's. This behavior in polycrystalline coatings

is rather difficult to measure unless either texture is observed in the microstructure or there is a dominance of one of the constitutive phases. TS coatings are known for their anisotropy due to the lamellar structure, but texture is rather low. So, TS coatings are considered anisotropic in the microscale due the interfaces and pores (interlamellar, globular, etc), but not in the atomic scale. Previous studies in the case of YSZ, (Kuroda 1991) affirm that CTE should not be affected by the amount or morphology of the porosity, and therefore, the expansion should not be anisotropic considering the lack of stiffness and low expansion of the air occupying the pores. However, (Berndt, C.C Herman 1982) sustain that the CTE can be anisotropic for YSZ due to changes in the crack network and interlamellar boundary distribution. They found that the CTE for a fixed composition $\text{ZrO}_2 - 8 \text{ wt\%} - \text{Y}_2\text{O}_3$, does not change before and after heat treatment (10 to 120 hours) at 1150°C . It is a fixed value around $10 \times 10^{-6} \text{ }^\circ\text{C}^{-1}$ for the in-plane orientation, but when testing the sample in the through-thickness direction, the value ranges from 2.9 to $23.5 \times 10^{-6} \text{ }^\circ\text{C}^{-1}$. In this reference samples of 0.5 mm in thickness were tested in free-standing form. Similar results are reported by (Wang, D. Berndt 1991) testing Al_2O_3 coatings. In the longitudinal direction, the CTE stabilizes after the first cycle to a value of $5.9 \times 10^{-6} \text{ }^\circ\text{C}^{-1}$. In the through-thickness direction the value keeps varying after cycles, and the reproducibility is low. It was found in the author's studies that testing short length samples generates measurements with high error due to the compromised resolution of the equipment.

The results presented by (Berndt, C.C Herman 1982) in the through-thickness direction which state that the CTE is different in that orientation than the longitudinal, are not consistently reproduced in the study. They attribute this lack of reproducibility to the continuous crack redistribution associated to shear and slip at points of contact between splats. On the other hand, studies of the authors (Nakamura and Liu 2007)(Y. Liu et al. 2007) have found that the mechanical behavior (stress-strain) which is highly dependent on crack opening and sliding, is reproducible during heating cycles for the same materials: YSZ, Al_2O_3 , and others. This observation would suggest that the mechanisms of continuous crack redistribution is not likely to occur, and that the anisotropy is not real but an effect of experimental error.

A very thick sample (30 mm) of Aluminum by flame spray was produced to test anisotropy in metal coatings. The CTE value obtained was the same for the in-plane and through-thickness orientations, as in Table 3 ($23.6 + 0.012T \times 10^{-6} \text{ }^\circ\text{C}^{-1}$ for the longitudinal orientation and

$23.6+0.0129T \times 10^{-6} \text{ }^{\circ}\text{C}^{-1}$ for the through-thickness orientation). However, this evidence does not necessarily rule out the observation by (Berndt, C.C Herman 1982), because of the different nature of the materials tested, but suggests that interlamellar pore closure or crack sliding (or opening) may not affect significantly the CTE as most of the thermal deformation occurs in the bulk areas of the splats and in the points of contact inter-splats.

3.4 Experimental Methods for CTE measurement

The coefficient of thermal expansion is obtained by monitoring the relative deformation of a finite portion of a sample material under controlled temperature as mentioned in Chapter 1. Various techniques to monitor the length change due to thermal expansion were also presented, including: high resolution displacement sensors LVDTs on contact push rods (most common method), non-contact optical imaging, and, optical/electron microscopy computed by image analysis. Monitoring curvature as function of temperature on a bilayer plate (coating-substrate) was presented as well. A less common method, the XRD monitoring of the d-spacing during *in-situ* heating, was also described. The push-rod technique applied to thermal spray coatings is described in details as follows.

3.4.1 Push rod Dilatometer

This instrument consists of an insulated furnace chamber with adjustable heating rate, where a sample is fixed against a movable pushing rod. The second end is in contact to a fixed support, the temperature increases consequently sample dilates and moves the rod whose displacement is registered by an LVDT. All the values of CTE reported by the author in Table 3 were obtained from a horizontal dilatometer “Thermische Analyse” model DIL 402C with an alumina pushrod (Figure 8).

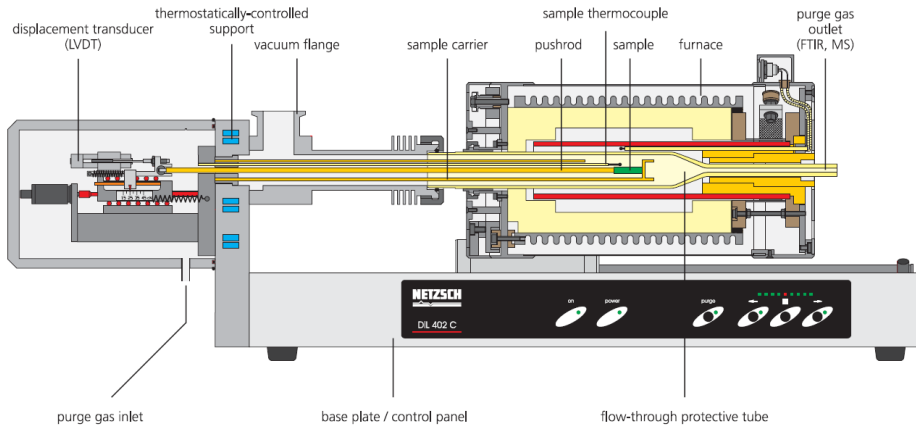


Figure 8. Schematic of Horizontal Dilatometer by NETZSCH model DIL402C (Netzsch 2006)

The dilatometer is connected to a thermal controller system TSAC 414/4 Jupiter both manufactured by NETZSCH (Netzsch 2006) The dilatometer is equipped with a high-resolution displacement transducer. Maximum resolution of the linear expansion is of 1.25 nm. It runs at temperatures up to 1600°C.

To measure thermal expansion, the instrument compares the linear expansion of the sample to the reference linear expansion of a calibration bar. Calibration is performed using a standard NBS sapphire sample, SRM 732, DIN 51045. Resulting data is extracted using standard differentiation methods between the calibration-run and the sample, both measured under similar experimental settings. Heating rate can be adjusted varying from 0.01°C/min, to 50°C/min. However, to avoid transient temperature gradients in the chamber, heating rates lower than 5°C/min are suggested. Also to avoid lengthy experiments a minimum of 1°C/min was used. The pushrod load is set in a standard load of 25 cN. All measurements were programmed from room temperature to the desire temperature. The experiments were conducted with recirculation of inert gas (N₂).

3.4.1.1 Sample Dimensions

Samples were deposited by standard parameters in the different spraying processes. All the samples to be measured were prepared as free standing shapes. Limitations on the samples sizes that can be used are referred by the manufacturer to be 25 mm in maximum length and 8 mm in maximum diameter. In the case of thermal spray, thick coatings are required to fulfill the lower

limit of sample cross-section. A quick study of sample size effect on the expansion measurements was carried out to determine the exact minimum sample dimensions. This analysis was developed using bulk Al6061-T6 varying length and cross sectional dimensions. The experimental results suggested that the minimum sample size in cross section should be 1 mm², whereas the appropriate length should be at least of 15 mm. The variability of the CTE observed with respect to sample size is produced by the low absolute deformation of the shorter samples, and possible buckling of the samples of small cross-section.

3.4.1.2 Sample preparation

Literature reports various types of samples used for CTE measurements. All samples are coatings deposited on the thick range (1 to 2 mm thickness) and are machined to free standing shapes. Samples can be sprayed on cylindrical rods of aluminum of 6 mm diameter, for instance; and later, the substrate can be machined or dissolved chemically (T. a. Taylor and Walsh 2004), resulting in a free standing coating tubes.

In this study, samples are sprayed over a flat surface to at least 1 mm thickness. The first step is to carefully cut the samples into the approximate required dimensions. Then the substrate is ground by using polishing equipment. Maximum care is taken during cutting and grinding process to avoid cracking or delamination of samples. Parallelism of sample ends is very important and considered during sample preparation. The typical final sample dimensions are the ones of a pillar of 25 mm length x 1 mm thickness x ~ 2 mm width. The initial sample length size is determined using a micrometer with 0.001 mm resolution. Wire cutting can also be used to machine samples with high accuracy.

3.4.1.3 Transient Temperature Gradients

The dilatometer experiments are regularly conducted at constant heating/cooling rates avoiding transient temperature gradients. However, the rate is difficult to be kept constant at low temperatures due to the large effect of convection of the surroundings, and at the temperature of inverting from heating to cooling due to transient effects. The analysis of the derivative of temperature change with respect to time (heating/cooling rate) permits identification of the points in which, temperature increase/decrease is not homogeneous and steady. This analysis was performed at different maximum temperatures and heating/cooling rates. From the transient temperature analysis temperature in the chamber stabilizes only at about 50°C when a low

variability of the heating rate from 0.2 to 1.4 °C/min is used. Similar deviation occurs at the inversion of heating to cooling and below 100°C during cooling, see Figure 9. As the heating rate increases to 5 or 10 °C/min, the deviation of heating/cooling rates from steady condition is more significant and it is reached at higher temperatures.

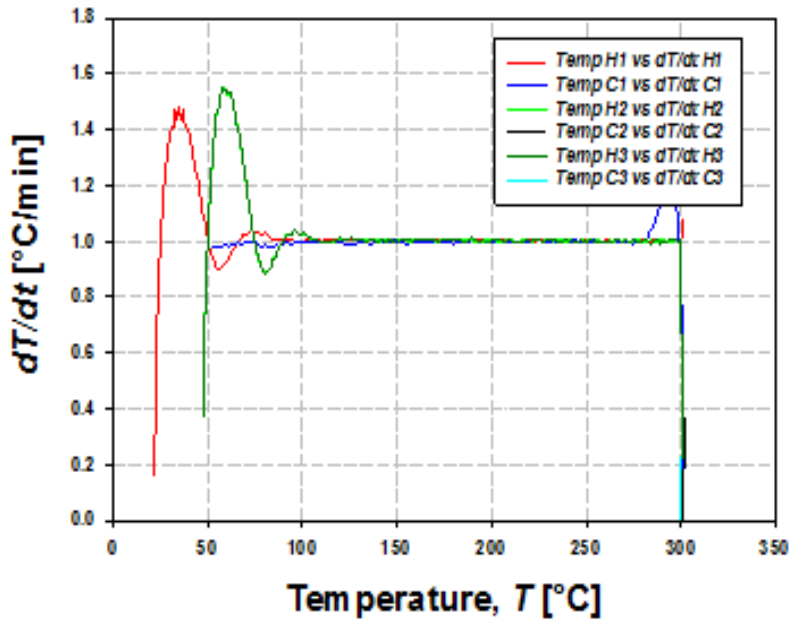


Figure 9. Analysis of temperature stabilization for the push-rod dilatometer at a heating/cooling rate of 1°C/min. Cycles reach a maximum of 300°C. The heating/cooling rate is stable after 100°C when heat transfer stabilization with the surroundings has been reached.

Thermal gradients analysis helps to identify temperatures at which the measured data points are in a homogeneous stabilized condition. Linear expansion and coefficient of thermal expansion versus temperature curves presented in this document are restricted to the temperature range in which effects of transient thermal gradient are minimum. The lack of homogeneous temperature (unstable heating and cooling rate) at the beginning and at the end of the cycle causes bias in the CTE results, as the temperature reading may not correspond to the actual temperature of the sample. A mechanism to allow for a better temperature stabilization in the chamber is suggested by the use of forced cooling (liquid nitrogen insertion in the chamber) near room temperature.

3.4.2 Process Induced Effects on Thermal Expansion: Materials and Processes

An investigation of the process effects influencing thermal expansion was carried out by testing coatings sprayed under different process parameters and techniques. Further characterization of microstructural features (e.g. oxide content, porosity), as well as correlation to the processing history (particle melting state, particle kinetic energy, residual stress state) will enable determination of whether thermal expansion for TS coatings is dependent on the processing.

Elemental metals (i.e. Ni, Al) were initially tested. Samples were sprayed by different techniques (atmospheric plasma spraying-APS, HVOF, cold spray-CS, Flame Spray), and it is expected them to show extreme differences in terms of microstructure, oxide content, hardening by impact, inter splat cohesion, etc.

NiCr as a representative of metal alloy materials was deposited within a broad process windows (various torches and conditions). Details of materials and processing are published elsewhere (Alfredo Valarezo and Sampath 2011).

YSZ coatings were also plasma spray deposited over a range of conditions with an F4 torch (Vaidya et al. 2008). Samples of different microstructure architecture (porosity content, stiffness, intersplat cohesion, etc) were obtained by changing process parameters and using two particle morphologies: fused and crushed powder (FC) and hollow spheres (HOSP).

3.5 Results and Discussion

A number of different effects can be observed in a heating cycle in a TS coating. Regarding the bulk material within the splats, as the temperature increases the atom-separation increases as the atoms find their equilibrium positions. This is measured as the volumetric expansion of the material. Besides that, the exposure of the material to heat during deposition causes microstructural progressive changes due to:

- Recovery or stress relief at $T_h \sim 0.3$ (where T_h is the homologous temperature $T/T_{melting}$)
- Polygonization at $T_h \sim 0.4$
- Grain growth at $T_h \sim 0.5$

- Increase in vacancy concentration
- Homogenization of the structure.

Outside the splats (in the splat boundaries, in the microcracks within splats, in the porosity and voids), as the temperature increases the structure changes due to:

- Growth of the intersplat contact area
- Intersplat interlocking and friction
- Surface diffusion that leads to microcrack healing and splat stiffening.
- Diffusion that leads to sintering of interfaces (at higher T_h), etc.

In this study, the discussion centers in the low temperature regime with heating cycles of $T_h < 0.55$

The occurrence of these effects will depend on the kinetics (time and temperature) and material specific behavior, including the processing effects such as residual stress, density, and heterogeneity of the structure. The abovementioned changes are important when studying the thermal expansion of TS coatings, especially because of the particular microstructure that includes chemical inhomogeneities due to the rapid solidification, defects, pores, etc. that affect the properties.

An “*anomalous*” behavior has been identified in the first heating cycle of all coatings, and it is particular to the defect annealing of the structure of the coatings. It is measured as a deviation from the nominal expansion behavior. This anomalous behavior has been called here as “*Thermal Shakedown*”. Evidence of differences on the first heat cycle expansion is presented for several materials. However, the analysis of the implications on defect annealing is discussed in detail in chapter 4.

It is known that due to the nature of the defects in TS, these coatings are anisotropic considering for instance: mechanical, thermal, or electrical properties (Sharma, Gambino, and Sampath 2006; S. Sampath et al. 2004). In this study, it was found that the thermal expansion, after *thermal shakedown*, is not anisotropic despite the layered nature of the coating. To complete the discussion of CTE and the relationship to the microstructure of coatings, a discussion of processing effects for the same material deposited by various techniques is presented. This will be discussed in section 3.3. Finally, the technique of extracting the CTE and the elastic modulus values of the coating by the curvature method is discussed as an alternative to produce design properties in a quick and reliable manner. This is presented in section 3.5.

3.5.1 Cyclic Heat Treatment

When performing cyclic expansion measurements of TS coating samples via dilatometry, the behavior of the first heating cycle shows an abnormal trend compared to the subsequent passes. This behavior has been found in all tested coating materials and this thermally activated behavior appears only during the first heating cycle. The samples expand more or less than in the subsequent passes. This results in an irreversible overall contraction or expansion of the original length of the sample. More prominent differences (shakedown) are observed in metallic samples than in ceramics, and the behavior is observed at low, medium, and high temperature cycles.

Figure 10 illustrates a typical temperature sequence: heating and cooling for three consecutive cycles at constant heating and cooling rates. Depending on the material, samples were cycled at different temperature ranges. It is highlighted that the heating/cooling rate is constant, except as the temperature approaches the lowest ranges due to the transient effects in the chamber of the dilatometer, as it was discussed in section 3.1.3 of this chapter.

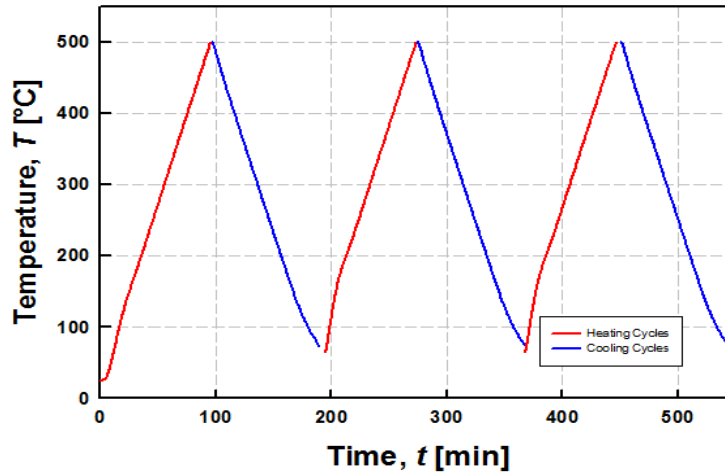
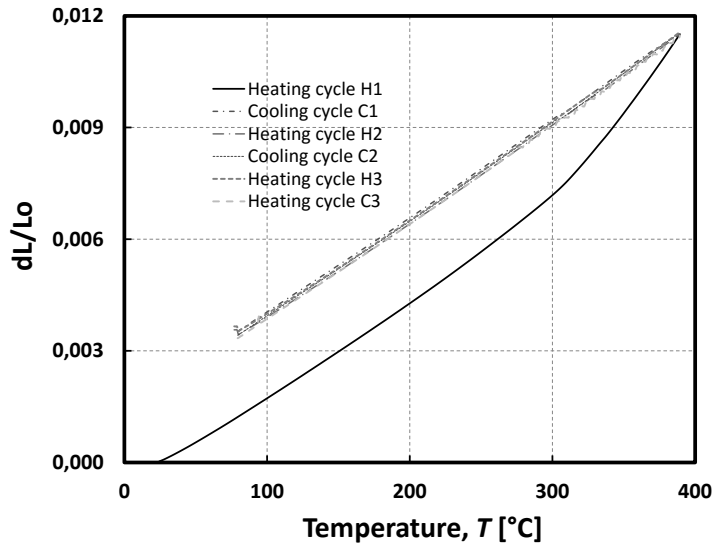


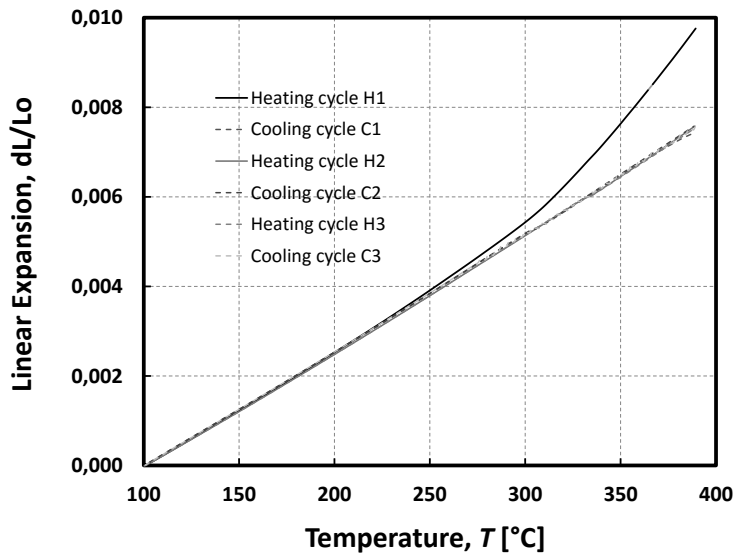
Figure 10. Typical time-temperature sequence for a heat cycling experiment to study thermal shakedown effect and the CTE in TS coatings.

In Figure 11a, the cyclic results of linear expansion ($\delta L/L_0$) for a temperature regime (up to 400°C) of an Al-sample coating sprayed by flame spray is presented. Figure 11a shows raw data illustrating the absolute linear expansion of the sample in various cycles. The sample dilates at a higher rate in the first cycle compared to the following, resulting in an overall irreversible expansion of the sample. Figure 11b shows tared data for the same experiment. Data is tared to the

absolute linear expansion of the sample after the shakedown heat cycle (first cycle) at a temperature at which constant heating/cooling rate is achieved (about 100°C) in the experiment. This allows the comparison of relative expansion in different cycles. For instance, in Figure 11b in the first heating cycle, the deviation from the nominal expansion starts at about 225°C, and increases as the temperature increases.



(a)



(b)

Figure 11. Linear expansion of an Al-sample deposited by flame spraying, as a function of temperature. Three heating/cooling cycles are presented: a) Raw data and b) Tared data (at 100°C) for comparison of relative expansion.

In Figure 10, the linear expansion from the corresponding cyclic experiment as presented (three heating and three cooling cycles) in Figures 9 is shown. Again the deviation from the nominal expansion behavior is observed in the first heating cycle, and deviates incrementally from 23×10^{-6} [$1/^\circ\text{C}$] (nominal) up to over 50×10^{-6} [$1/^\circ\text{C}$] at 380°C . The analysis of CTE is often more sensitive to deviations in the shakedown cycle compared to the linear expansion provided that CTE is the derivative of the linear expansion as a function of temperature. The deviation of the shakedown cycle apparently starts at about 175°C when observing the CTE curve (Figure 12) earlier than the 225°C observed in Figure 11b.

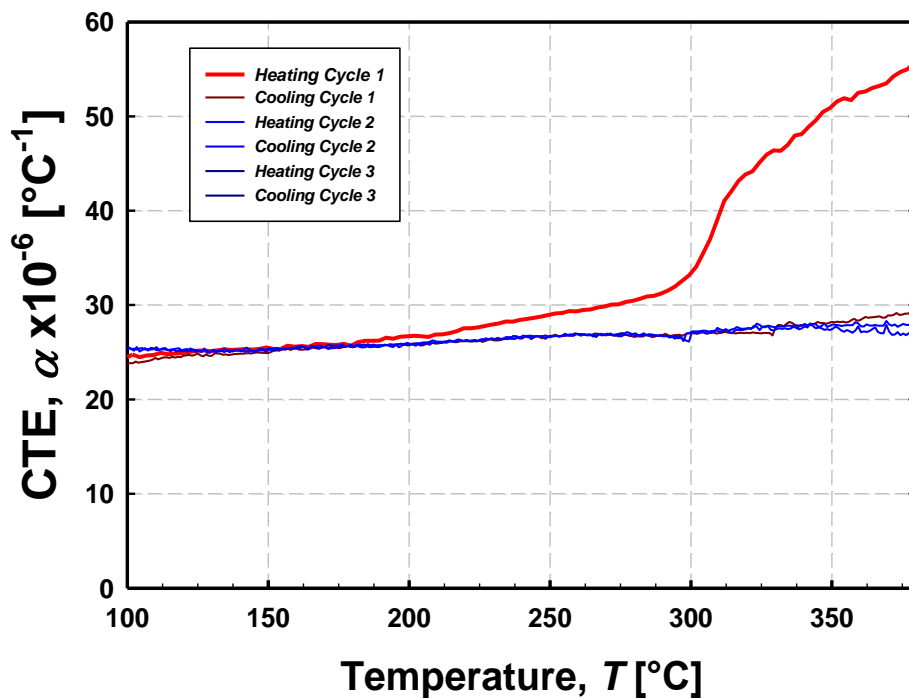


Figure 12. Coefficient of thermal expansion CTE of an Al-sample deposited by flame spraying as a function of temperature. Three heating/cooling cycles are presented. First heating cycle deviated from the nominal behavior which was achieved by all the following heating/cooling cycles.

Cyclic tests were carried out for all the dilatometry experiments presented here, and the CTE reported is obtained after the first heating cycle (any cooling or heating cycle can be used). All results about process induced effects as well as anisotropy are discussed after the *shakedown* cycle.

Although this is not the first study that identifies this behavior, it is probably the first one that has critically addressed the same. Investigation on expansion of YSZ and Alumina coatings, by (Wang, D. Berndt 1991) and (Berndt, C.C Herman 1982) reported for the first time this anomalous behavior which they attributed to experimental error of the dilatometer, and discarded this information.

Later, (J Ilavsky and Berndt 1998) reported as well this unique behavior of coatings during the first heating cycle at high temperature (above 800°C) in MCrAlYs, SS316, and YSZ composites. They suggested that the different behavior of the first cycle is the result of stress relaxation and/or oxidation. Their conclusion is based on comparing hardness values of the as-sprayed condition to the after heat cycling condition. An increase in hardness is attributed to oxidation whereas a decrease is attributed to stress relaxation. The study is limited to reporting these possible effects, oxidation and stress relaxation, on CTE during shakedown without discrimination between them. The authors did not discuss the possible precipitation of intermetallic phases that appear as peaks of the CTE vs temperature curves at specific temperatures for both alloyed materials (Taylor & Denman 1974).

Taylor et. al. (Thomas a. Taylor and Walsh 2004; T. a. Taylor and Walsh 2004) also reported thermal shakedown at high temperature cycles in various TS bond coats of several compositions and called it, residual sintering. High temperature thermal expansion tests (1100°C) were performed to find out the effect of the bond coat composition in the CTE. This study was intended to produce a new bond coat material with longer cycle life by reduction of thermal mismatch. Little attention was given to the shakedown behavior and was just attributed to sintering of interfaces.

Choi et. al. (Choi et al. 2007) on the analysis of the expansion of Aluminum cold spray samples conducted ten consecutive measurements. The study reported that repeated heat cycles reduces progressively the deviation of CTE from bulk, until reaching the bulk value after a number of cycles, or after annealing in air. The thermal shakedown was attributed to oxidation, in this case. They conclude that the thermal expansion of coatings is increased by oxidation and decreased by the presence of oxides. This study does not report the expansion behavior cycle by cycle. In the present document it has been found that the differences on the first heating cycle disappear right after the first cycle and not progressively as they (Choi et al. 2007) reported.

To address systematically the thermal shakedown effect, the CTE of samples of elemental metal coatings were tested initially to exclude possible effects of alloying. Also, samples of the same metal (e.g. Al) were prepared by several processes (e.g. HVOF, APS, cold spray, flame spray, etc) to rule out possible process induced effects, and finally, alloyed metal samples and other ceramics were also evaluated.

3.5.1.1 Thermal Shakedown Evidence on: Pure Metal Coatings

Alloying of the feedstock could eventually produce precipitation of different phases in the coating due to the effect of rapid solidification. Preferential oxidation during in-flight is also possible. During the first heating cycle, re-ordering of elements could be responsible for variation in the thermal expansion. Therefore, pure elements were chosen as initial material system.

Figure 13 shows the linear expansion during the shakedown cycle –thick line-, compared to the steady state behavior (equivalent to bulk expansion value) -thin line- of various pure metals deposited by different processes (the data is tared for comparison, similar to Figure 11b). The shakedown effect is considered positive when the sample irreversibly expands, or negative when it irreversibly contracts. In this set of data, the Ti and Al by Cold spray (CS), and the Ni by HVOF-DJ have a positive shakedown; whereas, the Ag by APS, and Ni by APS, HVOF-JK and CS, have a negative shakedown.

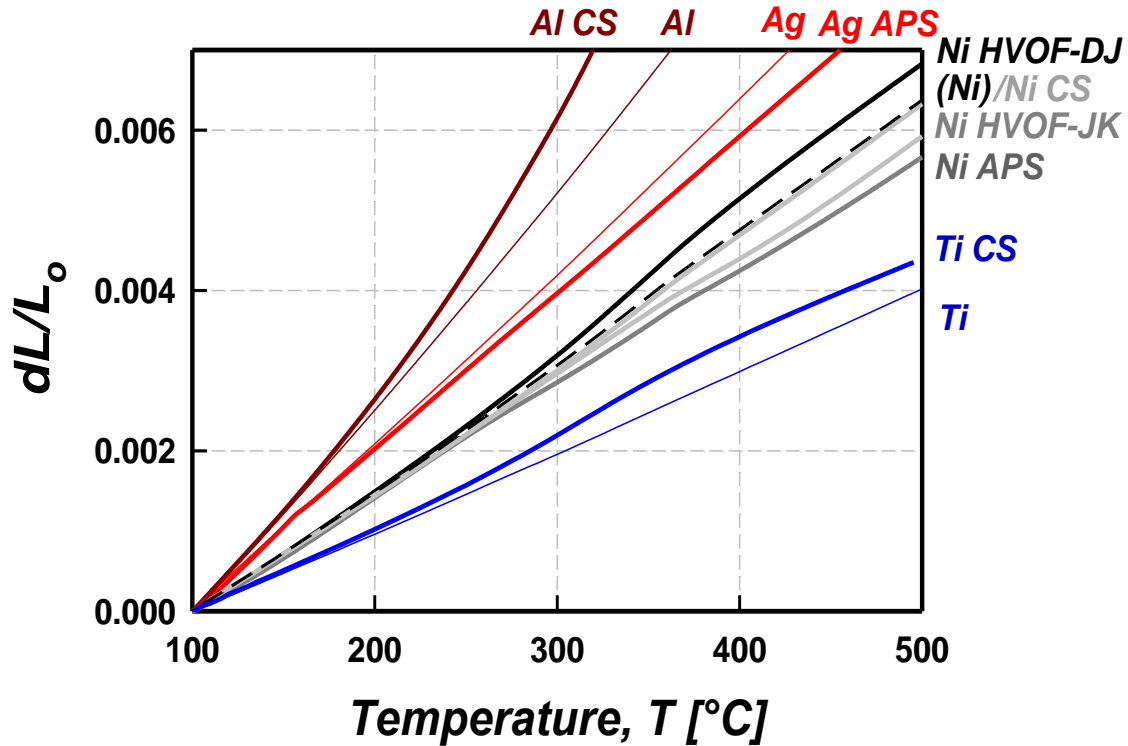


Figure 13. Comparison of the linear expansion during the first heating cycle –thick line–, and one after it (steady state behavior) -thin line- of various pure metals deposited by different processes. The thermal shakedown makes the linear expansion different in the first heating cycle than in the subsequent cycles.

Positive thermal shakedown can be attributed to an increase in vacancy concentration, relief of compressive stresses, and/or oxidation during heating; whereas, the negative thermal shakedown could respond to relief of tensile stresses, and/or annealing of defects (point, line). The magnitude of such effects will be discussed in chapter 4.

It is shown in Figure 13 that the shakedown effect appears in all of the TS coatings tested produced by different techniques. Ni, for instance; can show a positive or negative shakedown for the family of HVOF processes, whereas the cold sprayed Ni sample almost show no effect. However the cold sprayed Ti, or Al show large shakedown in contrast to the Ni sample. The magnitude of the deviation and the link to material and processing is not very clear at the moment.

3.5.1.2 Thermal Shakedown Evidence on: Process Induced Effects

Figure 14 shows CTE of various Al samples sprayed by three different spraying processes, atmospheric plasma spray, cold spray, combustion wire flame spray (FS-1). The results are

compared to the expansion behavior of the pure Al bulk material, to which all the samples approach after the shakedown cycle. Significant differences are found among the samples in the shakedown cycle. In every case, the shakedown is positive. The APS behavior is the closest to bulk, whereas the rest of samples (CS and FS-1) expand significantly more. At the temperature of 350°C the CTE for CS and FS doubles the CTE of the bulk. A second sample of FS (FS-2) was produced at a different time, and it showed a smaller effect. In conclusion, the shakedown effect responds to the processing of the coating.

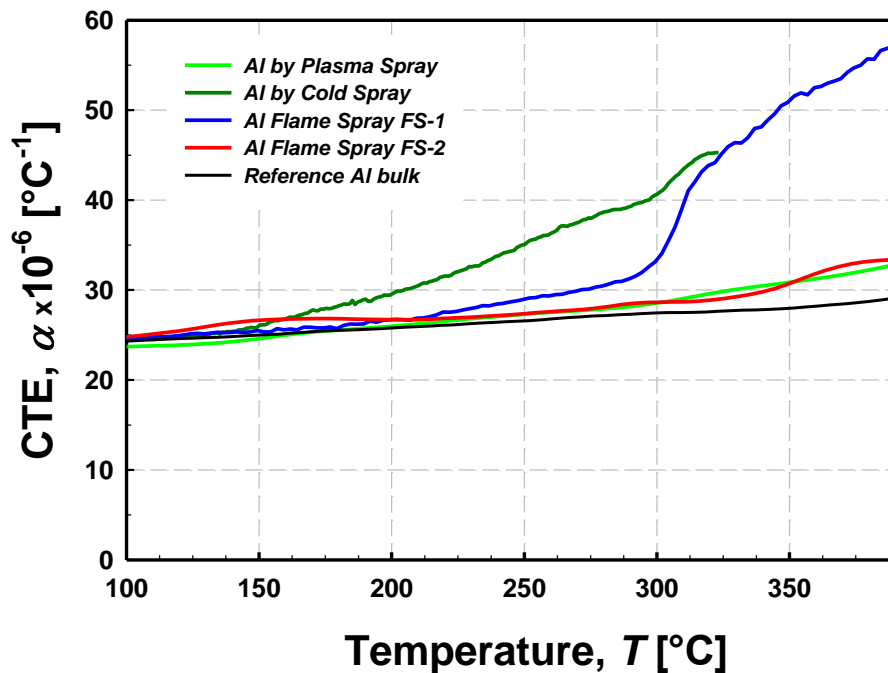


Figure 14. Comparison of the CTE during the first heating of Al-sample coatings sprayed by three different processes (atmospheric plasma spray, cold spray, FS-1 combustion wire flame spray. Shakedown is positive in all cases. First heating cycle –thick line–, and after it (steady state behavior) -thin line. The behavior reduces to the behavior of the bulk Al. FS-2 is another sample sprayed by combustion wire flame spray at a different time.

3.5.1.3 Thermal Shakedown Evidence on: YSZ coatings

It was found that ceramic coatings also showed a shakedown cycle, but with lower relative magnitude. Figure 15 shows CTE results of four different YSZ coatings by APS compared to a reference behavior after thermal shakedown. The shakedown behavior of samples sprayed at three different spraying conditions, namely, low, medium and high energy (deposited with HOSP

powder) are very similar, and slightly different than the stable condition. The shakedown of samples sprayed with fused & crushed powder (F&C) differs from the others, especially at the low temperature regime, and differs less to the reference behavior. Two peaks in all the three HOSP samples are identified in the shakedown cycle at about 330°C and 500°C. The same peaks are not present for the F&C sample. It is hypothesized that these peaks correspond to a phase change of the YSZ ($\text{ZrO}_2+8\% \text{ wt Y}_2\text{O}_3$) at those temperature. The equilibrium phase diagram registers a phase change at 500°C, where the tetragonal phase changes reversibly into tetragonal-cubic. The as-sprayed phase in YSZ plasma spray is typically tetragonal, although, some monoclinic and cubic phases can nucleate during the deposition due to the rapid solidification. According to the phase diagram (Jan Ilavsky and Stalick 2000; Scott 1975), some tetragonal phase transforms into cubic at around 525°C. Also, if there exist monoclinic phase, this changes into tetragonal at the same temperature. The effect in the CTE thermal shakedown is irreversible, therefore it is hypothesized that some monoclinic phase was deposited in the as-sprayed condition for the HOSP powder. Phase composition and the tetragonal phase yttria content may change significantly and rapidly, and even at considerably lower temperatures some compositional changes are reported. This change may be detrimental to deposit lifetime. Formation of monoclinic phase changed into tetragonal at 525°C creating a volume change. This volume change is comparable to literature reports similar. Values of volume change for this phase transformation is in the order of (0.2%).

Later, during the following heat cycles, the material behaves according to the phase diagram in equilibrium changing the low temperature phase tetragonal into tetragonal-cubic at higher temperature, and viceversa.

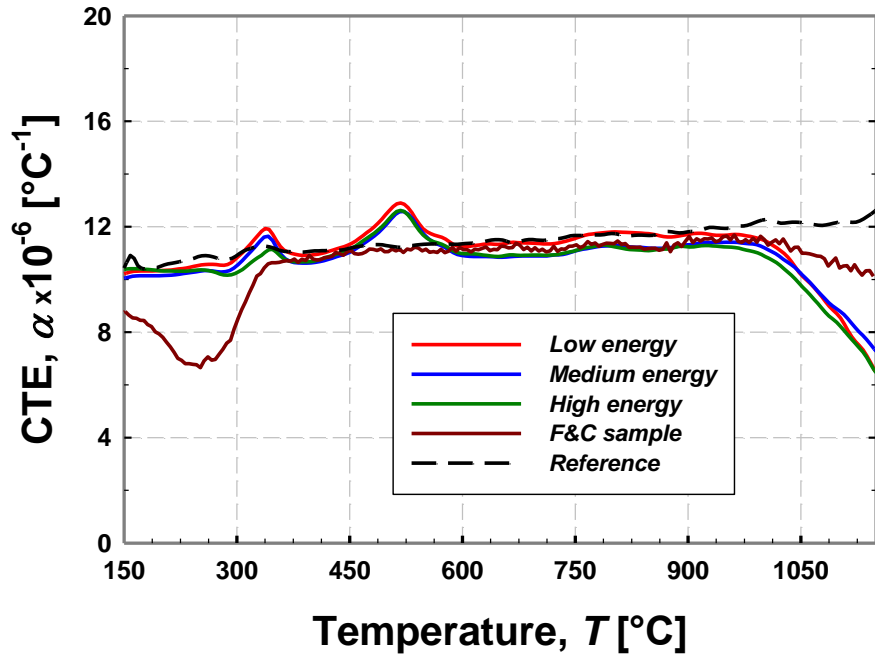


Figure 15. Comparison of the CTE during the first heating of YSZ coatings sprayed by APS- atmospheric plasma spray. Two feed stock materials were used: F&C fused and crushed, and HOSP hollowed spheres under three different spraying conditions, namely of low, medium, and high energy. The first heating cycle is presented for the four coating types. The behavior reduces to the one of the bulk YSZ -dashed line- after the first heating cycle.

The effect at 330°C for HOSP coatings is unknown at the moment. The behavior of F&C YSZ below 330°C is considered affected by a transient state of heat in the chamber during the experiment.

The relatively low difference of the CTE between the shakedown cycle and the subsequent ones responds to 1) the low energy stored as the structure relieves stress by microcracking during solidification; 2) the kinetics of annealing of defects is slow relative to the high melting point of the material $T_h < 0.3$; 3) the oxidation during the experiment is limited, etc.

It is noted that the phase transitions at 330°C, and 520°C, for HOSP occur as a rapid stretching of the structure followed by a contraction while heating. This type of strain changes are undesirable as they may lead to failure. Similarly, the phase change of monoclinic into tetragonal is considered undesirable, since this transformation is accompanied by a large volume change (Jan Ilavsky and Stalick 2000). It has been hypothesized that this could explain coating failures after few heating cycles (infant mortality) in YSZ coatings.

3.5.1.4 Discussion about Cyclic Heat Treatment

In a thermal expansion curve, the phase changes and/or magnetic/paramagnetic transitions can easily be identified as abrupt changes in the expansion rate at specific temperatures. These changes are reversible in nature. In the case of the thermal shakedown, as defined in here, the changes are irreversible and occur only in the first heating cycle. In most cases, it is observed that the deviation from the nominal behavior increases with increasing temperature.

This thermally activated phenomenon is believed to be a result of various progressive changes in the microstructure that include: stress relief, recrystallization (recovery, polygonization, and grain growth), crack/pore closure, oxidation, and sintering of inter-splat interface (at higher temperatures). Therefore, it is also assumed that thermal shakedown is affected by the processing of the sample, for instance, the nature of residual stress (compressive or tensile), amount of pores/cracks/metastable phases, grain sizes, intersplat bonding, etc.

In situ oxidation can be playing a role on shakedown behavior given that a perfect inert atmosphere is not achieved during the experiments and also oxygen could remain within the porosity after the spraying process.

Thermal shakedown was investigated by testing samples under cyclic conditions. First, pure metal materials (like, Ag, Ti, Ni, Al), the results show divergent results in the shakedown cycle. The effect can be positive (permanent elongation), or negative (permanent contraction) for the material, by just changing the process. Clear trends of processing to shakedown effects are not evident. Once the shakedown cycle has taken place, the CTE behavior approaches very closely to the bulk material.

Metal/alloy materials (Ni-20Cr) and more complex alloys with intermetallic precipitates (CoNiCrAlY and Inconel 718) have also been tested under inert atmospheres. Their shakedown behavior deviates relatively much more to the after shakedown cycle than for the pure metals. It is believed that due to the rapid solidification during particle deposition in TS, the resultant microstructure of the coating is chemically inhomogeneous, even for pure metals due to in-flight oxidation. This effect is more prominent for alloyed feedstock. With temperature, some intermetallic phases (e.g. in bond coats: γ' -Ni₃Al phase) precipitate. This phase precipitation is likely related to the changes in expansion rate occurring during the first heating cycle and it is irreversible.

The occurrence of the effect was largely tested and proven true in all experiments. The repeatability of the phenomena of shakedown was also investigated. Two pieces of the same specimen of Ni20%Cr were subjected to heat cycles. The specimen was deposited by HVOF-JK process and was tested under cyclic conditions. The shakedown effect was repeatable, as indicated in Figure 16 where shakedown repeatability was proven using two samples from the same Ni-20%Cr coating deposited via HVOF. From here, it can be concluded that the sampling size of the specimen (defined in 3.1.2) is appropriate to be a representative average of the contributing effects to the shakedown, allowing for reproducible results. A third sample of the same specimen was previously heat treated at 550 °C in vacuum for 2 hours, according to (ASM 2002). It was confirmed that the thermal shakedown disappears after the heat treatment.

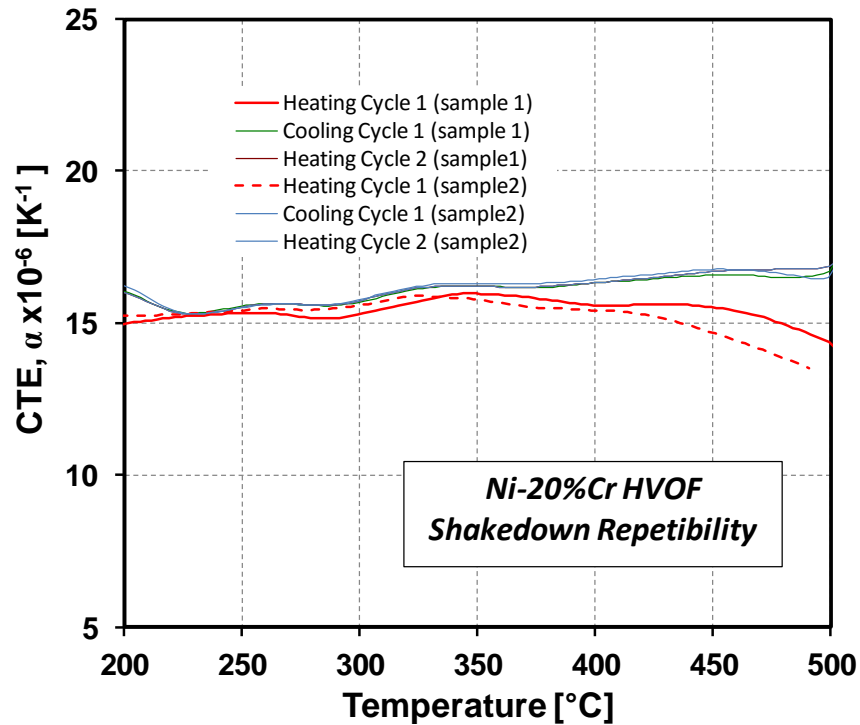


Figure 16 Analysis of shakedown repeatability, two samples from the same Ni-20%Cr HVOF coating were evaluated during three heating and cooling cycles up to 500°C.

3.5.2 Anisotropy in Coatings

As discussed previously in anisotropy section 3.3.2, there are no consistent studies in which TS coatings are not found to be anisotropic in thermal expansion. Some authors hypothesize the possibility that material expanding within a splat in its radial orientation (consider the splat as a disk, radial = in-plane orientation) may load a contiguous one by shear contact (the adjacent splat is not parallel). This would produce a difference in expansion in both directions since while a coating expands in the in-plane orientation, the shear loading affects the expansion of the through-thickness direction by adding mechanical strain to the thermal strain. However, this may be possible in a constrained scenario where splats are limited to expand in one direction but not in the other. This, for the experimental setup of linear dilatometers does not apply.

On the other hand, typically the expansion of composite materials as discussed in section 3.3.1 can be modeled considering a homogeneous distribution of the secondary phases. However if the composite material is a laminate (i.e. fiber reinforced polymer), or in general, the second phase has a preferential orientation, this determines a difference in the CTE in the longitudinal versus the transversal direction of the fibers. This anisotropy in the CTE of the composite rises from interaction between the thermal strain and the mismatch mechanical strain occurring between the matrix and the fiber, especially in the longitudinal direction. In the transversal direction, the mechanical mismatch strain is reduced. Several numerical models have been developed and applied to laminated composites ((B.Walter Rosen † 1970; Karadeniz and Kumlutas 2007; Hsueh, Becher, and Sun 2001). If the abovementioned concept were applied to TS coatings, an anisotropic response on CTE would be expected for coatings with a significant volume fraction and a homogenous and laminated distribution of a secondary phase (i.e. oxide).

The author here hypothesizes based on the previous discussion and on the following experimental results that the CTE for TS is not an anisotropic property unless a significant amount of a secondary phase is present in the microstructure with a regular laminated orientation.

A very thick sample (25 mm) of Al-sample by flame spray was produced to test anisotropy in metal coatings. The CTE value obtained was the same for the in-plane and through-thickness orientations, as reported in Table 3. Only, the shakedown behavior was found to be anisotropic, as presented in Figure 17.

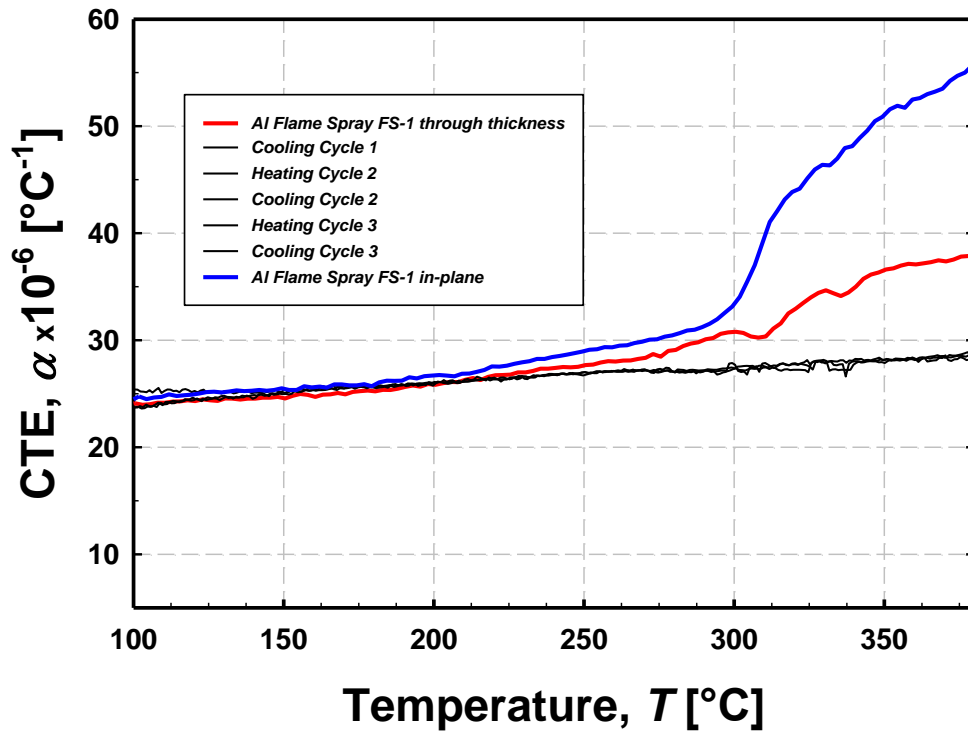


Figure 17 CTE of Al flame sprayed coatings using specimens oriented in the through-thickness and in-plane orientations for the shakedown cycle and after it. The line of reference bulk overlaps the behavior of the coating sample (in both orientations) after the first heating cycle.

As the shakedown is a kinetics-driven effect, the anisotropy is expected to occur due to the presence of inter-splat interfaces. Thus, the magnitude of strain relieved during shakedown is much larger for the in-plane than the through thickness orientation, as indicated by the magnitude of the shakedown effect. Also, the residual stress condition in TS coatings is considered an in-plane stress condition, which leaves the through thickness direction without any strain to relieve during the first heating cycle.

The CTE after shakedown for both in-plane and through-thickness directions resembles the bulk behavior of Al, in Figure 17. From here, it is concluded that features like oxides (Al_2O_3), pores, or cracks do not make CTE anisotropic, when testing a relatively large volume sample (compared to the splat or defects scale size). Although the coating formation commonly leads to a preferential geometric orientation of interlamellar oxides, when analyzing the microstructure (see Figure 28) of these samples, this “laminated” like microstructure is barely observed. This occurs likely due to the nature of the flame wire spray process in which splats are formed in a random

distribution of sizes and morphologies. This lack of significant anisotropy in the secondary phase distribution may be responsible of the apparent isotropic response of the CTE.

3.5.3 Process Induced Effects

As discussed before, the CTE property of a coating should be the same as the feedstock bulk material. However, the processing changes the CTE value because of changes in the composition of the coating due to presence of precipitates, oxides or vaporization of selected species during TS deposition.

In Table 3, a compendium of CTE values of various Al samples (shown also in Figures 7, and 14), and Ni is presented. The results are compared to bulk values. After the first heating cycle, the deviation on expansion behavior for all the samples tested compared to the bulk is minimum even though they have been processed by different TS technologies. This is explained by the low oxidation suffered by Al, and Ni, during the processing. The deviation from bulk values is in the range of the experimental error.

However, when investigating materials more sensitive to oxidation or processing effects such as Ni-20%Cr, the change in property value can be more significant (up to 10%). This was analyzed in section 2.1.1 and modeled by the rule of mixtures, Turner and Kerner models. The results in Figure 4, concluded that the deviation of the CTE value induced by the processing responds to the amount and nature of the secondary phases appearing in the coating.

In all cases above, the porosity effect is ruled out as the open air is not able to affect by expansion the surrounding material during heating. This is precisely observed in YSZ coating by plasma spraying. Here, YSZ coatings were deposited within a framework of a process map (Vaidya et al. 2005) to study process induced effects on CTE. The powder morphology used on the deposition of these coatings was hollow sphere powder (HOSP). Results are compared to one sample sprayed using fused and crushed (F&C) powder. Figure 18 shows that CTE differences are negligible among HOSP coatings of a process map and the F&C coating, although significant differences in particle temperature and velocity and microstructure (specifically porosity content) are observed, as seen in Table 5.

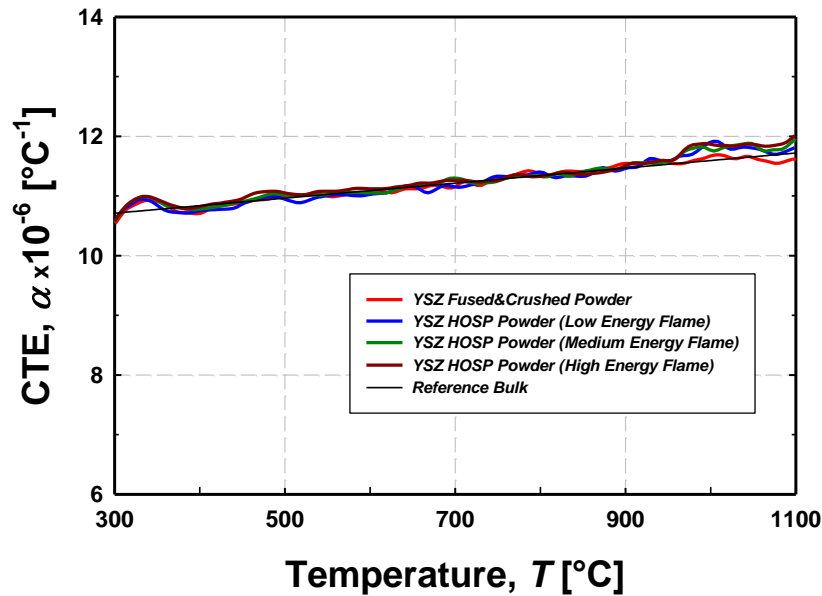


Figure 18. The CTE of various Ytria Stabilized Zirconia-YSZ coatings sprayed by APS- atmospheric plasma spray. The CTE is reported from the second heating cycle (after shakedown). Two feed stock materials were used: F&C fused and crushed, and HOSP hollowed spheres under three different spraying conditions, namely of low, medium, and high energy. The behavior of all samples is comparable to the behavior of the bulk YSZ.

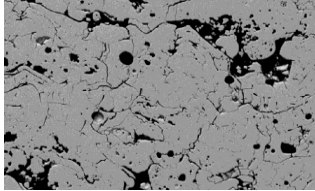
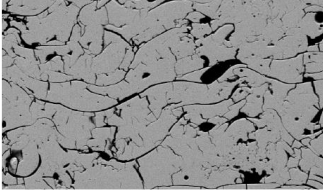
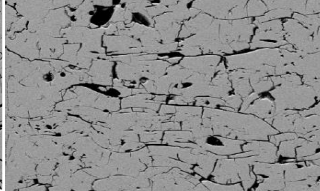
	LOW ENERGY TORCH	MEDIUM ENERGY	HIGH ENERGY TORCH
Condition			
Temperature[°C]	2978	3045	3105
Velocity [m/s]	139	173	208
Porosity [%]	27	18	17

Table 5. YSZ-APS coatings within a Process Map, average particle temperature and velocity by DPV, and porosity measurement by image analysis (Vaidya et al. 2008)(Chi 2008)

This confirms that the effect of porosity can be ruled out. On the other hand, different YSZ-phases can be deposited during APS processing, specifically tetragonal and less common, monoclinic and cubic. All of them have relatively the same expansion (Ochrombel et al. 2010)

except for the monoclinic-phase which is regularly found in less proportion. From here, it can be expected that all YSZ coatings by APS show about the same CTE value. In Table 3, the property range shows about 2.6% of variability around the nominal value, which again is within the experimental error.

Induced effects on CTE by processing are significant during the first shakedown cycle as it was discussed in section 4.1.3. However after that cycle, the CTE value is only dependent on composition.

3.6 Coefficient of Thermal Expansion-CTE by the Curvature Method

All the values of CTE presented previously are measured by instruments that monitor the change of length of a sample. LVDT's, optical, or laser sensors are regularly used. The longer the sample is, the more precise the measurement is. However, sample preparation in the case of coatings is difficult as the coating thickness needs to be large. Depositing thick coatings is often time consuming, expensive, and may lead to premature delamination due to residual stresses. As an alternative to the dilatometer measurement, the curvature principle applied to a coated plate is shown here. The principle of measurement is based on the analysis of a bilayer plate that bends when a thermal gradient is applied in response to the differences in thermal expansion of the two materials. In this method, a thin substrate is coated and subjected to a heat cycle while fixed in a two knife-edge setup or in a cantilever style. As long as, the following occurs:

- 1) There exists a difference of CTE of the two materials,
- 2) The thickness of coating (t_D) and substrate (t_H) are comparable ($t_H / t_D < 10$), and
- 3) The in-plane elastic modulus of coating (E_D) and substrate (E_H) are comparable ($0.5 < E_H / E_D < 2$);

Then, the bilayer plate bends significantly and can be measured with good precision (Kesler et al. 1997). The balancing of stresses through-the-thickness from a plane-stress condition that determines a unique curvature of the plate can be modeled analytically considering the thickness, the rigidity, and the CTE of each layer. The equation used by classical mechanics is the following:

$$\frac{\Delta K}{\Delta T} = \frac{6E'_D E'_s t_D t_s (\alpha_D - \alpha_s)}{E'^2_D t^4_D + 4E'_D E'_s t^3_D t_s + 6E'_D E'_s t^2_D t^2_s + 4E'_D E'_s t_D t^3_s + E'^2_s t^4_s} \quad \text{Equation 9.}$$

Where, $\frac{\Delta K}{\Delta T}$ is the rate of change of curvature due to a thermal gradient; E'_D, E'_s are the elastic modulus in-plane of the deposit and substrate respectively (the in-plane modulus is $E' = \frac{E}{1-\nu}$, where E is the Young's modulus); t_D, t_s are the thicknesses of the deposit and substrate respectively; and α_D, α_s are the coefficients of thermal expansion of coating and substrate respectively.

Here, the $\frac{\Delta K}{\Delta T}$ is obtained experimentally, and its value is a function of the thicknesses, in-plane elastic modulus, and CTE of each layer. This method has been used to obtain the elastic properties of TS coatings (Nakamura and Liu 2007; Matejicek and Sampath 2001) assuming known experimentally the $\frac{\Delta K}{\Delta T}$ and the CTE (α_D) of the coating. An instrumented heat cycle test has been developed to obtain $\frac{\Delta K}{\Delta T}$. Basically, the bending of the beam is monitored by three non-contact lasers that measure the displacement of three equidistant points. The bilayer plate is heated up in an oven that allows for controlled uniform heating. Any thermal gradient in the plate is minimized. When the CTE of the coating is not known experimentally, then the CTE of the bulk material is adopted.

Based on this principle, if two specimens of the same coating are produced on two different substrate materials, then the equation 9, can be used in a 2-equation systems (see equation 10) to calculate the CTE and the in-plane modulus of the coating.

$$\begin{cases} \left(\frac{\Delta K}{\Delta T}\right)_1 = \frac{6E'_D E'_{s1} t_{D1} t_{s1} (\alpha_D - \alpha_{s1})}{E'^2_D t^4_{D1} + 4E'_D E'_{s1} t^3_{D1} t_{s1} + 6E'_D E'_{s1} t^2_{D1} t^2_{s1} + 4E'_D E'_{s1} t_{D1} t^3_{s1} + E'^2_{s1} t^4_{s1}} \\ \left(\frac{\Delta K}{\Delta T}\right)_2 = \frac{6E'_D E'_{s2} t_{D2} t_{s2} (\alpha_D - \alpha_{s2})}{E'^2_D t^4_{D2} + 4E'_D E'_{s2} t^3_{D2} t_{s2} + 6E'_D E'_{s2} t^2_{D2} t^2_{s2} + 4E'_D E'_{s2} t_{D2} t^3_{s2} + E'^2_{s2} t^4_{s2}} \end{cases} \quad \text{Equation 10}$$

Where: $\left(\frac{\Delta K}{\Delta T}\right)_{1,2}, E'_{s1,2}, t_{D1,2}, t_{s1,2}$, and $\alpha_{s1,2}$ are known; and, E'_D and α_D are the unknowns to be resolved.

To validate the method, a Ni-20%Cr coating by HVOF-JK process was deposited onto two different substrate materials: Al-6061-T6 and Stainless Steel 316 (SS316). Sample dimensions are reported in Table 6. For the two substrates, the CTE's were measured via dilatometry, whereas

the elastic modulus and poisson ratios are assumed from literature. The coating was deposited in the same spraying session onto the two substrate materials by fixing them contiguously. The torch, controlled by a robotic arm, moved above the two samples in the same stroke. The coating thickness obtained was similar in the two substrates. It is expected that the coating microstructure and properties are the same onto the two substrates.

Material	Young Modulus, E , [GPa]	Possion Ratio, ν	In-plane Modulus*, E' , [GPa]	Thickness, t , [mm]	CTE, α , $\times 10^{-6}$ [$^{\circ}\text{C}^{-1}$]	Reference
Substrate 1: Al 6061-T6	68.9	0.33	102.8	3.154	22.76+0.0185T	Bejarano et al, Nakamura, Liu
Substrate 2: SS316	193	0.30	275.7	1.490	16.50+0.0071T	Bejarano et al,
Coating 1	-	0.30	-	0.233		
Coating 2				0.232		

* $E' = E/(1 - \nu)$,

Table 6. Experimental data used to obtain the CTE and Young’s modulus of the coating based on the curvature method, and equation 10.

Each sample was subjected to three consecutive heating cycles with continuous monitoring of the curvature and temperature evolution. The heating cycle reached 200°C. After spraying, the residual stress condition was different for each coating due to the differences in thermal stress during cooling of both systems. However, the heat cycle test assures loading the substrate and coating in the elastic regime, so the initial stress condition does not affect the measurement.

The curvature-temperature curves produced for both systems are shown in Figure 19. As the analytical model predicts in equation 9, the behavior of the bilayer is linear elastic.

The 2-equation system (equation 10) is solved at temperature considering ranges of temperature gradients of 10°C. The results then reflect the coating CTE and elastic modulus temperature dependence as shown in Figure 20.

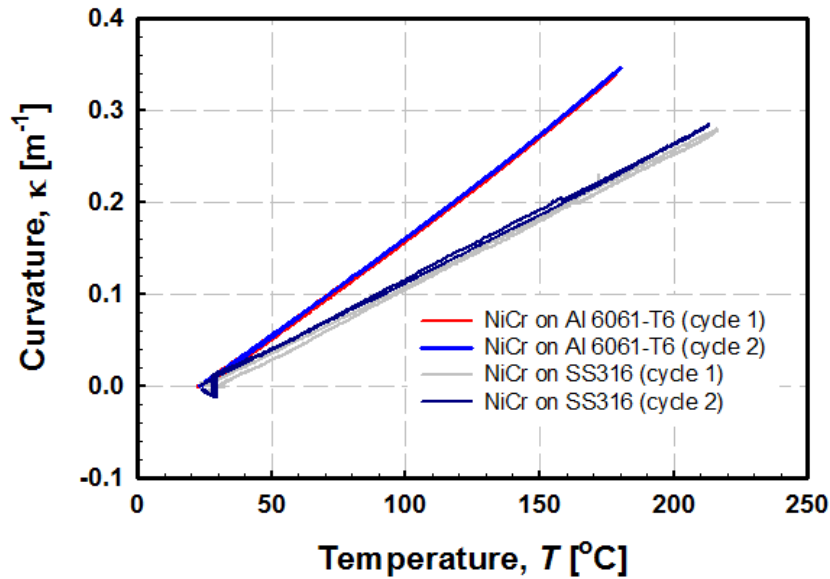


Figure 19 Curvature-temperature evolution of two coated plates subjected to heating/cooling cycles. One is the combination of a Ni-20%Cr coating onto Al-6061 T6 substrate, the other one is the combination of a Ni-20%Cr coating onto stainless steel 316 (SS316). Processing assures the coatings have the same properties in both substrates. The behavior is linear elastic. Two heating/cooling cycles are presented for each sample.

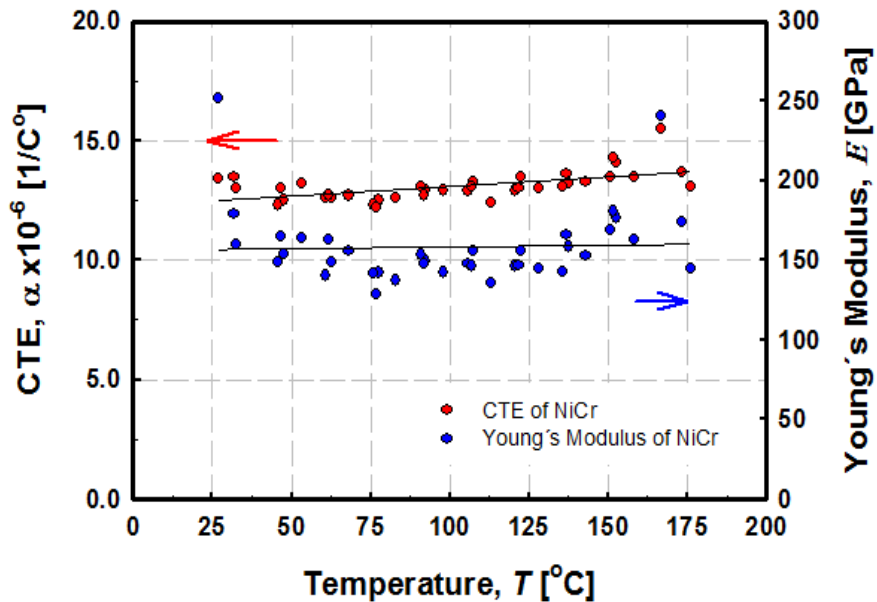


Figure 20. Calculated CTE and Young's modulus of a Ni-20%Cr coating based on the curvature method, data presented in Figure 19.

As compared to Table 3, the CTE of the coating varies from about $12,3 \times 10^{-6} \text{ }^{\circ}\text{C}^{-1}$ to $13,4 \times 10^{-6} \text{ }^{\circ}\text{C}^{-1}$, which is very similar or is in-the-range of coatings of the same compositions by HVOF. Even the temperature dependence, CTE increasing with temperature, is correctly reflected by the curvature method. The results validate the methodology, and offer an alternative method that can be of easy implementation in laboratory or production facilities. The main advantage of this technique lays on the fact that sample preparation is reduced to deposit a coating over two different plate materials, which is relatively easy to do in the same run, and there is no need of post-processing (sample cutting polishing, etc). Thin coatings can be used, whereas for dilatometry, thick coatings must be sprayed above 2 mm thick.

The value of elastic modulus is a fraction of the bulk value as it is typical for TS coatings, and ranges in between 70% of the bulk (bulk value reported for NiCr 215 GPa (Mankins, W.L., Lamb 1990)). Valarezo et. al. (a Valarezo et al. 2007; Alfredo Valarezo and Sampath 2011) reported a range of 50% to 60% of the bulk modulus for HVOF NiCr measured by instrumented indentation, is about 115GPa to 130 GPa for HVOF samples. The value here presented apparently shows to be larger than the reported in (a Valarezo et al. 2007) however, it should be noted that the measuring technique is quite different, especially sensing a different amount of coating material.

The curvature method does not show a singular behavior in the first heating cycle that could be considered the *shakedown* cycle. This could be because either the *shakedown* of this coating in particular was low, or the *shakedown* effect was affected by the applied mismatch strain from the substrate. The response of shakedown under applied strain is unknown at the moment.

3.7 Conclusions

In this chapter, the coefficient of thermal expansion (CTE) for TS coatings is discussed considering the fundamental behavior of the material and the possible influence of the property due to the particularities of the microstructure (oxide, pores, etc). Initially, a large compendium of CTE values for various metallic, ceramic, alloys, and cermet coatings is presented from literature and from tests developed by the author. The CTE values deviate from the bulk property only when significant oxidation (or presence of a second phase-byproduct of the TS processing) is present in the coating.

As a result of the experimental investigation conducted, appropriate sample sizing, preparation, and measurements are suggested for dilatometry measurements. Different techniques to obtain the expansion of samples are available. The values of CTE reported here were obtained mainly by the push rod dilatometry technique. Although other techniques such as: XRD, curvature method and DIC are also used.

All TS coating materials show an irreversible behavior manifested during the first heating cycle by measuring thermal expansion. The phenomenon is presented as an overall permanent elongation or contraction of the original sample length. The authors named this effect as *thermal shakedown* and it is attributed to annealing of defects (stress relief, recovery, sintering of cracks, etc) with temperature. For this reason, the compiled expansion data presented in this chapter corresponds to the second or third heating cycle. That is to say, the expansion values were extracted when the structure is stable and the CTE behavior is reproducible. The numbers of thermal expansion collected from other authors are not necessarily extracted in a cyclic manner.

Despite the anisotropy of the coatings due to their layered architecture, thermal expansion was found to be isotropic within the scope of this study. This was proven by analyzing a very thick coating material measured in both directions, in-plane and through-the-thickness. Only the first heating cycle was different for both samples due to shakedown, but after, they reached the same expansion value. However, further studies are suggested as it is hypothesized that a higher amount of a secondary phase preferentially oriented in the in-plane orientation may lead to anisotropy as suggested by the laminated composite theory.

Spraying processes and spraying parameters have an influence in the expansion response when phase changes occur (e.g. oxidation, precipitates) during spraying. Analytical models including rule of mixtures, Kerner and Turner models are used to predict the CTE behavior based on the properties of bulk material (feedstock) and oxides. When the feedstock oxidation is limited, the CTE approaches closely to the bulk value. The presence of microstructural defects related to porosity does not have an influence in the CTE.

Finally, the curvature method is discussed as an alternative technique to obtain the CTE of coatings without intensive sample preparation. There is no need to spray thick coatings to meet the requirements for dilatometry technique. The differences in CTE with this method compared to push-rod technique are small. It is highlighted that the method produces as well the Young's modulus of the coating with good approximation.

Chapter 4: Thermal Shakedown: Anomalous Expansion Behavior of Thermal Spray Coatings during Non-Isothermal Annealing

4.1 Introduction

Fully-molten or partially-molten particles are successively sprayed during TS process to build up the unique coating lamellar microstructure. The millions of overlapping splats are subjected to high deformation by impact, high temperature, and rapid solidification resulting in a complex system with high amount of microstructural defects. Also, TS coatings are known for being structures subjected to high strain (and high strain rates), and very rapid solidification: 10^6 - 10^8 K/s -(S. Sampath and Herman 1996).

Highly deformed structures often increase their internal stored energy. This energy can be correlated to accumulation of microstructural lattice defects, especially dislocations, grain boundaries, and microstrain (Raabe 2014). When these defects are found in a substantial amount in the microstructure of a material, the relief of them, via heat treatment, can cause a measurable volume change. For instance, this effect has been measured as an irreversible shrinkage of severely plastically deformed (SPD) materials during thermal expansion measurements by dilatometry (Sprengel et al. 2012). A similar behavior has been observed in thermal sprayed TS coatings. However, in this case, TS coatings not only can present an irreversible shrinkage but also it is possible to observe an irreversible dilation (Thomas a. Taylor and Walsh 2004; T. a. Taylor and Walsh 2004; J Ilavsky and Berndt 1998; Tsipas et al. 2004; Choi et al. 2007). Certainly, this behavior responds to defect annealing at temperature, and it will be discussed in detail.

The high number of defects in TS coatings is a result of the processing via the rapid melting and rapid solidification of small portions of material projected from the torch to a substrate to form a layer. Splats solidify presenting columnar grains that grow perpendicular to the substrate orientation (aligned with the orientation of the stream of particles) (Deshpande, Sampath, and Zhang 2006; Chraska and King 2001). The directionality of the columnar grains respond to the heat dissipation towards the substrate. As the coating grows thicker elongated and equiaxed grains can be found depending upon the substrate temperature and the roughness (Safai and Herman 1977). Grains of the order of nanosize and microsize have been observed, as a consequence of the rapid solidification. (Safai and Herman 1977; Deshpande, Sampath, and Zhang 2006; Franetovic, Stubicar, and Bonafacic 1980; a Valarezo et al. 2007; Wu et al. 2007; G. Bolelli et al. 2010). Each

splat is composed of a number of grains (small, in the thinnest regions; and larger in the thicker), and defines a significant amount of grain boundaries (Wu et al. 2007). Dislocation densities as high as 10^{15} m^{-2} have been measured in Al 7075 cold spray coatings (Rokni et al. 2015), and are confirmed in this study via analysis of XRD results. Residual stresses are also inherent to TS coatings due to the rapid quenching, impact, and thermal mismatch between dissimilar materials (i.e. between the oxides formed during in-flight of the molten particles, and between dissimilar coating/substrate materials). As the coating progressively is build up by successive impingements, the roughness increases and the chaotic formation creates unfilled gaps namely, micropores, pores (inter-splats, interlamellar), cracks, etc. Chemical segregation in alloyed materials is also possible due to oxidation in flight, and convection during melting, impact, and solidification (Safai and Herman 1977). All these structural defects contained in the microstructure affect the properties of the material, and specifically, here, the dilation during a non-isothermal annealing process.

Several authors have reported changes in property values due to annealing of defects in TS coatings, and some results in metal alloys are cited here. Transport properties, for instance, electrical resistivity in Ni20%Cr coatings evolve from $300 \mu\text{ohm/cm}$ to $400 \mu\text{ohm/cm}$ during a heating cycle to 500°C (Prudenziati and Gualtieri 2008); for TiO_2 , resistivity of the coatings increases with air annealing at 550°C when the coatings are reoxidized (Sharma et al. 2006). Property values in coatings are often a fraction of the bulk material especially due to the presence of intersplat interfaces, which will also sinter (diffusion takes place making them to disappear) at more elevated temperature and with time. Finally, several authors have also reported previously, the anomalous behavior of dilation of TS coatings, which in some cases has been disregarded and in others, they have been explained it as a result of *in situ* oxidation of the samples (Choi et al. 2007) or chemical homogenization of the material (J Ilavsky and Berndt 1998; Berndt, C.C Herman 1982).

Coating properties are known to depend on the complexity of the microstructure and architectural defects that are strongly related to the deposition process (S. Sampath et al. 2004; Varis et al. 2014; Vaidya et al. 2005), some results are discussed in this context. The anomalous dilation behavior related to strain energy relief has been observed in all types of TS coating materials (ceramics, metals, alloys and cermets) with different magnitudes. An in depth study is developed for only two metal/alloys as it was identified that the relief effect is enhanced in these materials due to the presence of a larger amount of defects. Implications of this behavior are not

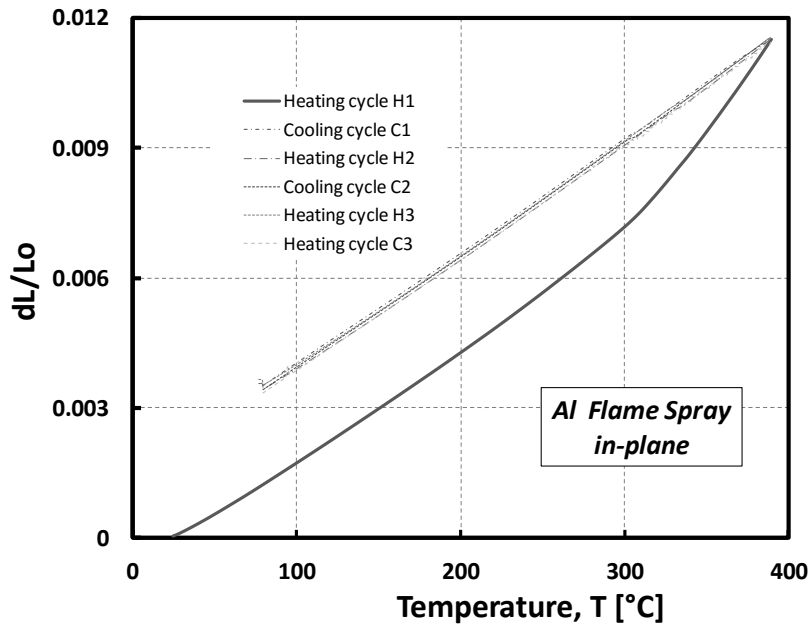
only dimensional but functional. When coatings are used in passive applications the dimensional changes as function of temperature introduce thermal stresses, whereas in applications where coatings are functional, it will give origin to bias in the signals produced; for instance, in electronics and sensors applications (Sanjay Sampath 2010).

To systematically study this effect, an Al coating (99% pure) was deposited by flame spraying and a Nickel-5% w.t. Aluminium (Ni-5Al) alloy coating was deposited by the arc spraying technology. Samples were studied using various characterization techniques. At the atomic scale, X-ray diffraction (XRD) at temperature was used to determine changes in the lattice parameter of the coating, and monitor the progressive annealing of defects in the diffraction pattern. At the micro-scale, the digital image correlation (DIC) method was utilized to evaluate thermal expansion in splats. High resolution images were taken at different temperatures on a hot-stage plate and evaluated with Matlab software. DIC method was applied on the microscale, observing and analyzing individual splats. The macro-scale analysis was carried out with dilatometry (DIL) using a contact based instrument. Atmosphere and heating rates were controlled. Furthermore, evaluation of inhomogeneities on the microstructure was done by elemental mapping using scanning electron microscope (SEM) on both materials. To evaluate possible phase changes and/or oxidation, differential scanning calorimetry (DSC) and thermogravimetry (TG) was employed.

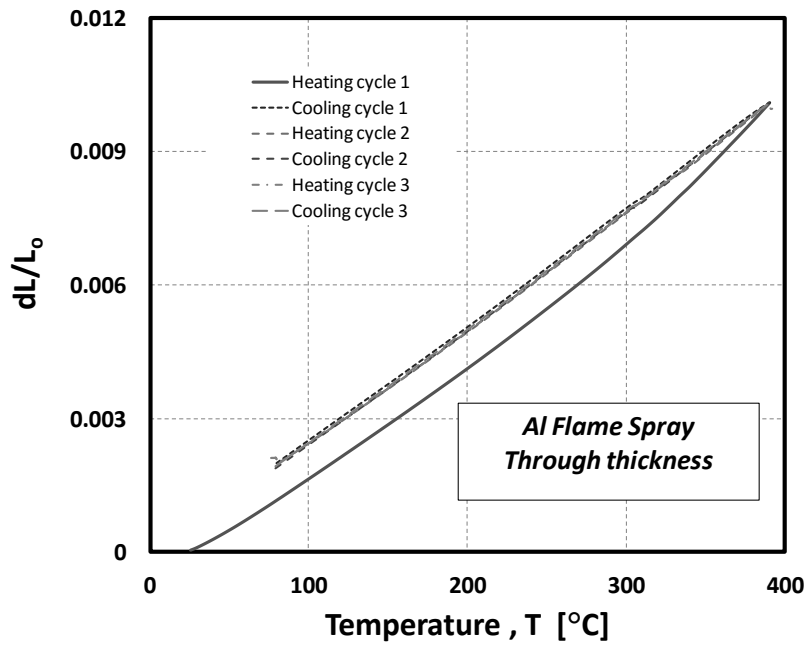
4.1.1 Research Problem Statement

To illustrate the anomalous dilation in the first heating cycle, in Figure 21a, 21b and 19c, the linear expansion of the Al-sample (19a). in-plane and 19b). through-thickness orientation) and in Ni-5Al-sample (19c). in-plane orientation) coating respectively is presented. The results are measured by a push-rod dilatometer. The linear expansion is plotted assuming zero linear expansion at room temperature for the first heating cycle. The Al-sample shows a permanent elongation of the sample on the order of +0.27% for the in plane orientation and +0.11% through thickness strain at 380°C in the in-plane direction (sample obtained from a portion of the material parallel to the substrate), whereas for the Ni-5Al sample the deformation measured was of -0.25% permanent shrinkage. Temperature range for Al-sample experiments was from room temperature to 350 °C and for Ni-5Al sample from room temperature to 700°C. The maximum temperature for each material corresponds to the 0.56 and 0.5 of homologous temperature, respectively. Figure 21, shows the results form Al and Ni5% Al in the in plane direction. After

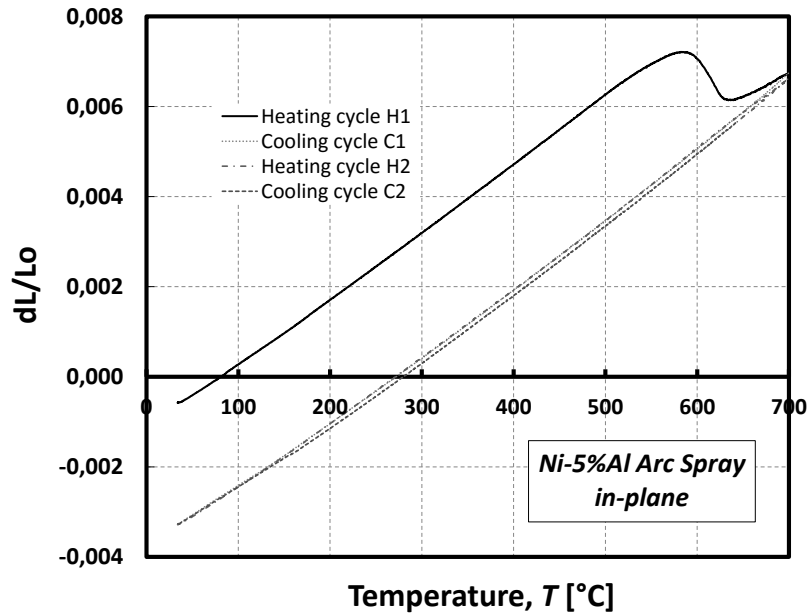
the annealing, the expansion behavior of the material is consistent with that of the bulk, and its measurement is reproducible at any heating/cooling cycle.



(a)



(b)



(c)

Figure 21. Linear expansion of an a) Al-sample coating by flame spray in the in-plane orientation, b) Al-sample coating by flame spray in the through-thickness and c) Linear expansion of a Ni-5Al sample coating by arc spray in the in-plane orientation.

The amount of strain relieved in the first heating cycle is discussed considering the mechanisms of defect annealing: 1) recovery, 2) recrystallization and 3) grain growth. Therefore, the evolution of dislocation density, grain size, and microstrain are analyzed to explain the behavior and the orders of magnitude of the deformation. Homogeneity of the microstructure and oxidation during non-isothermal annealing is revised to neglect their effect on the overall relieved strain. The differences between in-plane and through-thickness tests are explained based on the anisotropic behavior of TS coatings that determine a greater number of defects in the former orientation.

4.2 Experimental Methods for Shakedown Magnitude Analysis

4.2.1 Materials and Processes

The two specimens used in this study were prepared by two different spraying techniques.

- 1) A 99% pure Aluminum (Al) coating was deposited using a flame spray torch Metco 12E

(Oerlikon-Metco, Westbury, NY-USA) using acetylene as fuel, with feedstock material in the form of solid wire, grade 1100, Metco-Al of 3.2 mm wire diameter (Oerlikon-Metco, Westbury, NY-USA). Spraying parameters are the ones suggested by the gun manufacturer, and are summarized in Table 7. Two specimens were produced at different times to investigate the reproducibility of the effects. These samples will be named Al-FS-1 (for flame spray, aluminum sample 1); and Al-FS-2 (for flame spray, aluminum sample 2).

Table 7. Thermal spraying parameter for Al-sample: flame spraying

Parameter	Value	Parameter	Value
Fuel type	Acetylene	Spray Distance (mm)	
Fuel Pressure (kg/cm ²)	0.9 – 1.1	Torch Transverse Speed (mm/s)	40
Oxygen Pressure (kg/cm ²)	2 – 2.5	Substrate Material	Steel
Carrier Air Pressure (kg/cm ²)	4.5 – 5	Substrate thickness (mm)	4

2) A solid solution alloy of Nickel-5% w.t. Aluminum (Ni-5Al) sample was deposited using the arc spray process, torch Tafa 8830 (Tafa-Praxair, Concord, NH, USA) using feedstock material in the form of solid wire of 1/16” diameter. The material used was a Tafa bondArc 75B, a Ni-5% w.t. Al alloy (Tafa-Praxair, Concord, NH, USA) from the category of bond coat materials. The spraying parameters are the ones suggested by the manufacturer and are listed in Table 8.

Table 8. Thermal spraying parameter for Ni-5Al-sample: wire arc spraying

Parameter	Value	Parameter	Value
Current (A)	200	Spray Distance (mm)	200
Voltage (V)	29	Torch Transverse Speed (mm/s)	40
Carrier Air Pressure (kPa)	410	Substrate Material	Steel
Substrate thickness (mm)	4		

Coatings were of 25 mm thick for the Al-sample FS-1, and 12.5 mm thick for the Ni-5Al-sample and Al-FS2. Thickness was obtained by depositing various layers of about 0.075-0.100 mm per pass. Free standing specimens were machined to be tested by different methods, including cutting saws and/or discharge wire cutting. From sample Al-FS-1, a pillar from the vertical (through-thickness) direction was used to study the anisotropic behavior of the material. Splats of both materials Al, and Ni-5Al were collected on flat polished Al-substrates, and Stainless steel 304 substrates, by rapidly moving the torches in front of the substrates.

4.2.2 Elemental Mapping by SEM

The microstructure of the as-sprayed coatings was evaluated by optical microscopy (Nikon Eclipse Microscope, Tokyo, Japan) and by scanning electron microscopy (SEM), utilizing a JEM-2100 SEM, operating at 200 kV. Samples were prepared via standard metallographic preparation procedure. The as-sprayed coatings were cut using a precision saw, grade 15HC diamond blade and then mounted (infiltrated with Buehler EPO-THIN low viscosity epoxy using vacuum impregnation). The polishing was carried out on a semiautomatic system using procedures outlined for thermal sprayed metallic coatings in technical notes published by manufacturer Buehler (Lake Bluff, Illinois, USA). Fine polishing steps were done with cloth polishing with 9 and 3 μm diamond suspensions particles and a final step of 0.05 μm alumina suspension.

It is of interest to analyze the elemental distribution/extent of oxidation in these coatings because oxidation can influence the thermal expansion response as indicated in chapter 3, (section 3.3) where TS coating's expansion behavior is compared to composite material. Figure 22, shows the elemental distribution of nickel, aluminum and oxygen and some contaminants on the Ni-5Al sample by arc spraying. It is observed that nickel is predominant while the Aluminum tends to oxidize. Al is concentrated on the outer surface of the splats together with the oxygen. Oxygen and Aluminum are segregated towards splat boundaries forming Al_2O_3 (Deshpande, Sampath, and Zhang 2006). Some residues of carbon are a by-product of the polishing cloths.

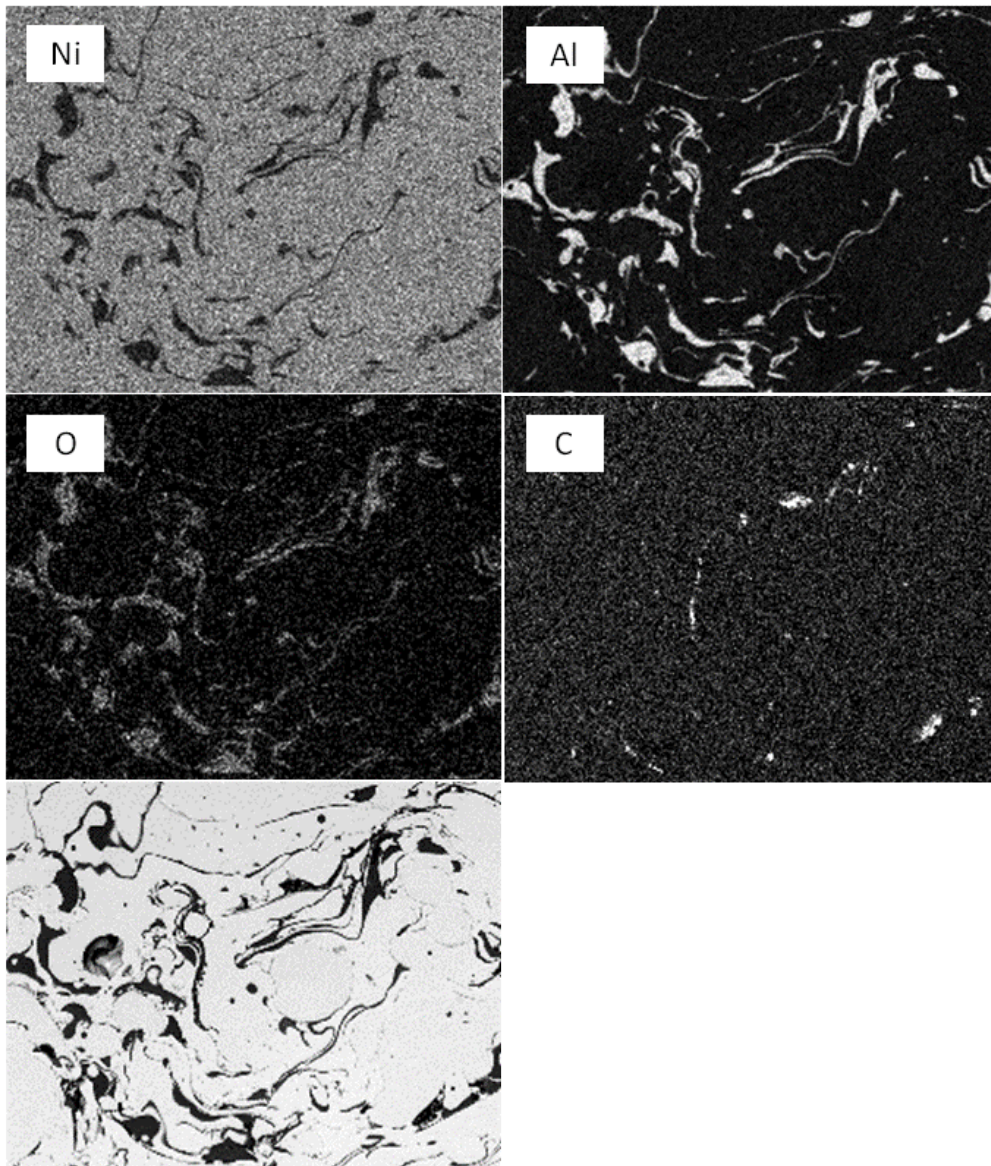


Figure 22 Elemental mapping of nickel, aluminum, oxygen and carbon, in Ni-5Al-sample by arc spraying.

Figure 23, shows the actual percentage of the components on the elemental distribution of Ni5%Al sample. Nickel is predominant with about $92 \pm 2\%$, and a variation on aluminum present with $5.08 \pm 0.47\%$, oxygen $0.37 \pm 0.01\%$, and carbon as contaminant in about $2.7 \pm 0.35\%$. The elemental content was measured in nine different points of the polished surface of the coating.

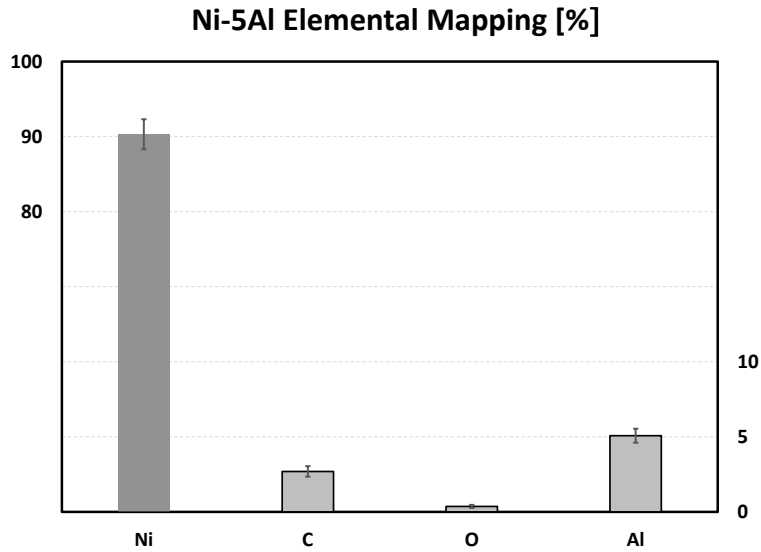


Figure 23. Elemental distribution of Ni5%Al Arc-spray coating. Percentage of constituents

The same elemental mapping analysis was done for Al-sample by flame spraying. Figure 24 shows the presence of oxygen in the boundaries of splats, and carbon as contaminant. This presence of oxygen is minimum, and it is very likely to occur on the particles during in-flight.

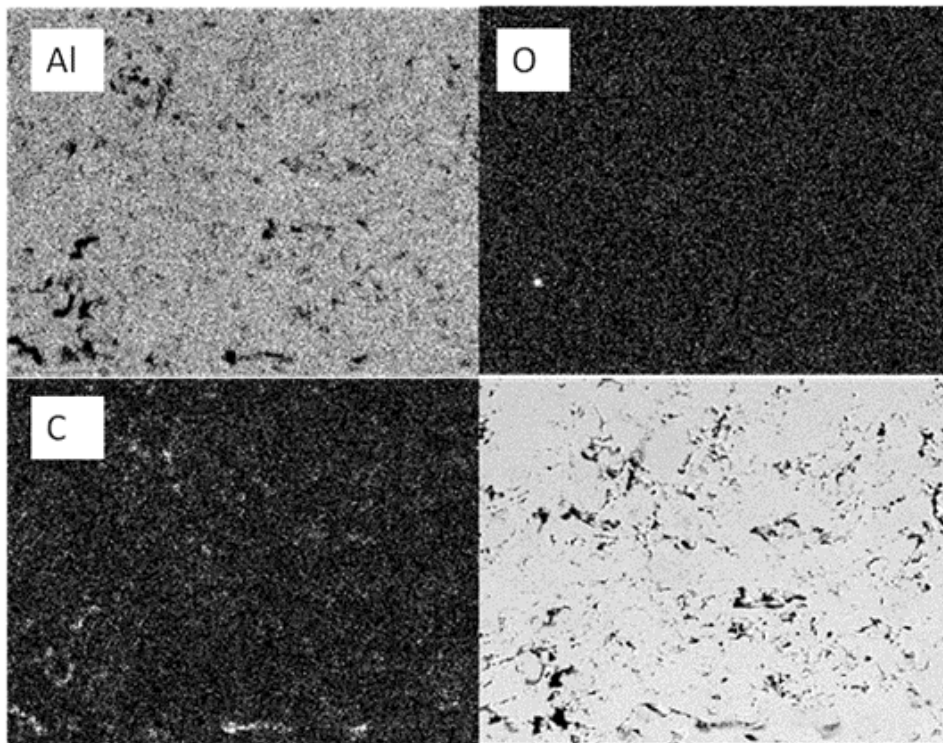


Figure 24. Elemental mapping of aluminum coating, Aluminum and Oxygen together with some Carbon as a contaminant on the process

Figure 25, indicates the percentage amount of each constituent evaluated in nine areas of a polished coating. The resulting values are: aluminum 97.45±2%, oxygen 0.39±0.2% and carbon 2±1%.

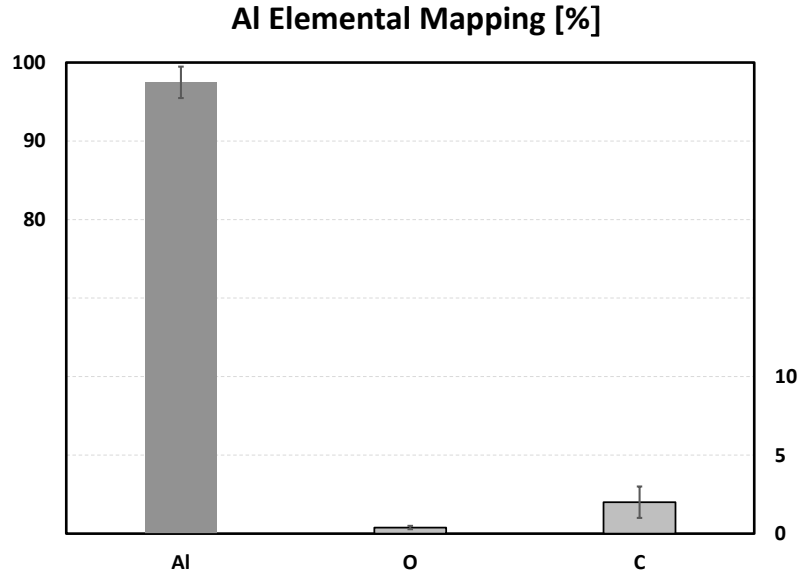


Figure 25. Elemental distribution of Al Flame Spray coating. Percentage of constituents

4.2.3 X-Ray Diffraction (XRD) at Temperature

Monitoring of the lattice parameter during *in situ* heating/cooling was conducted for Al- and Ni-5Al-samples. The diffraction pattern of both samples was obtained via XRD while heating and cooling the samples, according to the procedure described as follows. Continuous Θ - 2Θ scans were performed on a Panalytical Xpert diffractometer with an XRK 900 Anton Parr furnace with flowing $N_2/4\%H_2$ gas, from nominally 15° to 112° (2Θ) using Cu $K\alpha_1$ radiation ($\lambda=1.540598 \text{ \AA}$), $K\alpha_2$ radiation, and a X'Celerator detector. For Al-sample the intensity height was adjusted to the (111) peak. For Ni-5Al-sample, the scans ranged from 5° to 80° , 2Θ Mo $K\alpha_1$ using radiation ($\lambda=0.709319 \text{ \AA}$) and $K\alpha_2$ radiation, and the same X'Celerator detector. All scans used $1/4^\circ$ fixed slits and $1/2^\circ$ anti-scatter slit. A 10 mm mask was used and temperature collection varied from 27°C to 50°C , and after, in steps of 25°C up to 350°C . The sample was cooled in similar way, in steps of 25°C steps to 30°C and temperature profile was repeated. For Ni-5Al-sample, temperature was controlled in steps of 25°C from 50°C to 800°C . The sample was kept for 25 min. at each temperature for the counting of the diffraction.

Jade software (MDI Materials Data, Liver more, California) was used to profile fit Al-sample and Ni-5Al-sample diffraction patterns. A search of match was conducted using Jade and High Score software and ICDD database. The silicon standard 640 examined with the same optics was refined and used as the standard for size - strain analysis for the samples. Two analyses were conducted. The profile fit of the Al (111) peak and also the Ni-5Al (111) peak at various temperatures was used to evaluate the change in the lattice parameter as the sample anneals. The second analysis focused in the narrowing of the peak, which is associated to annealing of imperfections and grain growth (increase in the crystallite size). So, the XRD pattern results at various temperatures were also used to calculate the mean grain diameter [d]; the microstrain [ε]; and from here, the dislocation density [ρ] changes of the samples at approximately room temperature, and following annealing at various temperatures.

Grain size and dislocation density values were calculated following the Williamson–Hall method (Williamson and Hall 1953). B , the peak broadening term, was calculated by computing the equation 11, that includes the full width at half-maximum (FWHM) values of the diffracted peaks (B_{abs}), obtained experimentally; and the peak broadening accounted by the instrument (B_{inst}), obtained using a Gaussian function from a silicon standard 640 reference sample:

$$B = \sqrt{(B_{abs})^2 + (B_{inst})^2} \quad \text{Equation 11.}$$

Now, using Equation (12), according to (Williamson and Hall 1953; Williamson Smallman 1956), the values of d and ε were obtained from the slope and intercept, respectively, of the $B \cdot \cos(\theta_B)$ vs. $\sin(\theta_B)$ curve by performing a linear regression analysis at every temperature tested.

$$B \cos \theta_B = \frac{K\lambda}{d} + \varepsilon \sin \theta_B \quad \text{Equation 12.}$$

where λ is the wavelength of Cu $K\alpha_1$ and Cu $K\alpha_2$ radiation, i.e. 1.54 Å, K is ~0.9 according to (Klug and Alexander 1954) θ_B is the Bragg angle, and B is the peak broadening term, obtained in equation 11. Dislocation density [ρ] can be quantified by using the equation 13:

$$\rho = \frac{2\sqrt{3}\varepsilon}{db} \quad \text{Equation 13.}$$

Where b is the magnitude of the Burgers vector b , for Al (0.286 nm), calculated from lattice parameters and confirmed (Rokni et al. 2015). This relationship (Equation (13)) is commonly used when studying aluminum alloys subjected to severe plastic deformation (Rokni et al. 2015). In this context, considering the typical high strain rates (approaching 10^9 s^{-1}) and high cooling rates (approaching 10^7 - 10^9 K-s^{-1}) (S. Sampath and Herman 1996) experienced by TS coating, thus, it is rational to use Equation (13) for estimation of dislocation density in this study.

4.2.4 Push rod (and Dual Push rod) Dilatometers

Dilatometry measurements were carried out with a single or dual push rod. Instrument consists of an insulated furnace chamber with adjustable heating rate, where a sample is fixed against a movable pushing rod. The second end is either in contact to a fixed support, or to a movable pushing rod. Sample is heated up or cooled down with controlled temperature and in some cases purging inert gas or vacuum atmosphere. The system measures precise dimensional changes of a specimen brought to temperature change. This is the most common method to extract linear dimensional changes through a wide temperature range. The displacement is registered using an LVDT. A single push rod dilatometer (Netzsch Thermische Analyze DIL402, Netzsch Group, Selb, Germany) (Netzsch 2006) was used and also a number of thermal expansion measurements were carried out on a dual push rod dilatometer (Theta Dilatronic, Theta Industries, Port Washington, NY). Thermal expansion was measured over the temperature range from room temperature RT to 400°C and 700°C for Al and Ni-5Al respectively in a controlled atmosphere. The temperature of the specimen was determined using a type S (Pt versus Pt-10%Rh) thermocouple. Measurements were with a standard heating and cooling rate of 5 K/min. The length of the sample was measured relative to a standard sapphire specimen (5 mm diameter 25 mm long).

4.2.5 Differential Scanning Calorimetry (DSC) and Thermal Gravimetry (TG) Measurements

A Q2000 DSC (TA Instruments, New Castle, USA) instrument was used to determine phase changes related mainly to oxidation, homogenization or possible precipitations. Simultaneous TG measurements were conducted to verify the change in weight. The

measurements were done using 5.0 mm-diameter by 1.0 mm-thick disks that were prepared by cutting pieces from the original thick coating specimens. Samples weight was (35.24 mg). Measurements were made in the temperature range from 25°C to 400°C for Al and from 25°C to 700°C. Hermetically sealed aluminum pans and lids were used during the DSC runs, and all tests were conducted in helium (He) flowing (5 sccm) environment. Heating and cooling rates of 20°C/min were used.

4.2.6 Digital Image Correlation (DIC) Technique for strain field monitoring

DIC is an optical non-invasive technique that allows measurement of displacements and deformations on the surface by analyzing two dimensional (2-D) high resolution digital images of the object, in this case subjected to a change in temperature. Two stages have to be considered for this evaluation. The first step is related to sample preparation. Samples were prepared by standard metallographic technique, assuring very flat surfaces perpendicular to the orientation of the digital camera. The camera was mounted on a Stereo Microscope of 10X magnification.

The samples need to have an appropriate and randomly distributed gray scale or speckle pattern. This pattern allows to have a correct scan of the image for the analysis. For the experiment, the contrast in the image produced by the features of pores and oxides were used as the gray scale pattern. After obtaining the sequences of images, the correlation is run in MatLab R2013a (Matworks Inc.). In this step tracking of surface displacement is evaluated in correlation with pixels on the image (Wang and Tong 2013; Thompson and Hemker 2010)

4.3 Results and Discussion

Dilatometry has been identified as a powerful tool to identify the evolution of the structure of the materials upon heating for several studies. Reversible changes in the materials can be identified via dilatometry as inflections in the linear expansion of the sample, which correspond to phase transformations i.e. martensitic transformations in steels (Naderia, Saeed-Akbarib, and Bleckb 2008), magnetic-paramagnetic transitions -Curie temperature (Nix F.C. MacNair D. 1941), etc. Other non-reversible changes have been monitored via dilatometry such as consolidation of powders during sintering (Cipitria, Golosnoy, and Clyne 2009a; Cipitria, Golosnoy, and Clyne 2009b), oxidation (Choi et al. 2007), defect annealing in severely plastically deformed (SPD)

materials (Sprengel et al. 2012), intercalation reduction reactions in the first charge of batteries, change in electrical properties of graphite electrodes, (Ohzuku, Matoba, and Sawai 2001), etc. Dilatometry experiments applied to TS coatings, as seen in Figure 21, show an irreversible change producing a macroscopic length modification, shrinkage or dilation, due to various mechanisms occurring during a heat annealing cycle. This effect, so called here as “thermal shakedown” behavior, is evident only during first heating cycle. This effect occurs in lower or higher magnitude in all coating materials deposited by different spraying processes. The hypotheses of some of the mechanisms that can lead to have this effect on TS coatings are described below.

- 1) The annealing of large number of the defects can lead to significant volume change. The presence of large amounts of dislocations (1-D defects), and grain boundaries (2-D defects) determine an excess volume that upon heating, can determine an overall shrinkage of the structure. By means of the analysis of XRD patterns at temperature during heating and cooling, the change in dislocation density and grain size can be determined. The order of magnitude of this change can be defined.
- 2) Another hypothesis to be considered is the consequence of the interaction of microstructural intrinsic defects produced by the TS processing: interfaces, oxides, pores, cracks, etc., during a heat treatment. As coatings are formed by a number of splats that solidify in irregular morphologies with large retained residual stress when they are heated up, these splats tend to undergo stress relief. Splats can be found mostly constrained (attached to other splats), but other regions (near to pores) can be found unconstrained. Simultaneously, as the splats expand while heating, they create new contact areas (shear or normal contacts) causing possibly friction between splats. This can increase or alter the shakedown behavior.
- 3) As it has been discussed previously, large residual stresses can be found in the splats and in the overall coating. Measurements of residual stress profiles reported in literature (A Valarezo et al., n.d.; Matejicek et al. 2003) describe large magnitudes of the stress, and significant variations through the thickness, depending upon the processing conditions. Therefore, residual stress is taken into account as an important mechanism to explain the order of magnitude of strain relaxation during the shakedown cycle.
- 4) Diffusion mechanisms can act during the shakedown cycle, including: oxidation, new phase precipitation, and homogenization of the atomic structure. Particularly, TS coatings

have larger surface area per volume than the bulk materials due to the splat structure, and porosity. This would make TS coatings more prone to oxidation, however many of the splats surface can be found covered by oxides produced during in-flight. This would decrease the kinetics of oxidation reactions. On the other hand, atomic disorder can occur due to convection mechanisms during particle melting, in-flight, and impact. Atomic reordering is likely to occur during the first exposure of the sample to heat, after deposition.

5) Sintering is a well-known process that result in the densification of a porous structure. Sintering in TS coatings may occur in cracks within splats, and between splats in the intersplat interface; with no applied-pressure. Dilatometry (regularly used in sintering of ceramics has been used to monitor the magnitude of the shrinkage due to sintering; for instance, in YSZ coatings (Cipitria, Golosnoy, and Clyne 2007) during isothermal heat treatments, but there are no references regarding metallic TS coatings. The experiments developed in this chapter are at about $0.5 T_H$, with which, the effect of sintering is reduced; however the possibility of its occurrence is not fully ruled out.

In Table 9, these hypotheses are made specific for the case of the Al- and Ni-5Al-samples. The possible mechanisms causing or affecting the dilation behavior reversibly or irreversibly (shakedown) for these two materials are described. The key experiment(s) selected to study each mechanism are proposed as well.

Table 9. Mechanisms that alter the dilation behavior of TS Al- and Ni-5Al-samples during a heating/cooling cycle.

Mechanism	Nature of the mechanism	Irreversible change during first heating		Experimentation
		Yes	No	
Kinetics of Defect Annealing & Material Specific Properties	<ul style="list-style-type: none"> ▪ Annealing of defects: dislocations, recrystallization, grain growth. ▪ Oxidation: Al₂O₃ formation on the surface of exposed materials to oxygen in the Al-samples; and similarly Al₂O₃ formation in the Ni-5Al-sample (preferential oxidation of Al) (Deshpande, Sampath, and Zhang 2006) 	x		<ul style="list-style-type: none"> ▪ Annealing of defects: Evaluation of dislocation density change, and grain size change by XRD at temperature ▪ Oxidation: DSC, and DTA-TG tests
	<ul style="list-style-type: none"> ▪ Increase in vacancy concentration ▪ Phase transformations 		x	<ul style="list-style-type: none"> ▪ Vacancy concentration: comparison between dilation

				of the d-spacing, vs the linear expansion. ▪ Phase transformation: DSC and DTA-TG tests
Kinetics of Defect Annealing due to Processing Effects	<ul style="list-style-type: none"> ▪ Relief of residual stresses ▪ Homogenization (chemical homogenization by diffusion) ▪ Sintering of interfaces 	x		<ul style="list-style-type: none"> ▪ Relief of residual stresses: XRD monitoring of d-spacing and peak shift due to stress relief ▪ Homogenization: cyclic tests-heating/cooling of DSC and DTA-TG ▪ Sintering:
Mechanical Effects	<ul style="list-style-type: none"> ▪ Splat unraveling/Distortion of splats due to relief of intrinsic stresses and thermal stresses ▪ Inelastic mechanical shakedown, due to sliding, friction, shear contact, axial contact, etc. between splats 	x		<ul style="list-style-type: none"> ▪ Splat unraveling/Distortion of splats: observation of splats via Digital Image Correlation (DIC) ▪ Inelastic mechanical shakedown: N/A
	<ul style="list-style-type: none"> ▪ Thermal stresses between the coating material and oxides within the same splat. 		x	<ul style="list-style-type: none"> ▪ Thermal stresses: Digital Image Correlation (DIC) N/A

The contribution to the “thermal shakedown” of the several mechanisms is discussed considering the possible strain gradient that each proposed mechanism could account in the overall shakedown strain gradient (defined here as the strain difference between the first heating cycle and the subsequent heating and cooling cycles). The summation of the overall non reversible gradients of strains caused by the mechanism described in Table 9, should be equal to the shakedown strain gradient. The overall shakedown strain gradient is shown for Al-sample, and Ni-5Al in Figure 26. Equation 14 summarizes the contribution of each mechanism to the shakedown strain, thus:

$$\Delta\varepsilon_{sh} = \Delta\varepsilon_{G.B.} + \Delta\varepsilon_{\rho} + \Delta\varepsilon_{R.S} + \Delta\varepsilon_{others} \quad \text{Equation 14}$$

Where:

$\Delta\varepsilon_{sh}$ is the shakedown strain gradient (the difference between the linear expansion in the first annealing cycle with respect to the steady state behavior of the same sample in subsequent tests); $\Delta\varepsilon_{G.B.}$ is the strain gradient due to grain boundary annihilation, $\Delta\varepsilon_{\rho}$ is the strain gradient due

to dislocation annealing, $\Delta\varepsilon_{R,S}$ is the strain gradient due to residual stress relief, and the $\Delta\varepsilon_{others}$ is the summation of oxidation, sintering and other possible effects that might occur during heating, but that for the Al- and Ni-5Al system are considered negligible.

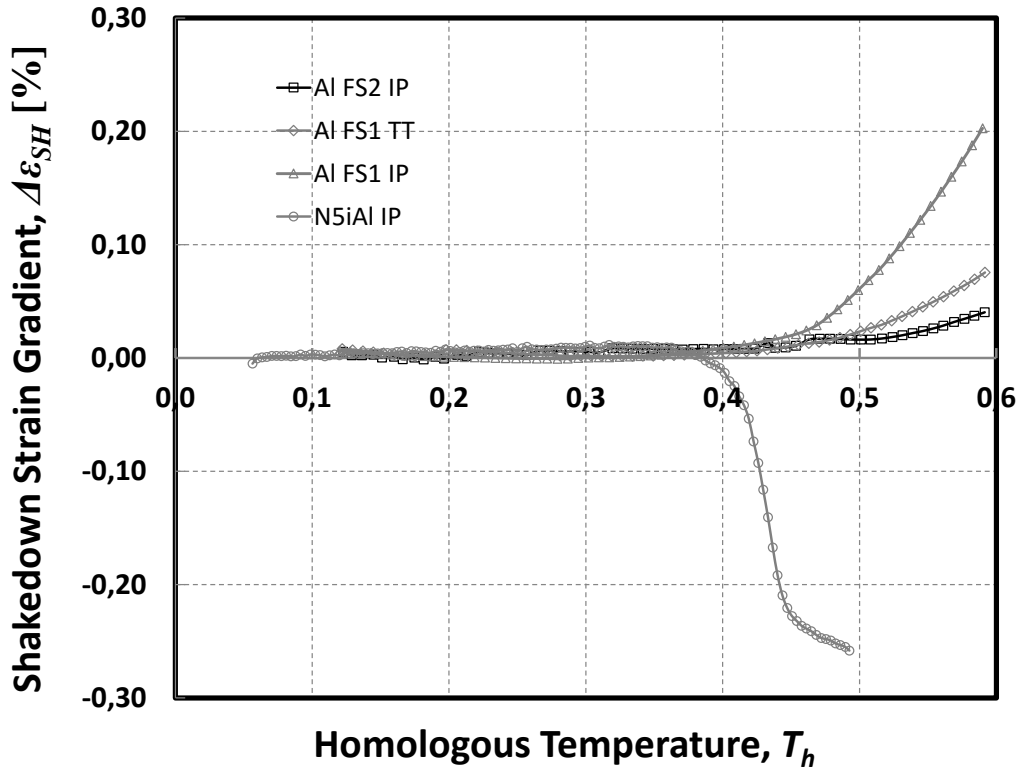


Figure 26. Shakedown strain gradients of Al-sample FS-1, in the in-plane (IP) and through-thickness (TT) orientation (FS1 refers to the process: flame spray-FS, and 1 to the first batch of samples), Al-sample FS-2 in the in-plane orientation from batch 2, and Ni-5Al-sample by arc spraying in the in-plane orientation only.

In Figure 26, the shakedown strain gradient is presented as a function of homologous temperature. As the temperature increases, the shakedown strain gradient increases as the energy available allows for the evolution of the microstructure to an equilibrium state. The shakedown strain gradient appears about above 200°C (0.3 T_h) for Al-sample and above 400°C (0.3 T_h) for Ni-5Al-sample. It is highlighted that this temperature corresponds to the recrystallization temperature for both materials. For Al-sample, two specimens are presented, one sample (Flame spray FS1) in the in-plane orientation, and the through-thickness orientation and another one (Flame spray FS2) for the in-plane orientation only. Ni-5Al sample is presented only in the in-

plane orientation. For Al-sample FS-1 in the in-plane orientation, the $\Delta\varepsilon_{sh} = +0.20\%$ and for the through-thickness was of $\Delta\varepsilon_{sh} = +0.08\%$. The differences in shakedown due to the anisotropy of the Al-coatings lies on the kinetics of the defect annealing varying in the through-thickness versus the in-plane orientation. The through-thickness orientation includes: 1) a higher number of inter-splat interfaces which can lead to a slower kinetics of grain growth and dislocation annealing in the grain boundaries, especially near the interfaces; and 2) near zero residual stress as plane-stress condition normally occurs in these coatings. It should be noted that the latest condition still includes some deformation in the through-thickness direction due to “Poisson effect” as the in-plane stress is relieved

Al-sample FS-2 in the in-plane direction will be studied in detail. The maximum shakedown strain gradient at 390°C was on the order of $\Delta\varepsilon_{sh} = +0.040\%$, whereas for the Ni-5Al-sample the maximum shakedown strain gradient registered at 700°C was $\Delta\varepsilon_{sh} = -0.250\%$. The magnitude of strain corresponding to the mechanisms contributing to the shakedown is discussed as follows.

4.3.1 Microstructure Characterization:

The Al- and Ni-5Al-samples were tested initially to identify the similarity of the splat-structure in different regions of the coating, and assure that the sample dimensions for the different characterization techniques are representative of each coating. SEM (Figures 27 and 28) and (Figures 22 to 25). Elemental mapping techniques were used to scan different regions of the sample. The typical oxide formation (Al_2O_3) in the intersplat interfaces for both coatings is identified. SEM micrograph of as sprayed Ni-5Al-sample sprayed by Arc spray are shown in Figure 27. The images show characteristic features of arc spray coatings. Images were taken in different regions of samples seeking to analyze similarity of coating distribution. Micrographs show homogeneous distribution of splats, pores and oxides. This was quantified by elemental mapping in Figure 23, showing very small relative standard deviations. This allows to conclude that the samples show homogeneous microstructures.

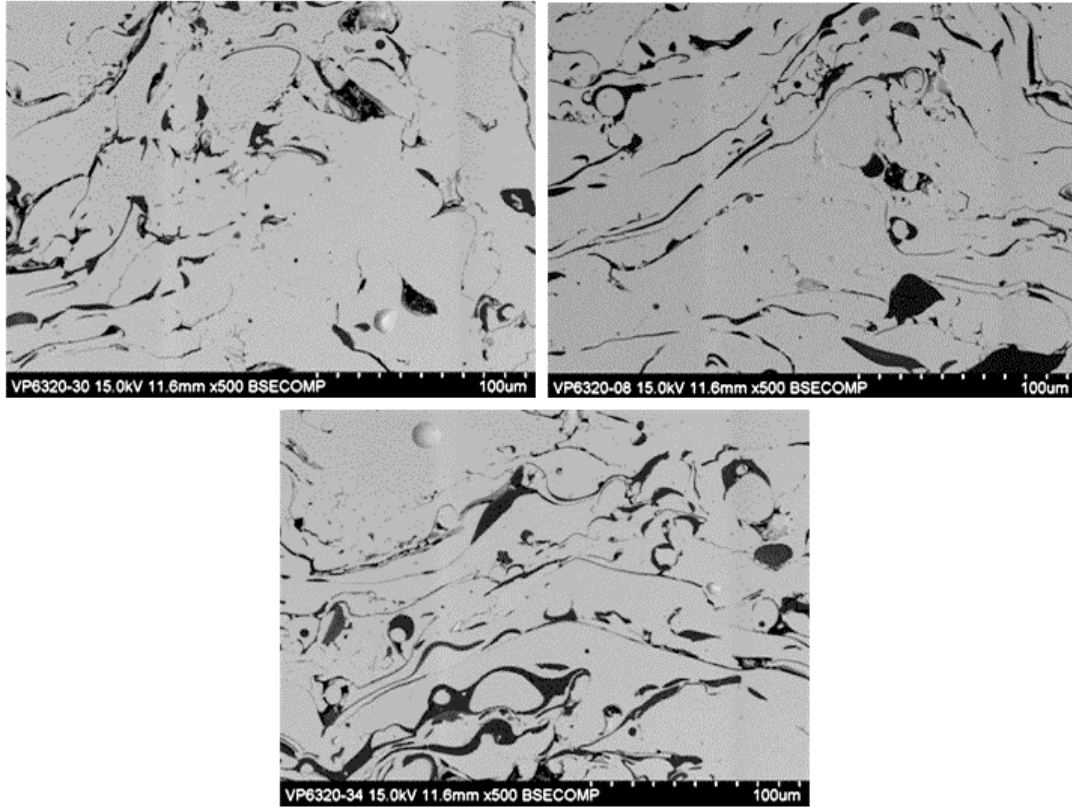


Figure 27. Cross-sectional micrographs of Ni-5Al-samples obtained from three different positions by SEM

The same micrograph analysis was carried out for the Al-sample. Similarity of the microstructures was also identified based on observation of various different regions of the sample, as it is shown in Figure 28; and also regarding the elemental mapping in Figure 25.

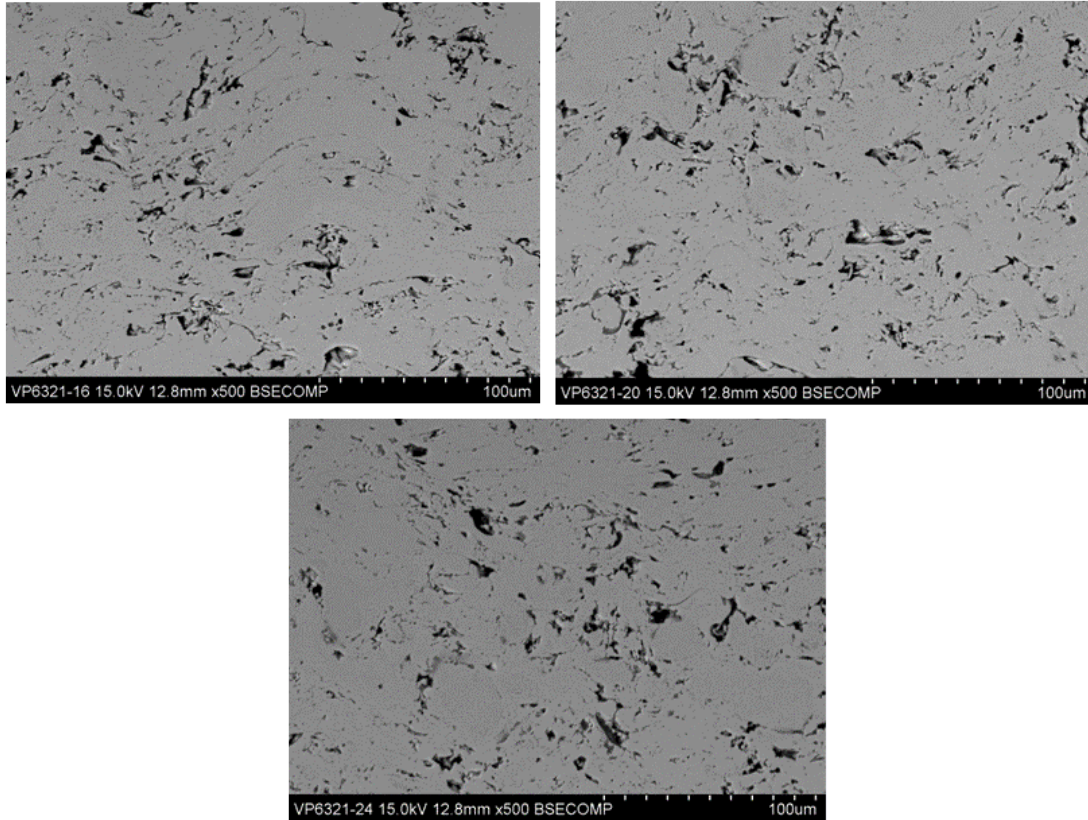


Figure 28. Cross-sectional SEM micrographs of Al-samples FS-2 for three different regions of the sample.

It is concluded that microstructural features for both samples are homogeneously distributed and samples are representative of each coating.

4.3.2 Differential Thermal Analysis and Thermal Gravimetry

The DTA–TG curves of the Al- and Ni-5Al-samples in flowing atmosphere of argon at a heating rate of 5°C/min are shown in Figure 29. These experiments were developed to investigate possible phase changes during the shakedown thermal cycle, such as phase precipitation, homogenization of the microstructure, decomposition of phases, or oxidation.

No evidence of any significant weight loss nor endothermic or exothermic phase changes were identified for any of the two materials. This leads to the conclusion that neither oxidation nor phase changes occur for the coatings when exposed to a heating cycle. This analysis was conducted in similar cyclic manner like the expansion measurements, and there is no evidence of the shakedown effects.

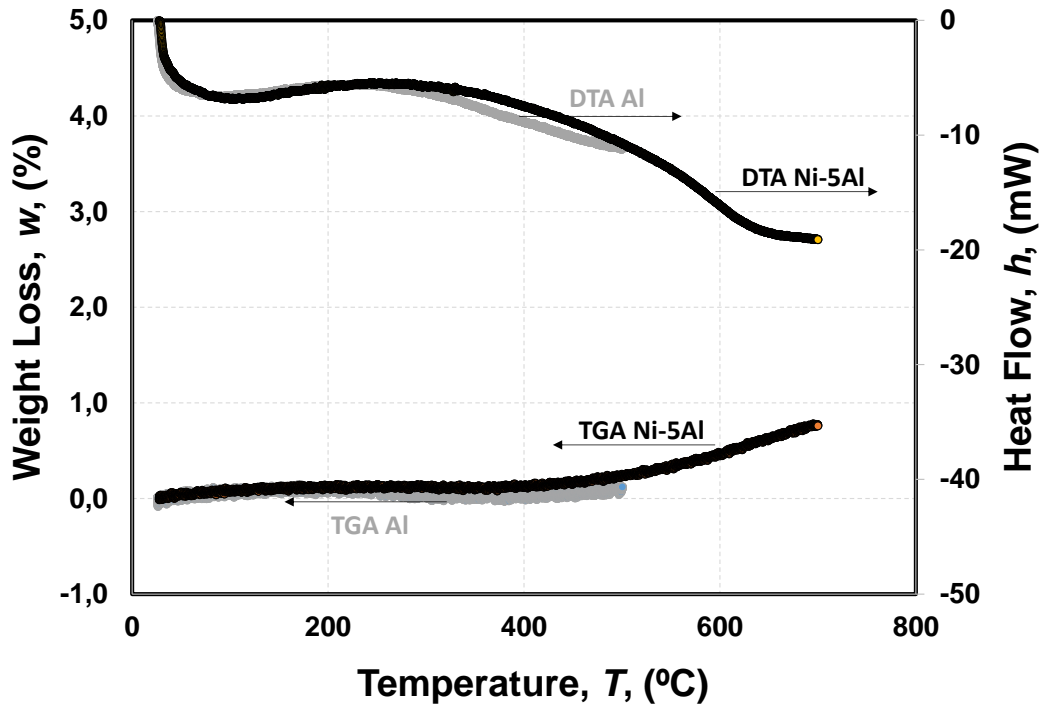
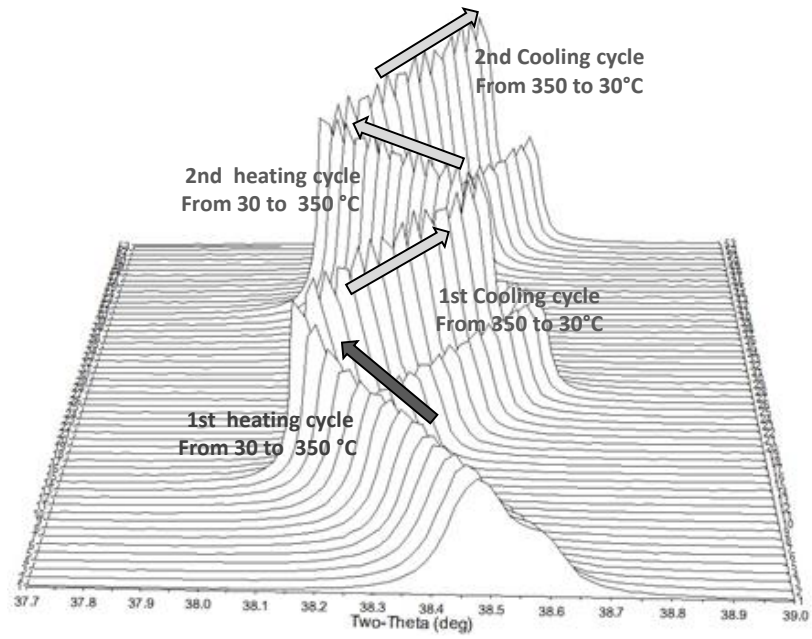


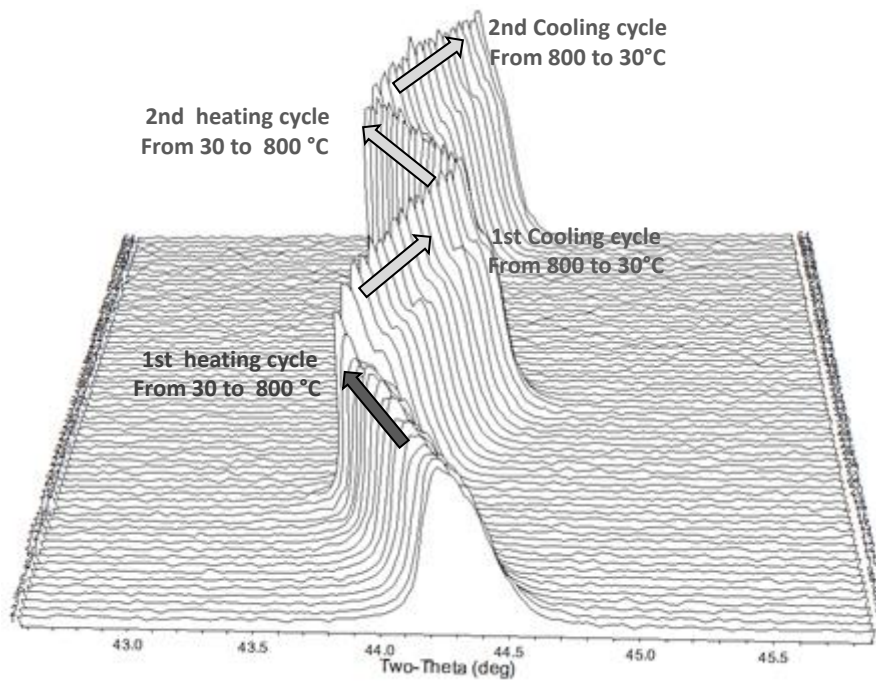
Figure 29. DTA–TG curves at a specified heating rate of 5°C/min in air with a flow of Ar, for Al-sample FS-2 and Ni-5Al-sample.

4.3.3 D-spacing, shift of the peak

Al- and Ni-5Al-samples by flame spray and arc spray respectively, were tested in a diffractometer according to the method described in (section 4.2.3). Figure 30 shows XRD measurements of Al-sample (Figure 30a) and Ni-5Al-sample (Figure 30b) as they are progressively heated up. The position of the (111) peak of Al, as well as the (111) peak of Ni-5Al samples, register a shift in the 2-theta angle towards lower values indicating an increase in the interatomic distance of the lattice as the material expands, whereas on cooling down the peak shifts to the original position. Diffraction patterns are shown every 25°C. Refinement (narrowing and growing) of the peak is observed as a result of annealing of defects and relaxation of residual stresses during the first heating cycle.



(a)



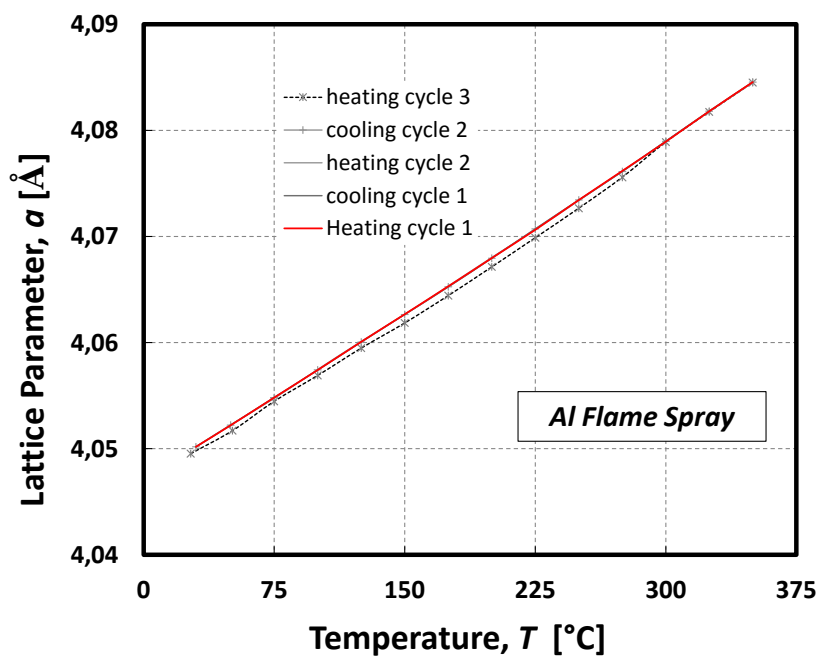
(b)

Figure 30. In situ monitoring of a) the (111) peak of Al-sample flame sprayed and b) and (111) peak Ni-5Al-sample arc sprayed coating by XRD while heating and cooling. Procedure is described in section 4.2.3. Two-heating cycles are presented. The average peak position shifts with temperature in response to the increased interatomic separation to reach equilibrium.

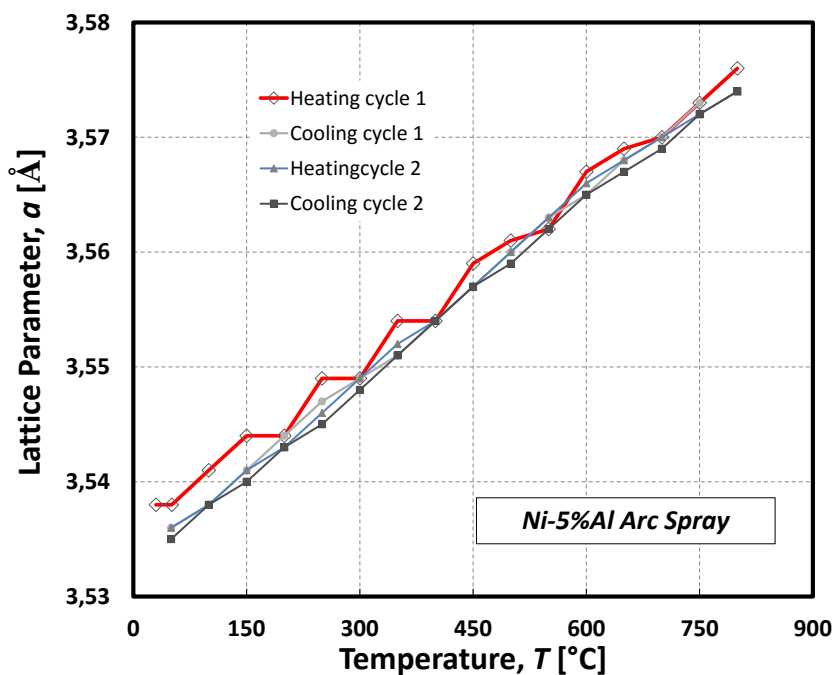
When analyzing the dilation effect at the atomic level under these temperature cycle regimes, results show deviation of the lattice expansion in the first annealing cycle from expected expansion property, as indicated summarized in Figure 31 showing the lattice parameter evolution with temperature and cycles. Deviation is evident only during first heating cycle, similarly to the dilation results measured by the dilatometer. Subsequent cooling and heating cycles present a stable lattice expansion response which is comparable to the expansion property of the bulk material. This deviation is associated with residual stress relief in the sample as the d -spacing changes with temperature.

For Al-sample in Figure 31a, the stress is identified to be compressive in nature as the measured lattice parameter in the first heating cycle is shorter than the one in the equilibrium state. The calculated strain gradient at $0.3 T_h$ was about +0.022% (positive means the lattice was enlarged irreversibly due to annealing). It is noted that the amount of strain gradient between the first heating cycle and the stable one represents the recovery of the lattice at discrete temperatures, thus it does not represent the absolute residual stress relief since the measurement is carried out at temperature while annealing of defects is occurring concurrently.

For Ni-5Al-sample in Figure 31b, the behavior does not show a remarkable stabilization after the first annealing cycle. The overall change of the lattice parameter suggests a relief of tensile residual stress in the first heating cycle. The largest calculated strain gradients are: at 50°C (-0.060%), at 350°C (-0.058%), and, at 450°C (-0.056%), (negative means the lattice decreased to the equilibrium state at that temperature). These strain gradients are significantly large, and may account for part of the thermal shakedown strain gradient (on the order of -0.250% measured by dilatometry for NiAl). The Ni-5Al alloy may experience homogenization during the first annealing cycles. Some depletion of Al occurs during the formation of the Al_2O_3 (Figures 22, 28), and therefore, during the first heating cycle the material may experience some diffusion effects to homogenize the structure, and this can affect the measurements of the lattice parameter.



(a)



(b)

Figure 31. The lattice cell parameter- a (d -spacing) as a function of temperature for a) an Al-sample flame sprayed coating, and b) a Ni-5Al-sample arc sprayed coating. Both coatings relieve stress during first heat cycle.

In order to approach the shakedown problem, in a more systematic manner, only the XRD patterns of the Al-sample are analyzed in detail as follows.

4.3.4 X-ray Diffraction Analysis and Mechanisms Contributing to the Shakedown Effect

The energy stored in the coating during deposition is released with temperature as a consequence of defect annealing. These defects include vacancies, dislocations, grain boundaries, intersplat interfaces, etc. Presence of these defects creates an excess volume in the material. In TS coatings residual stresses are also known to account for some amount of the energy stored in the system. In this section, the analysis of the XRD patterns at temperature allows to quantify the order of magnitude of the contributions to shakedown from annealing of dislocations and grain boundaries. Analysis of these contributions are compared to the permanent macroscopic length change, shakedown strain, presented as measured by the push-rod dilatometer.

4.3.4.1 Excess Volume due to increase in Vacancies Concentration

Besides the natural increase in the interatomic distances with temperature, creation of vacancies will increase the overall length of the sample. Therefore, an increase in vacancy concentration will increase the expansion of the material. This increase is reversible and does not contribute to shakedown. However, in this section, the strain accounted for vacancy concentration increase (C_v) is calculated to be compared with the known values of Al-bulk. C_v can be determined by using equation 15. This analysis was first performed by (Simons and Balluffi 1960; Nenno and Kauffman 1959).

$$C_v = 3 \left(\frac{\Delta L}{L_o}(T) - \frac{\Delta a}{a_o}(T) \right)$$

Equation 15

Where a is the lattice parameter and L is sample length. Therefore, the excess volume can be obtained from equation 15, by computing the dilatometer results for L and the XRD results for a . in equation. The linear strain corresponding to $C_v = 2.19 \times 10^{-4}$, this is about **0.022%** strain. This is equivalent to the Al-bulk value reported in literature as 3×10^{-4} (Feder and Nowick 1959) This results proves that the coating in terms of excess volume due to vacancy creation behaves similar

to a bulk material, despite the fact that the coating has larger surface area per unit volume compared to a bulk material.

The excess volume (equivalent to volumetric expansion) is defined for an isotropic material as three times the linear expansion as shown in the equation 16.

$$\frac{\Delta V}{V} = 3 \frac{\Delta L}{L} \quad \text{Equation 16}$$

From here forward, only the linear expansion will be considered, although the reader should keep in mind that the effects are volumetric and isotropic.

4.3.4.2 Excess Volume due to Dislocation: Analysis of Narrowing of the Peak

Microstructure evolution during annealing will change the lattice parameter (due to strain relief), grain size, microstrain, and dislocation density as a function of temperature. The analysis of the narrowing of the peak using the Williamson–Hall method allows determination of grain size and dislocation density changes (described in 4.2.3)

As the XRD peak shifts with temperature (shown in Figure 30), it also gets taller and narrower during heating/cooling cycles (Figure 32). Narrowing of the peak is associated to annealing of imperfections in the structure that mainly reduces the amount of dislocations present in the microstructure by recovery.(Raabe 2014), in the initial stage. The presence of dislocations is responsible of microstrain energy in the structure. The strain relaxation is associated to the number of dislocations annealed when the material is exposed to temperature. In Figure 32, the narrowing of the peak at 50°C in different time of the heating and cooling cycles is shown.

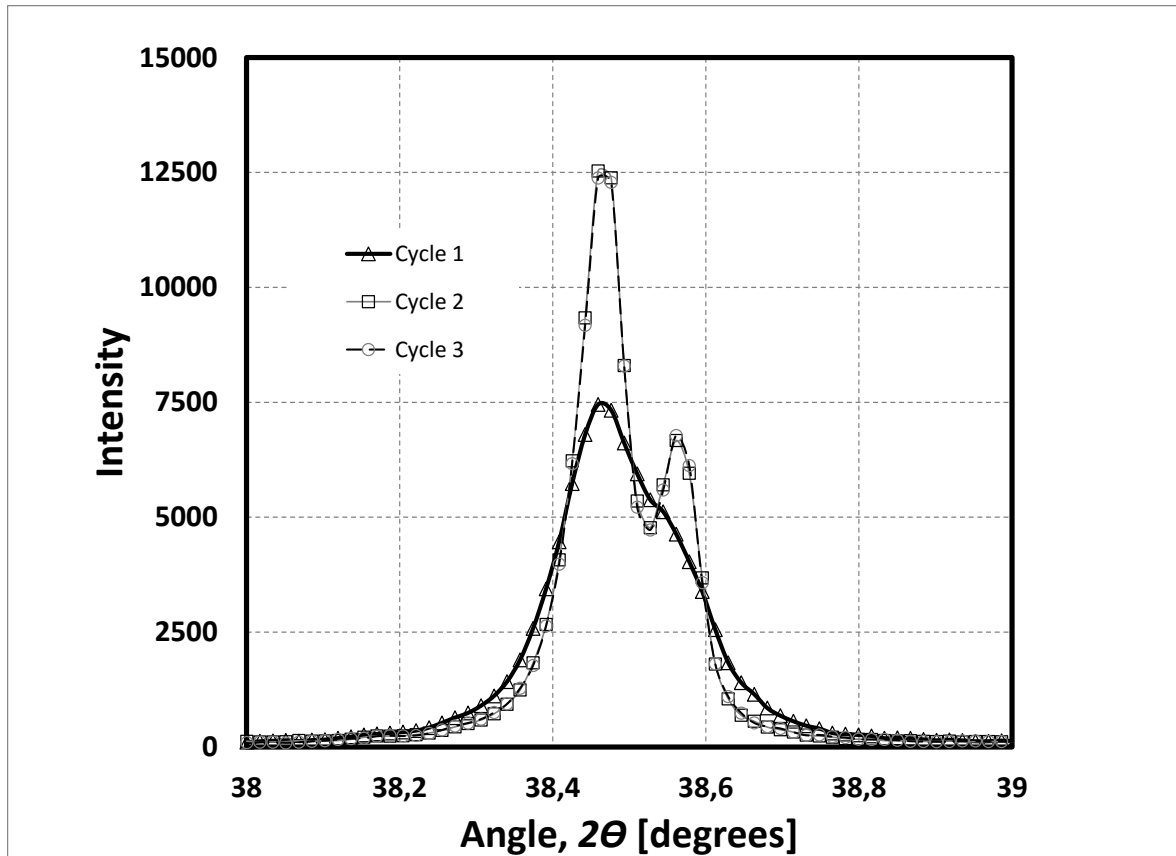


Figure 32. Narrowing of a (111) peak of Al-sample at a fixed temperature of 50°C during a heating/cooling cycle. XRD is carried out using Cu-K α 1, and K α 2 radiation.

At higher temperatures, recrystallization and grain growth occur. The full width at medium height (FWMH) at various peaks of the pattern were determined and used according to the Williamson-Hall Method to determine for each temperature in every cycle: the grain size (d) and microstrain (ϵ), and from here, the dislocation density (ρ), according to equations 11-13. The evolution of ρ and d with temperature in the first heating cycle is shown in Figure 33. Both parameters experience a significant change. Dislocation density varies from $21 \times 10^{14} \text{ m}^{-2}$; to $1 \times 10^{14} \text{ m}^{-2}$; while the average grain size changes from about 150 nm to almost 500 nm.

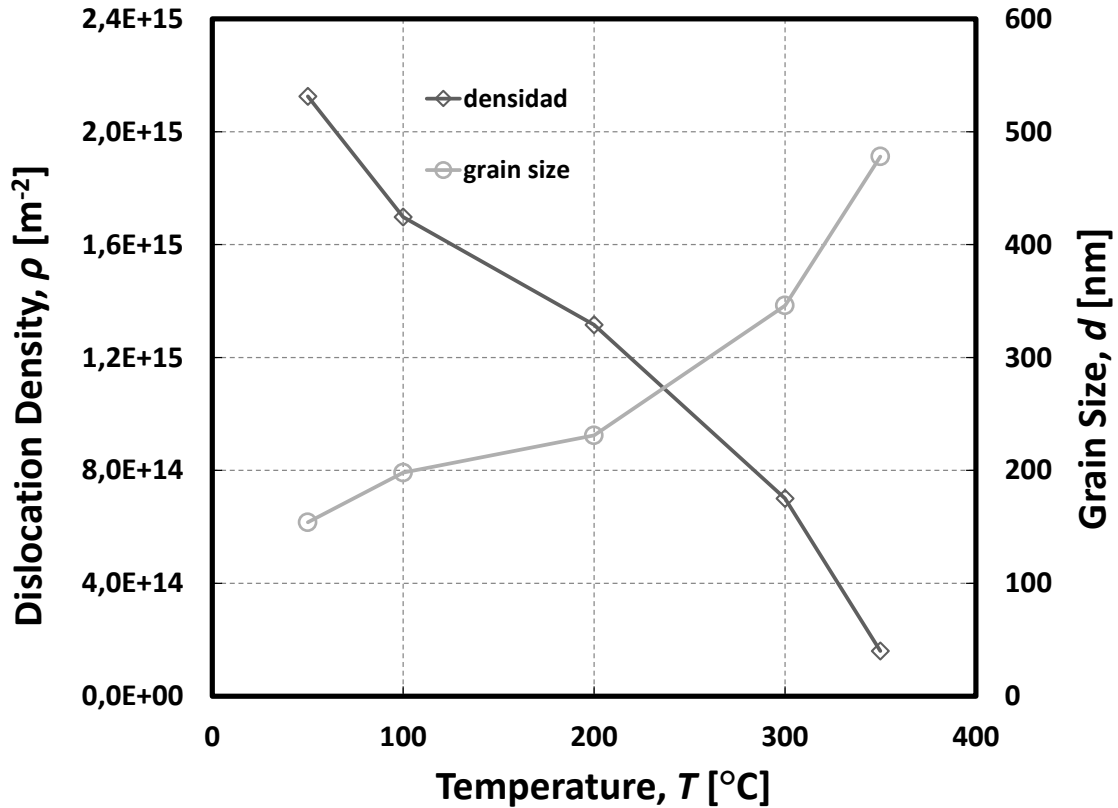


Figure 33. Dislocation density (ρ) and grain size (d) evolution during a heating cycle. Measurements of XRD are carried out at various temperatures 50°C, 100°C, 200°C, 300°C and 350°C. Williamson Hall method is used to analyze the XRD pattern and determine ρ and d .

The annealed excess volume $\Delta V/V_{disloc}$ corresponding to the change in dislocation density can be calculated from equation 17.

$$\frac{\Delta V}{V_{disloc}} = 0.5b^2\rho$$

Equation 17

Where b is the burgers vector for Al (0.2862 nm calculated from lattice parameters). (ρ) corresponds to the change of dislocation density from initial 50°C to 350°C. The excess volume (volumetric strain) contribution to the shakedown as determined by the dislocation annealing is estimated to be 0.615×10^{-3} . Therefore, the linear strain contribution is **0.021%**.

4.3.4.3 Excess Volume due to grain boundaries

The contribution from the grain boundary can be calculated by using equation 18:

$$\frac{\Delta L}{L}\Big|_{initial} - \frac{\Delta L}{L}\Big|_{final} = e_{GB} \left(\frac{1}{d_{initial}} - \frac{1}{d_{final}} \right) \quad \text{Equation 18}$$

Where e_{GB} is the grain boundary excess volume, a reasonable value for Al is 0.02 nm (Williamson and Hall 1953; Wolf 1989). Using the change of average grain sizes in Figure 32, from 50°C to 350°C, the contribution of the excess volume of the grain boundary in the shakedown strain is of 0.010%.

4.3.5 Digital Image Correlation (DIC) of unconstrained splat

Commonly, splats solidify in irregular shapes that emulate disks or flakes. In this section, it was found that splats morphology change drastically when they are heated up. Splats tend to unravel and relax the stored energy resulting in a change in shape. The residual stress associated with the spraying process is relieved during the recovery process and can be correlated to the distortion of these shapes. The microscopic splat distortion was recorded by DIC. The observation of a single unconstrained splats (delaminated) heated up under temperature control reflects the magnitude of the strain and actual deformation. To evaluate the magnitude of the geometric changes, it is necessary to track points of the splat by analyzing several high resolution images to determine the distortion. This is done through the DIC technique while in-situ heating the splat, and taking images at specific temperatures and later analyzed them with the use of specialized software.

Results of DIC analysis on two unconstrained splats are presented on Figure 34, thermal strain versus temperature is plotted. This correlation method using the DIC process again shows differences between the thermal shakedown (first heating) cycle and the subsequent ones. This alteration on expected dilation values are evident and expected because of the similitude on previous analysis carried out. However, two aspect are highlighted:

1. The shakedown effect also appears at the microscale, in similar orders of magnitude (even higher) in comparison to the macroscale, which suggests that the mechanisms producing the shakedown strain gradient act at the splat level, and that the results of the shakedown strain is not the summation of effects on millions of splats.
2. Although not shown in Figure 34, the shakedown strain is three-dimensional, which explains the deformation in the through-thickness dimension as well. It has been

observed that splats unravel in highly deformed areas of itself. It is hypothesized that the stress relief not only produces a relaxation of the lattice parameter but as a consequence of the relief there exists a substantial distortion of the shape of the splat. The summation of distortion plus stress relief, at the end, magnify the shakedown strain. It is highlighted that these results were observed in delaminated splats, because of the limitation of the experimental set up.

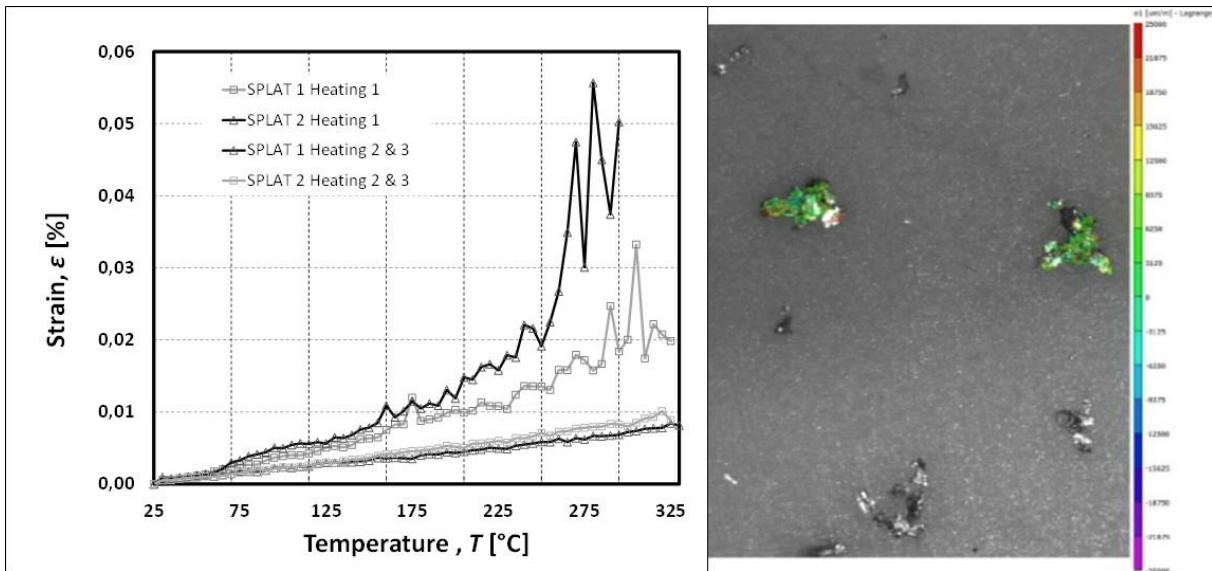


Figure 34. Analysis of deformation of splats of Al-FS2 samples by the Digital Image Correlation (DIC) Technique– Heating and Cooling Cycles up to 325°C. On the right hand side, the change in thermal strain as a function of temperature. On the left hand side, an image of two analyzed splats at temperature (280°C), the colors reflect the strain change with respect to the first image at room temperature.

4.3.6 Analysis of Results

The overall irreversible length change in TS coatings was first determined from dilatometry measurements. The total shakedown strain measured in macro scale via dilatometer on the Al-FS2 sample was of about +0.040%, as indicated in Figure 26.

Several mechanisms are hypothesized to have contributions on this behavior. The “Thermal Shakedown Strain”, $\Delta\epsilon_{sh}$, defined in equation 14 identifies some of the mechanisms acting. First at atomic level, the presence of lattice defects was analyzed. Annealing of defects was quantified by analysis of the XRD patterns. It was discussed that vacancy creation will have a reversible contribution, whereas, dislocations density and grain boundaries excess volume (Oberdorfer et al.

2014) will create a contraction on the sample when the defects are annealed. For these reason the two contributions are negative. Later, at the microscale, the observation of splat annealing revealed other mechanisms, whose contribution instead was positive.

Considering the hypotheses proposed in Table 9, the mechanisms related to “Kinetics of Defect Annealing & Material Specific Properties” are summarized as follows. The contributions of strain gradient quantified from diffraction analysis on the dislocations and grain boundary annealing were of -0.021% and -0.010%, respectively. Since these two types of defects contribute to an excess volume in the microstructure that gets annealed during heat cycle, they reduce the total length of the sample. The strain gradient corresponding to the possible kinetics driven mechanism due to oxidation, homogenization of the microstructure, or phase changes, are considered negligible according to the results from DTA/TG in section 4.3.2.

The mechanisms related to “The Kinetics of Defect Annealing due to Processing Effects”, highlighted the effect of residual stress, homogenization of the microstructure, and sintering. The residual stress as for section 4.3.3, was discussed to be compressive and produce a +0.022%, positive strain gradient. The homogenization criteria is neglected according to section 4.3.1., as mentioned before, and the sintering effect is also neglected as the maximum annealing temperature was below $0.6 T_h$.

Finally, the mechanisms related to “Mechanical Effects” in Table 9, proposed the contribution of effects of splat unraveling accounting for distortion of the microstructure. DIC results from section 4.3.5 suggest that the effect of splat distortion can be large and in the order of magnitude of +0.040% and slightly superior. It is highlighted that the contributions of distortion and “mechanical effects” in general, must be summed on the structure and therefore, it is possible that they represent the remaining difference in equation 14. This factor may account for part of the strain gradient that is measured as an overall expansion of the structure.

To resolve for the equation 14 presented initially in this section (4.3), shakedown gradient due to distortion effects should be considered as suggested by the DIC results. Other mechanism may act like intersplat sliding, friction, shear contact, axial contact, etc. However, these mechanisms have not been addressed in this study, and thus, remain within the strain gradient $\Delta\epsilon_{others}$.

$$\Delta\varepsilon_{sh} = \Delta\varepsilon_{G.B.} + \Delta\varepsilon_{\rho} + \Delta\varepsilon_{R.S} + \Delta\varepsilon_{distorion} + \Delta\varepsilon_{others}$$

$$0.040\% = (-0.010\%) + (-0.021\%) + (0.022\%) + \Delta\varepsilon_{distorion} + \Delta\varepsilon_{others}$$

$$\Delta\varepsilon_{distorion} + \Delta\varepsilon_{others} = +0.049\%$$

Equation 19

Despite that the previous analysis does not fulfill thoroughly every contributor to the shakedown gradient strain and its absolute value, the analysis of order of magnitude for each contributor is remarkable. As it has been cited in this chapter, all TS coatings tested so far, have shown the shakedown behavior. Some coatings present a permanent contraction while others a dilation, but all the strains are in the range of $\sim 0.010\%$. This number is reasonable when compared to the results of annealing of materials with high level of dislocations ($\sim 10^{14} \text{ m}^{-2}$), and small grains sizes ($\sim 100 \text{ nm}$) which is the case of TS coatings due to the rapid solidification and impact.

4.4. Conclusions

TS coatings store a significantly large amount of energy from the deposition process. This energy can be correlated to accumulation of microstructural defects, especially dislocations, grain boundaries, microstrain, and residual stress. During the first exposure to heat, the as-sprayed coating experience a rapid annealing of imperfections that result in a permanent macroscopic length change of the sample, named here as thermal shakedown. The length change can be positive or negative, meaning coating samples expand or contract during the first heating cycle. All types of coatings exhibit this behavior that is enhanced in metal and alloy materials due to the large amount of defects they store after the rapid cooling and solidification.

Differences on the thermal expansion from the first heating cycle respect to the subsequent ones was analyzed in two systems: a 99% pure Al-flame spray coating, and a Ni-5Al alloy arc sprayed coating. For Al-sample, the shakedown strain gradient (difference between the thermal strain in the first heating cycle versus the thermal strain due to natural heating) was of $+0.040\%$, and for Ni-5Al-sample of -0.250% . Microstructural examination of the constituents of the coatings by elemental mapping was carried out to evaluate the possible contributions to the expansion difference due to presence of different phases or oxides. Also homogeneity of the microstructures

was analyzed to identify possible phase segregation. Uniformity of the coating was evident from this examination.

X-rays diffraction with temperature was measured to analyze lattice expansion change with temperature cycles. The shakedown was evident on the lattice parameter variation on the first heating cycle. Analysis of the peak narrowing and shifting was used to determine the contributions of defect annealing (dislocation density change and grain growth) on the shakedown behavior exhibited by the Al-sample. Analysis of the results demonstrates the presence of nano-grains, and high amount of dislocations in the coating comparable to SPD (severely plastically deformed) materials.

It was identified that an excess volume in the structure of the coating material anneals reducing the size of the sample by 0.010% due to grain growth (grain boundary annihilation), and 0.022% due to dislocation annihilation. Reactions like oxidation and phase changes might also add to the shakedown but they were found negligible via DTA/TG analysis. Residual stress annealing analyzed by XRD shown an irreversible expansion contributing to the shakedown in about 0.022%. Finally, the analysis via Digital Image Correlation-DIC showed a substantial deformation observed as splat-distortion due to stress annealing. It is hypothesized that the splat distortion, and other possible effects (shear contact, intersplat friction, etc.) may account for the difference in strain gradient required to explain all the contributions to the shakedown strain.

Chapter 5: Future Work

5.1 Introduction

In this dissertation, several aspects of research have been described, all related to thermal spray coatings and their thermal expansion behavior. In chapter 1, the fundamental theory about thermal expansion in bulk materials, and its application to thermal spray coatings was presented. In chapter 2, the technical hypotheses that motivated the development of this work were addressed. The investigation was focused mainly in measuring the thermal expansion property (CTE) of TS coatings and identifying particularities in comparison to bulk material. In chapter 3, the influence of deposition process and parameters on expansion property was explored. Also, analysis of the anisotropic behavior of TS coatings and its CTE was examined. The experimental results and analysis led to determine that deviations of CTE from bulk property arise only in the presence of a second phase, distinct to the feedstock, as byproduct of the spraying process (i.e. oxidation). When this second phase (e.g. oxides, precipitates) is limited, deviations from bulk are minimum. Analytical models based on bulk properties were applied and the results were compared to experimental findings. Typical TS microstructural features such as: pores or cracks, were found not to have an influence on the expansion property. In chapter 4, the *thermal shakedown* effect (described as a permanent length change of a TS coating during a non-isothermal heating cycle) was studied in depth for two system-materials, namely Al and Ni-5Al. Although, all types of coatings exhibit this shakedown behavior, this effect is enhanced in metal and alloy materials due to the large amount of defects that these materials store after the rapid cooling and solidification. Several mechanisms responsible for this behavior were evaluated with different techniques, including: dilatometry, XRD and DIC. After the analysis of results, it was concluded that the thermal shakedown is associated to a rapid annealing of defects.

Several other related research aspects have been explored yet not fully investigated within this dissertation. Some of the topics and previous results are proposed for future research work and presented as follows in this chapter.

5.2 Thermal stresses in TS coatings: analysis of thermo-mechanical behavior of coatings via dilatometry

Coatings are commonly subjected to stresses by thermal loading due thermal expansion mismatch in service. To study the effect of thermal strain mismatch on the thermo-mechanical

elastic and/or inelastic behavior, including shakedown and sintering rates, a special sample was prepared by coating an Al-6061 substrate beam spray coated on both sides with YSZ by APS process. Figure 35, shows a schematic of a double side coated sample (sandwich composite) analyzed in a dilatometer test. Coating thickness was of 0.5 mm on each side and the substrate thickness was 3.2 mm. An analytical linear elastic model was developed to extract the elastic modulus and calculate the “stress vs. mismatch thermal strain” curve. The sample was sprayed on the in situ coating property (ICP) sensor, (1 x 9 in. flat plate). Slabs in the transversal direction (1 in. length) were cut and polished to be measured in the dilatometer. Ex-situ coating property ECP measurements were done on the sample when only one side was coated. ICP and ECP provide the information of residual stress and non-linear elasticity of a single coating. (Y. Liu et al. 2007; Yajie Liu et al. 2008)

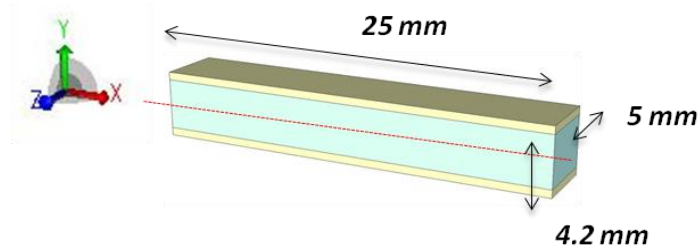


Figure 35. Schematic of sandwich composite sample. Al-6061 substrate of 3.2 mm thickness is coated in both sides with YSZ coating by APS of 0.5 mm thickness

The methodology to estimate the thermo-mechanical behavior of the coating consists on the measurement of three thermal strains: ε_{tc} thermal strain of the coating, ε_{ts} thermal strain of the substrate, and ε_o thermal strain of the composite. As illustrated in Figure 36, when the sandwich composite is subjected to a temperature change, the YSZ coating develops its natural thermal strain and is subjected to an additional strain inserted by the substrate. The applied strain on the coating will be $(\varepsilon_{tc}-\varepsilon_o)$ in tension, whereas the applied strain to the substrate will be $(\varepsilon_o-\varepsilon_{ts})$ in compression.

The overall length of the composite sandwich is mostly defined by the stiffer of the components, in this case the Al substrate.

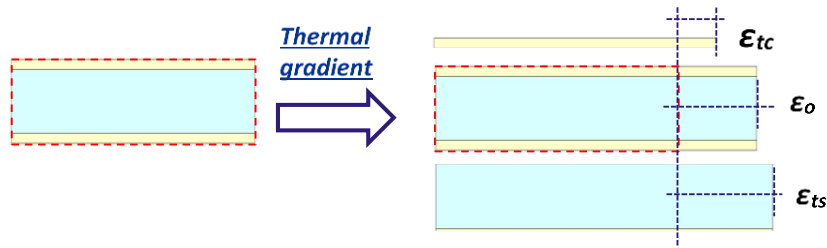


Figure 36. Illustration of sandwich composite sample subjected to an increase in temperature (positive temperature gradient). ϵ_{tc} is the thermal strain of YSZ coatings (free standing), ϵ_{ts} is the thermal strain of Al substrate (free standing), and ϵ_o is the resultant strain of the composite

The sandwich sample was fabricated with layers in both sides to equate the presence of thermal stresses and thus, avoid bending of the sample. Figure 37 shows the linear expansion (thermal strain) of each of the individual components and the composite sample, as measured by the push-rod dilatometer described in chapter 3. As the Al substrate is thicker, this component drives almost all the expansion of the composite. The linear expansion of the composite is as expected smaller than the stiffer component and larger than the more compliant component –YSZ coating. The large difference of linear expansion between substrate and coating assures a significantly large applied strain to the coating ($\epsilon_{tc}-\epsilon_o$) in tension and small applied strain to the substrate in compression ($\epsilon_o-\epsilon_{ts}$).

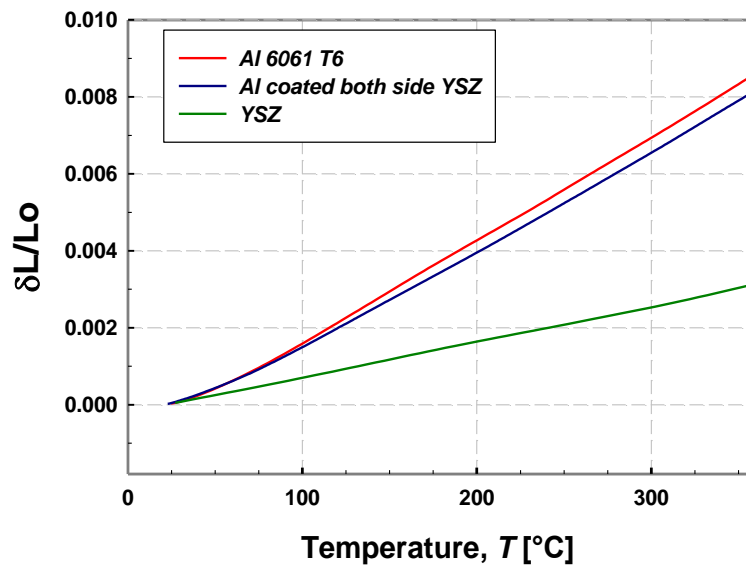


Figure 37. Linear expansion (thermal strain) of free standing coating (YSZ), substrate material (Al-6061-T6) and sandwich composite coating (YSZ on both sides of Al substrate)

The calculation of the stresses is presented here. The stress (σ) of the coating in side #1 is (c_1) and coating in side #2 is (c_2), as well as the substrate (s) are:

$$\sigma_{c1} = E'_{c1} \cdot \varepsilon_{c1} = E'_{c1} \cdot (\varepsilon_o - \varepsilon_{Tc}) = E'_c \cdot (\varepsilon_o - \alpha_c \cdot \Delta T) \quad \text{Equation 20}$$

$$\sigma_{c2} = E'_{c2} \cdot \varepsilon_{c2} = E'_{c2} \cdot (\varepsilon_o - \varepsilon_{Tc}) = E'_c \cdot (\varepsilon_o - \alpha_c \cdot \Delta T) \quad \text{Equation 21}$$

$$\sigma_{s1} = E'_s \cdot \varepsilon_s = E'_s \cdot (\varepsilon_o - \varepsilon_{Ts}) = E'_s \cdot (\varepsilon_o - \alpha_s \cdot \Delta T) \quad \text{Equation 22}$$

Where E' is the in-plane modulus of the components $E/(1-\nu)$, and α is the CTE. Applying the boundary condition to a symmetric sample:

$$\sum F = 0 \quad \text{Equation 23}$$

Here, the neutral axis is in the middle of the sample, H is half of the thickness of the substrate, and h is the thickness of the coating:

$$\int_{-H-h}^{-H} \sigma_{c1} \cdot dA_{c1} + \int_{-H}^{+H} \sigma_s \cdot dA_s + \int_{+H}^{+H+h} \sigma_{c2} \cdot dA_{c2} = 0 \quad \text{Equation 24}$$

Solving for E'_c :

$$E'_c = -\frac{(\varepsilon_o - \varepsilon_{Ts}) \cdot (H)}{(\varepsilon_o - \varepsilon_{Tc}) \cdot (h)} E'_s \quad \text{Equation 25}$$

Solving for Stresses:

$$\sigma_{c1} = E'_{c1} \cdot \varepsilon_{c1} = E'_{c1} \cdot \left(\frac{(\varepsilon_{Ts} - \varepsilon_{Tc}) \cdot E'_s \cdot H}{E'_c \cdot h + E'_s \cdot H} \right) \quad \text{Equation 26}$$

$$\sigma_{s1} = E'_s \cdot \varepsilon_s = -E'_s \cdot \left(\frac{(\varepsilon_{Ts} - \varepsilon_{Tc}) \cdot E'_c \cdot h}{E'_c \cdot h + E'_s \cdot H} \right) \quad \text{Equation 27}$$

From here, and using the experimental data in Figure 37, the elastic modulus of the coating E'_c can be extracted as a function of temperature in Figure 38, as well as, the stress-strain behavior of the coating, calculating the stress using E'_c and $(\varepsilon_{tc} - \varepsilon_o)$ as the applied strain.

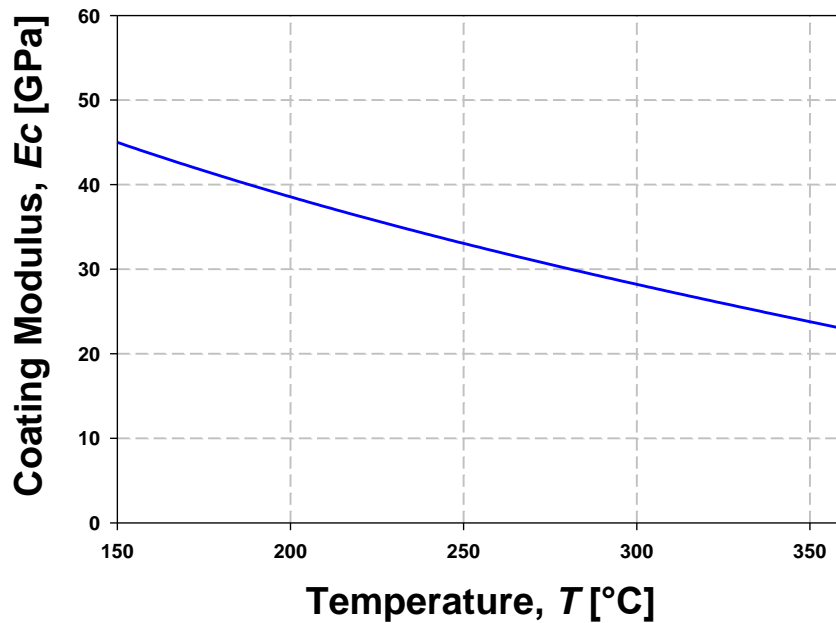


Figure 38. Coating modulus of YSZ coating obtained from uniaxial monitoring of sandwich composite expansion

5.2.1 Considerations

The presented procedure allows to determine the mechanical properties of a coating of known CTE. For the analysis, the shakedown effect was neglected as it did not appear for this type of sample, probably as for the YSZ, this effect was measured to be of low strain levels. However, the methodology demonstrates to be a powerful tool to study the thermal stress engineering problem including the evaluation of the mismatch thermal strain and the mechanical properties of the coating, which are often unknown. For the case of YSZ, the non-linear elastic behavior was identified by this alternative method.

5.2.2 Suggestions

The methodology presented here may allow to study the shakedown effect of metal/alloy coatings deposited over a substrate. The studies so far regarding thermal shakedown have been carried out on free standing coatings. There is no evidence yet that the shakedown effect appears on coatings constrained by the substrate. Some evidence on ECP tests, have shown that the first heating cycle is different that the subsequent, however this is not the rule. The ECP technique may

not be as sensitive as to differentiate the shakedown effect. However, this technique of double-side sprayed samples may allow the study of the shakedown effect on coatings under applied thermal mismatch strains.

The studied case (Aluminum substrate - YSZ coatings) was utilized to promote the thermal mismatch between the two materials. In high temperature applications as in TBC's, the materials are different but the mismatch strain levels are similar. Additionally, other effects start playing a role during a high temperature heating cycle, such as annealing, growth of TGO, creep, etc. Thus, the presented technique may be a powerful tool to learn of the TBC-system behavior in a more compelling way, which may include the analysis of shakedown, study of the anelasticity of the YSZ coating at temperature, study of the sintering effects, etc.

The presented technique may also allow to extract the properties CTE and Elastic Modulus of the coating if two samples of the same coating are prepared on two different substrate materials, as it was describe in Chapter 3 using the curvature technique.

5.3 Shakedown Behavior at Elevated Temperatures

In Chapter 4, the studies of *shakedown behavior* were conducted in relatively low temperature regimes (below $0.5 T_H$). Some exploratory experiments were conducted in the dilatometer for materials at higher temperatures, i.e. Ni-20%w.t.Cr samples deposited by HVOF, as seen in Figure 39. It was of particular interest to study the dilation behavior of the coating in a cycling manner (heating-cooling various cycles) at low-temperature regimes, up to 500°C, and followed by a high-temperature regime, up to 900°C in the same sample. The results show re-activation of the shakedown behavior. The absolute value of shakedown strain gradient $|\Delta\varepsilon_{SH}|$ (difference of linear expansion between the first heating cycle and the steady state cycle) increases as the temperature increases, and it is larger for the high temperature regime.

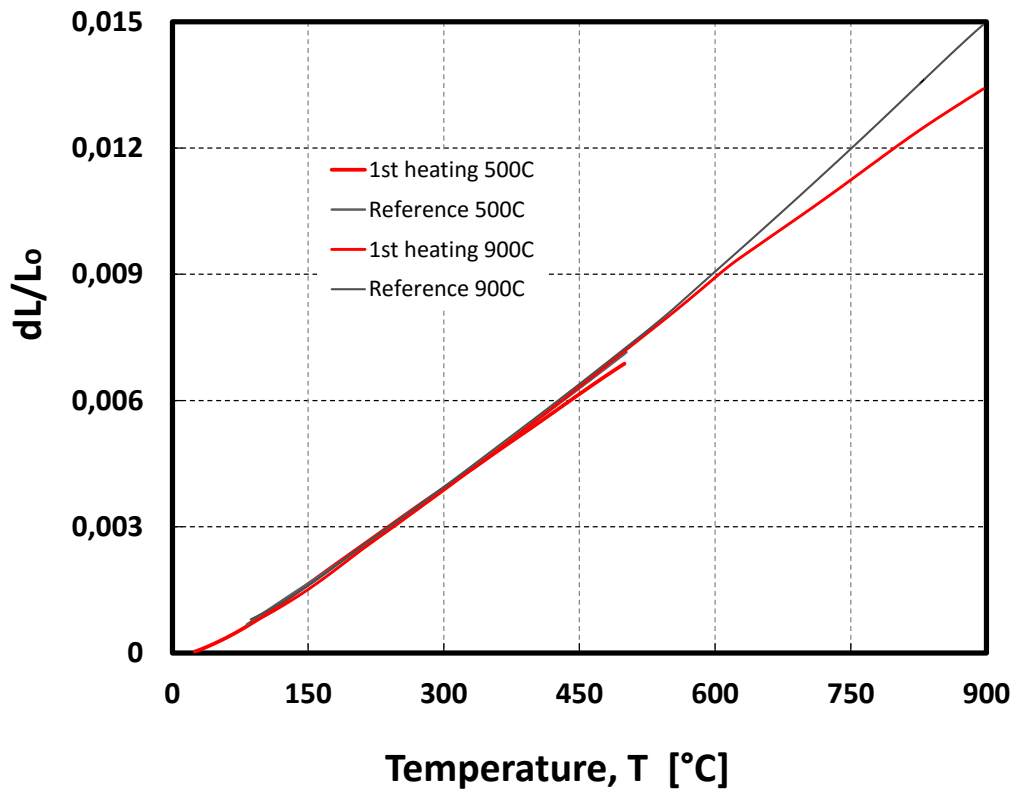


Figure 39. Shakedown behavior of Ni-20Cr sample tested in a cyclic manner: heating-cooling. Low-temperature regime reached up to 500°C, and high-temperature regime reached up to 900°C. There are three subsequent cycles for each regime (data of shakedown linear expansion is tared to the reference behavior).

5.3.1 Considerations

Different mechanisms responsible for the shakedown behavior should be activated at high-temperature regimes. The following mechanisms are proposed as responsible for the reactivation of the shakedown effect (consider Table 9, in Chapter 4, as reference):

1. Annealing of grain boundary defects: grain growth.
2. Oxide formation on the surface of exposed materials to oxygen (i.e. preferential oxidation of Cr in Ni-20Cr) (Valarezo et al. 2007)
3. Sintering of interfaces.
4. Chemical homogenization by diffusion and new phase precipitation (i.e. second order phase transformation for Ni-20Cr at around 550°C (Chan, Pan, and Lee 2006)
5. Splat unraveling/Distortion of splats.

6. Inelastic mechanical shakedown, due to sliding, friction, shear contact, axial contact, etc. between splats.

Defects, such as: residual stresses, dislocations, grain boundaries; must have been already annealed in the low-temperature regime. In the high-temperature regime, mechanisms 1) to 3) should be responsible of a negative shakedown (permanent contraction of the sample); whereas mechanisms 4) to 6) may result in a positive or negative shakedown.

5.3.2 Suggestions

It is proposed to conduct experiments controlling the kinetics of the mechanisms responsible for the *shakedown* at high temperature regimes. The proposed experiments below may allow to find out the order of magnitude of the effect of each mechanism in the *shakedown strain gradient*. Isothermal annealing experiments followed by (or mixed to) non-isothermal annealing heat cycles may allow to discern the effect of mechanisms that are less sensitive to time, specifically, sintering of interfaces and oxide formation. It is suggested to choose a material system of very well-known behavior at temperature and bulk properties; together with a large shakedown response. Table 10 shows the proposed techniques and experiments linked to the mechanisms abovementioned:

Table 10. Proposed experiments and experimental techniques to investigate the mechanisms responsible of *shakedown* at high-temperature regimes.

Mechanism	Proposed Experimentation
Annealing of grain boundary defects: grain growth.	Microstructure observation and grain size measurements
Oxide formation	DTA-TG experiments together with push-rod dilatometry in isothermal and non-isothermal temperature cycles.
Sintering of interfaces	Push-rod dilatometry in isothermal followed by non-isothermal temperature cycles.
Chemical homogenization by diffusion and new phase precipitation	DTA-TG experiments together with push-rod dilatometry in isothermal and non-isothermal temperature cycles

Splat unraveling/Distortion of splats	DIC experiments in isothermal and non-isothermal temperature cycles
Inelastic mechanical shakedown, due to sliding, friction, shear contact, axial contact, etc. between splats.	

5.4 Kinetics: Heating Rate Effect on Shakedown

In the low-temperature regime (below $0.5 T_H$), some exploratory experiments were conducted for Al-flame sprayed sample (Al-FS2) by changing the heating rate in a push-rod dilatometer. As most of the mechanisms responsible for the shakedown effect proposed in Table 9-chapter 4, are kinetics driven; then, increasing the heating rate should reduce the time for defect annealing resulting in a smaller absolute *shakedown strain gradient*. Figure 40 shows contradictory results to the previous hypothesis. In the Figure, three pieces of the same sample (Al-FS2) were tested in a push-rod dilatometry and exposed to three different heating rates: 3°C/min, 10°C/min and 20°C/min. The shakedown cycle as linear expansion, is shown for the three heating rates. The sample tested at 3°C/min has more time to anneal defects compared to the sample tested at 20°C/min, and therefore its absolute shakedown strain gradient should be larger. However, the results are contradictory. When testing the sample at 10°C/min, the absolute shakedown strain gradient is larger than sample at 3°C/min and even the sample at 20°C/min. This behavior suggest that there might be a heating rate at which the shakedown strain gradient may reach a maximum. There is not a clear trend in this behavior. At the moment, the author has not been able to explain the results.

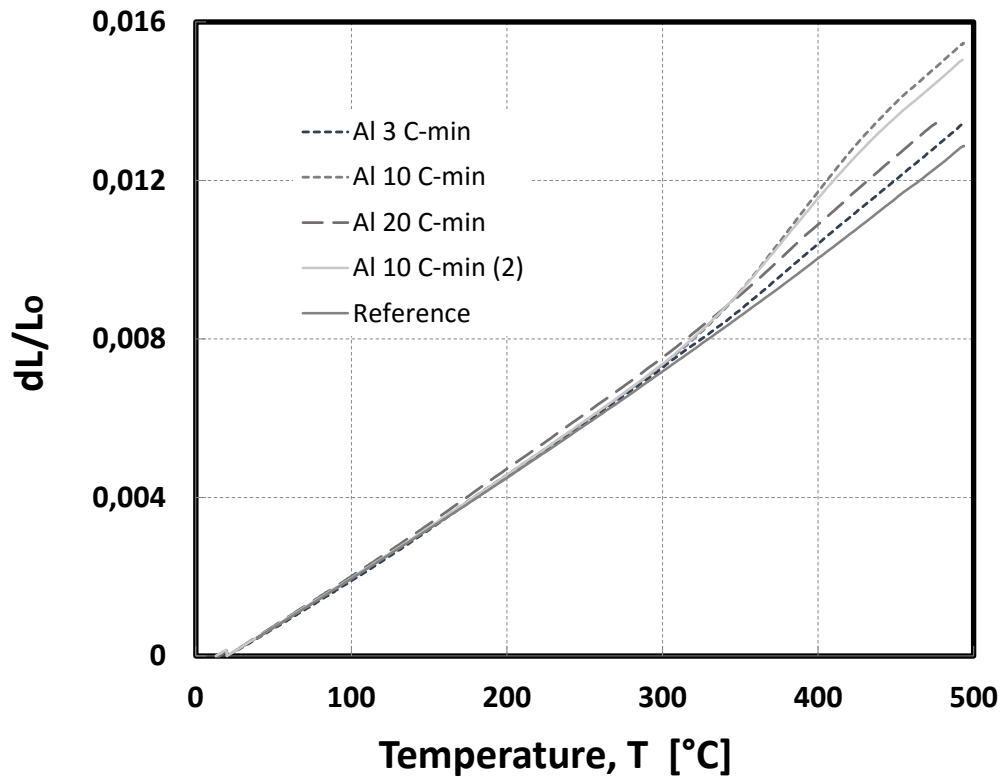


Figure 40. Linear expansion dL/L_0 of an Aluminum-flame sprayed coating (Al-FS2) tested in a push-rod dilatometer at three different heating rates: 3°C/min, 10°C/min, 20°C/min. Only the shakedown first heating cycle is considered, and compared to the steady state behavior. For 10°C/min, two different samples were tested.

5.4.1 Considerations

In Table 9-Chapter 4, mechanisms that are kinetics driven (i.e. annealing of dislocations, recrystallization, sintering, homogenization, etc.) should respond consistently to the heating rate. That is to say, more time of exposure to heat, should allow more time for defects to be annealed. On the other hand, the mechanical mechanisms may be responsible for the results in Figure 40 as they do not necessarily depend on heat exposure, this includes: splat unraveling/distortion of splats due to relief of intrinsic stresses and thermal stresses; inelastic mechanical shakedown, due to sliding, friction, shear contact, axial contact, etc. between splats; and, thermal stresses between the coating material and oxides within the same splat. The proposed mechanical mechanisms are likely

dependent on the thermal gradients within the coating (non-steady state temperature) produced by higher heating rates.

5.4.2 Suggestions

More extensive testing is proposed to validate the results shown in Table 10. The analysis of the procedure, and possible effects from the chamber of the dilatometer, at higher heating rates must be analyzed. An alternative technique to the push-rod dilatometry, such as DIC, may clarify the response of the acting mechanisms on shakedown and their response to the heating rate.

5.5 Shakedown Effect under Vacuum Conditions

Some exploratory experiments were also conducted for Al-flame sprayed sample (Al-FS2) by changing the environment of the inside chamber (vacuum vs. purging Argon) in a push-rod dilatometer at a constant heating rate of 3°C/min. The reduction of O₂-partial pressure should minimize the oxidation effects. The thermal gravimetric tests already suggested a minimal contribution to oxidation in the temperature range of room temperature up to 350°C. So, it would be expected that the vacuum condition would not affect the dilation behavior. However, Figure 41 shows a significant reduction of the *shakedown strain gradient* under vacuum conditions. Additional experimentation is suggested.

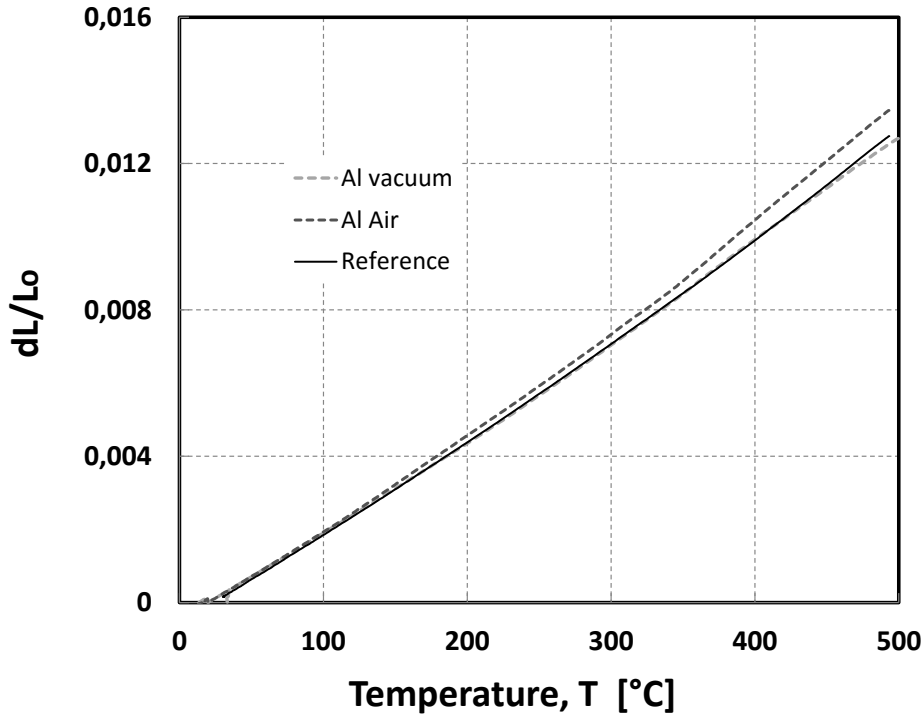


Figure 41. Linear expansion dL/L_0 of an Aluminum-flame sprayed coating (Al-FS2) tested in a push-rod dilatometer under vacuum conditions and under purging-Ar-environment. Only the shakedown first heating cycle is considered, and compared to the steady state behavior.

5.5.1 Considerations

The reduction of O_2 -partial pressure, N_2 -partial pressure, air humidity, etc., are unlikely to have a significant effect over the kinetics-driven-mechanisms responsible for shakedown cited in Table 9-chapter 4. The vacuum environment may affect the kinetics on the surface of the sample and exposed splats but in a limited degree. It is hypothesized that the mechanical mechanisms such as “splat unraveling/distortion of splats”; and “inelastic mechanical shakedown, due to sliding, friction, shear contact, axial contact, etc. between splats”; may be affected in a more significant manner if the surface chemistry of the splats is changed by the vacuum. The oxygen enriched surface of the splats due to the spraying process, may be affected by the low partial pressure of the surroundings and therefore change the characteristic sliding/contact, namely the friction coefficient, between splats during the dilation test.

5.5.2 Suggestions

More extensive testing is proposed to validate the results shown in Figure 39. Manipulation of O₂-partial pressured towards a richer condition than purging Ar, should clarify whether the surrounding environment is affecting the friction coefficient between splats. Also, as it was hypothesized in section 5.3, the heating rates may affect the mechanical-mechanisms of the shakedown, experiments conducted under vacuum conditions and at different heating rates should reflect consistent results. For instance, if there is a heating rate at which the shakedown strain gradient is maximum that should be shown as well in vacuum conditions unless the low partial pressure rules out all the mechanical effects. Testing other system materials in vacuum (i.e. SPD-superplastically deformed materials) that have shown similar shakedown behavior under environmental conditions, may also enlighten the possible explanations. The effect of porosity can be ruled out in the analysis for SPD materials.

References

- AL-Mangour Bandar, Mongrain. R., Irissou, E., and Yue, S. 2013. "Improving the Strength and Corrosion Resistance of 316L Stainless Steel for Biomedical Applications Using Cold Spray." *Surface and Coatings Technology* 216. Elsevier B.V.: 297–307. doi:10.1016/j.surfcoat.2012.11.061.
- ASM. 2002. *ASM Handbook*. <http://products.asminternational.org/hbk/index.jsp>.
- Berndt, C.C., Herman, H. 1983. "Anisotropic Thermal-Expansion Effects in Plasma Sprayed ZrO₂-8Wt-Percent Y₂O₃ Coatings." *Ceramic Engineering and Science Proceedings* ISSN 0196-6219; v. 4 p. 792-801
- Bolelli, G., Kazi Sabiruddin, Lusvarghi, L., Gualtieri, E., Valeri, S., and Bandyopadhyay, P. P. 2010. "FIB Assisted Study of Plasma Sprayed Splat-Substrate Interfaces: NiAl-Stainless Steel and Alumina-NiAl Combinations." *Surface and Coatings Technology* 205 (2). Elsevier B.V.: 363–71. doi:10.1016/j.surfcoat.2010.06.057.
- Bolelli, G., Cannillo, V., Lusvarghi, L., Rosa, R., Valarezo, A., Choi, W. B., Dey, R., Weyant, C., and Sampath, S. 2012. "Functionally Graded WC-Co/NiAl HVOF Coatings for Damage Tolerance, Wear and Corrosion Protection." *Surface and Coatings Technology* 206 (8-9). Elsevier B.V.: 2585–2601. doi:10.1016/j.surfcoat.2011.11.018.
- Brindley, W. J. 1997. "Properties of Plasma-Sprayed Bond Coats." *Journal of Thermal Spray Technology* 6 (1): 85–90.
- Brossard, S., Munroe, P. R., and Hyland, M. M. 2010. "Study of the Splat Formation for HVOF Sprayed NiCr on Stainless Steel Substrates and the Effects of Heating and Boiling Pre-Treatments." *Journal of Thermal Spray Technology* 19 (5): 990–1000. doi:10.1007/s11666-010-9502-3.
- Chan Kwai, S., Yi-Ming Pan, and Yi-Der Lee. 2006. "Computation of Ni-Cr Phase Diagram via a Combined First-Principles Quantum Mechanical and CALPHAD Approach." *Metallurgical and Materials Transactions A* 37 (7): 2039–50.
- Chivavibul, P., Watanabe, M., Kuroda, S., and Komatsu, M. 2008. "Evaluation of HVOF-Sprayed WC-Co Coatings for Wood Machining." *Surface and Coatings Technology* 202 (21): 5127–35. doi:10.1016/j.surfcoat.2008.05.024.
- Choi, W. B., Li, L., Luzin, V., Neiser, R., Gnäupel-Herold, T., Prask, H. J., Sampath, S., and Gouldstone, A. 2007. "Integrated Characterization of Cold Sprayed Aluminum Coatings." *Acta Materialia* 55 (3): 857–66. doi:10.1016/j.actamat.2006.09.006.
- Chraska, T., and King, H. 2001. "Transmission Electron Microscopy Study of Rapid Solidification of Plasma Sprayed Zirconia - Part I. First Splat Solidification." *Thin Solid Films* 397 (1-2): 30–39. doi:10.1016/S0040-6090(01)01360-8.
- Cipitria, A., Golosnoy, I. O., and Clyne, T. W. 2007. "Sintering Kinetics of Plasma-Sprayed

- Zirconia TBCs.” *Journal of Thermal Spray Technology* 16 (5-6): 809–15. doi:10.1007/s11666-007-9080-1.
- Cipitria, A., Golosnoy, I. O., Clyne, T. W. 2009a. “A Sintering Model for Plasma-Sprayed Zirconia TBCs. Part I: Free-Standing Coatings.” *Acta Materialia* 57 (4). Acta Materialia Inc.: 980–92. doi:10.1016/j.actamat.2008.10.024.
- Cipitria, A., Golosnoy, I. O., Clyne, T. W. 2009b. “A Sintering Model for Plasma-Sprayed Zirconia Thermal Barrier Coatings. Part II: Coatings Bonded to a Rigid Substrate.” *Acta Materialia* 57 (4). Acta Materialia Inc.: 993–1003. doi:10.1016/j.actamat.2008.10.058.
- Clarke, D., and Phillpot, S. 2005. “Thermal Barrier Coating Materials.” *Materials Today* 8 (6): 22–29. doi:10.1016/S1369-7021(05)70934-2.
- Clarke, D., Matthias Oechsner, and Nitin, P. Padture. 2012. “Thermal-Barrier Coatings for More Efficient Gas-Turbine Engines.” *MRS Bulletin* 37 (10): 891–98. doi:10.1557/mrs.2012.232.
- Davis, J. R. 2004. *Handbook of Thermal Spray Technology*. ASM International.
- Deshpande, S., Sampath, S., and Zhang, H. 2006. “Mechanisms of Oxidation and Its Role in Microstructural Evolution of Metallic Thermal Spray Coatings - Case Study for Ni-Al.” *Surface and Coatings Technology* 200 (18-19): 5395–5406. doi:10.1016/j.surfcoat.2005.07.072.
- Duane, C. Wallace. 1965. “Thermal Expansion and Other Anharmonic Properties of Crystals.” *Phys. Rev.* 139 (2).
- Dugdale and MacDonald. 1955. “Vibrational Anharmonicity and Lattice Thermal Properties.” *Phys. Rev.* 99 (1905-1955).
- Edrissy, A., Perry, T., and Alpas, A. T.. 2005. “Investigation of Scuffing Damage in Aluminum Engines with Thermal Spray Coatings.” *Wear* 259 (7-12): 1056–62. doi:10.1016/j.wear.2005.02.048.
- Evans, A. G., Clarke, D. R., and Levi, C. G.. 2008. “The Influence of Oxides on the Performance of Advanced Gas Turbines.” *Journal of the European Ceramic Society* 28 (7): 1405–19. doi:10.1016/j.jeurceramsoc.2007.12.023.
- Evans, A.G., Mumm, D.R., Hutchinson, J.W., Meier, G.H., and Pettit, F.S. 2001. “Mechanisms Controlling the Durability of Thermal Barrier Coatings.” *Progress in Materials Science* 46 (5): 505–53. doi:10.1016/S0079-6425(00)00020-7.
- Feder and Nowick. 1959. “Use of Thermal Exasnsion Measurement to Detect Lattice Vacancies near the Melting Point of Pure Lead and Aluminum.” *Phys. Rev.* 109.
- Franetovic, V., Stubicar, A., Bonefacic, A. 1980. “Electron-Microscopic Study of Grain-Size Distribution Function in Splat-Cooled Aluminium.” *Journal of Material Science* 15: 353–58.
- Freund, L. B., Suresh, S. 2005. *Thin Film Materials; Stress, Defect Formation, and Surface Evolution. Materials & Manufacturing Processes*. Vol. 20.

- Graham and Hagy. 1971. "Thermal Expansion --1971." In *Thermal Expansion Symposium*, edited by American Institute of Physics. New York.
- Hsieh, C. L., and Tuan, W. H.. 2007. "Thermal Expansion Behavior of a Model Ceramic-Metal Composite." *Materials Science and Engineering A* 460-461 (January): 453–58. doi:10.1016/j.msea.2007.01.109.
- Hsieh, C.L., and Tuan, W. H. 2006. "Elastic and Thermal Expansion Behavior of Two-Phase Composites." *Materials Science and Engineering A* 425 (1-2): 349–60. doi:10.1016/j.msea.2006.03.073.
- Hsueh, C. H., Becher, P. F., and Sun, E. Y. 2001. "Analyses of Thermal Expansion Behavior of Intergranular Two-Phase Composites." *Journal of Materials Science* 36 (1): 255–61. doi:10.1023/A:1004890415316.
- Hwang, Jong-Hyun, Myoung-Seoup Han, Dae-Young Kim, and Joong-Geun Youn. 2006. "Tribological Behavior of Plasma Spray Coatings for Marine Diesel Engine Piston Ring and Cylinder Liner." *Journal of Materials Engineering and Performance* 15 (3): 328–35. doi:10.1361/105994906X108611.
- Ilavsky, J., and Berndt, C.C. 1998. "Thermal Expansion Properties of Metallic and Cermet Coatings." *Surface and Coatings Technology* 102 (1-2): 19–24. <http://www.sciencedirect.com/science/article/B6TVV-3VX9XC4-3/2/9b9f78bdf5730c6fc7531e50ec2ecafe>.
- Ilavsky, J., and Judith, K. Stalick. 2000. "Phase Composition and Its Changes during Annealing of Plasma-Sprayed YSZ." *Surface and Coatings Technology* 127 (2-3): 120–29. doi:10.1016/S0257-8972(00)00562-4.
- Johnston R.E., and Evans, W.J. 2007. "Freestanding Abradable Coating Manufacture and Tensile Test Development." *Surface and Coatings Technology* 202 (4-7): 725–29. doi:10.1016/j.surfcoat.2007.05.082.
- Karadeniz, Z. Haktan, and Dilek Kumlutas. 2007. "A Numerical Study on the Coefficients of Thermal Expansion of Fiber Reinforced Composite Materials." *Composite Structures* 78 (1): 1–10. doi:10.1016/j.compstruct.2005.11.034.
- Kerner, E.H. 1956. "The Elastic and Thermo-Elastic Properties of Composite Media." *Proc. Phys. Soc.* 69: 808.
- Kesler, O., Finot, M., Suresh, S., and Sampath, S.. 1997. "Determination of Processing-Induced Stresses and Properties of Layered and Graded Coatings: Experimental Method and Results for Plasma-Sprayed Ni-Al₂O₃." *Acta Materialia* 45 (8): 3123–34. <http://www.scopus.com/inward/record.url?eid=2-s2.0-0031200102&partnerID=tZOtx3y1>.
- Kittel, C. 2004. "Introduction to Solid State Physics". New York, John Wiley & Sons. 8th Edition, ISBN : 978-0-471-41526-8.
- Klug Harold P., Alexander Leroy E.. 1974. "X-Ray Diffraction Procedures: For Polycrystalline

- and Amorphous Materials” New York, John Wiley & Sons, 2nd Edition, ISBN: 978-0-471-49369-3 Kroupa, F., and Dubskey J.. 1999. “Pressure Dependence of Young’s Moduli of Thermal Sprayed Materials.” *Scripta Materialia* 40 (11): 1249–54. doi:10.1016/S1359-6462(99)00120-7.
- Kuroda, S., Clyne, T.W. 1991. “The Quenching Stress in Thermally Sprayed Coatings.” *Thin Solid Films* 200 (1): 49–66. doi: 10.1016/0040-6090(91)90029-W
- Leigh, S., Lin, C., Berndt, C.C..1997. “Elastic Response of Thermal Spray Deposits under Indentation Test.” *Journal of the American Ceramic Society* 80 (8): 2093–99.
- Li, L., Hitchman, N., Knapp, J. 2010. “Failure of Thermal Barrier Coatings Subjected to CMAS Attack.” *Journal of Thermal Spray Technology* 19 (1): 148–55.
- Lih Wei Cheng, Yang, S. H., Su, C. Y., Huang, S. C, Hsu, I. C., and Leu, M. S. 2000. “Effects of Process Parameters on Molten Particle Speed and Surface Temperature and the Properties of HVOF CrC/NiCr Coatings.” *Surface and Coatings Technology* 133-134: 54–60. doi:10.1016/S0257-8972(00)00873-2.
- Lima, R., Libardi, R., Camargo, F., Fals, H.C., Ferraresi, V.A. 2014. “Assessment of Abrasive Wear of Nanostructured WC-Co and Fe-Based Coatings Applied by HP-HVOF, Flame, and Wire Arc Spray” 23 (October): 1097–1104. doi:10.1007/s11666-014-0101-6.
- Liu, Y., Nakamura, T., Srinivasan, V., Vaidya, A., Gouldstone, A., Sampath, S.. 2007. “Non-Linear Elastic Properties of Plasma-Sprayed Zirconia Coatings and Associated Relationships with Processing Conditions.” *Acta Materialia* 55 (14): 4667–78. doi:10.1016/j.actamat.2007.04.037.
- Liu, Y., Nakamura, T., Dwivedi, G., Valarezo, A., and Sampath, S. 2008. “Anelastic Behavior of Plasma-Sprayed Zirconia Coatings.” *Journal of the American Ceramic Society* 91 (12): 4036–43. doi:10.1111/j.1551-2916.2008.02789.x.
- Lypthout, C., Nylén, P., Manescu, A., and Pirling, T. 2008. “Residual Stresses Distribution through Thick HVOF Sprayed Inconel 718 Coatings.” *Journal of Thermal Spray Technology* 17 (5-6): 915–23. doi:10.1007/s11666-008-9242-9.
- Mankins, W.L., Lamb, S. 1990. *Nickel and Nickel Alloys*. ASM Intern.
- Matejcek, J., and Sampath, S. 2001. “Intrinsic Residual Stresses in Single Splats Produced by Thermal Spray Processes.” *Acta Materialia* 49 (11): 1993–99. doi:10.1016/S1359-6454(01)00099-4.
- Matejcek, J., Sampath, S., Gilmore, D., and Neiser, R. 2003. “In Situ Measurement of Residual Stresses and Elastic Moduli in Thermal Sprayed Coatings Part 2: Processing Effects on Properties of Mo Coatings.” *Acta Materialia* 51 (3): 873–85. doi:10.1016/S1359-6454(02)00477-9.
- Naderi, M. Saeed-Akbarib, A., and Bleckb, W. 2008. “The Effects of Non-Isothermal Deformation on Martensitic Transformation in 22MnB5 Steel.” *A, Materials Science and Engineering* 487 (1): 445–55.

- Nakamura, T., and Liu, Y. 2007. "Determination of Nonlinear Properties of Thermal Sprayed Ceramic Coatings via Inverse Analysis." *International Journal of Solids and Structures* 44 (6): 1990–2009. doi:10.1016/j.ijsolstr.2006.08.012.
- Nenno Soji, Kauffman, J.W. 1960. "Detection and Determination of Equilibrium Vacancy Concentration in Al." *Journal of the Physics Society of Japan*, 15(2): 220-226, doi: 10.1143/JPSJ.15.220
- Netzsch. 2006. "Netzsch DIL 402." *Netzsch Instruments N.A.* <http://www.dilatometers.com/products.htm>.
- Nix, F.C., MacNair, D. 1941. "Thermal Expansion of Pure Metals." *Physical Review Letters* 60: 597–605. doi: 10.1103/PhysRev.60.597.
- Oberdorfer B., Lorenzoni B., Unger K., Sprengel W., Zehetbauer M., and Wu R. 2010. "Absolute Concentration of Free Volume-Type Defects in Ultrafine-Grained Fe Prepared by High-Pressure Torsion" 63: 452–55. doi:10.1016/j.scriptamat.2010.05.007.
- Oberdorfer, B., Setman D., Steyskal, E.M., Hohenwarter, A., Sprengel, W., Zehetbauer, M., Pippan, R., and Wu, R. 2014. "Grain Boundary Excess Volume and Defect Annealing of Copper after High-Pressure Torsion" 68: 189–95. doi:10.1016/j.actamat.2013.12.036.
- Ochrombel, R., J. Schneider, B. Hildmann, and Saruhan, B. 2010. "Thermal Expansion of EB-PVD Yttria Stabilized Zirconia." *Journal of the European Ceramic Society* 30 (12). Elsevier Ltd: 2491–96. doi:10.1016/j.jeurceramsoc.2010.05.008.
- Ohzuku Tsutomu, Naoki Matoba, and Keijiro Sawai. 2001. "Direct Evidence on Anomalous Expansion of Graphite-Negative Electrodes on Charge by Dilatometry" 98: 73–77.
- Paul S., a. Cipitria I. O. Golosnoy, L. Xie, M. R. Dorfman, and T. W. Clyne. 2007. "Effects of Impurity Content on the Sintering Characteristics of Plasma-Sprayed Zirconia." *Journal of Thermal Spray Technology* 16 (5-6): 798–803. doi:10.1007/s11666-007-9097-5.
- Pawlowski Lech. 2008. *The Science and Engineering of Thermal Spray Coatings. Composite Structures*. John Wiley & Sons, Hoboken-New Jersey, 2nd Edition
- Pollock et al. 2012. "Multifunctional Coating Interlayers for Thermal-Barrier Systems." *MRS Bulletin* 37 (37): 923–31.
- Prudenziati Maria, and Magdalena Lassinantti Gualtieri. 2008. "Electrical Properties of Thermally Sprayed Ni- and Ni20Cr-Based Resistors." *Journal of Thermal Spray Technology* 17 (3): 385–94. doi:10.1007/s11666-008-9187-z.
- Raabe, Dierk. 2014. "Recovery and Recrystallization: Phenomena, Physics, Models, Simulation." In *Physical Metallurgy (Fifth Edition)*, 2291–2397. doi:http://dx.doi.org/10.1016/B978-0-444-53770-6.00023-X.
- Rabiei, A., Mumm, D. R., Hutchinson, J. W., Schweinfest, R., Rühle, M., and a. Evans, G. 1999. "Microstructure, Deformation and Cracking Characteristics of Thermal Spray Ferrous Coatings." *Materials Science and Engineering A* 269 (1-2): 152–65. doi:10.1016/S0921-

5093(99)00132-X.

- Raj, S.V., and Palczer, A. 2010. "Thermal Expansion of Vacuum Plasma Sprayed Coatings." *Materials Science and Engineering: A* 527 (7-8). Elsevier B.V.: 2129–35. doi:10.1016/j.msea.2009.11.064.
- Rajendran, R. 2012. "Gas Turbine Coatings - An Overview." *Engineering Failure Analysis* 26. Elsevier Ltd: 355–69. doi:10.1016/j.engfailanal.2012.07.007.
- Rangaswamy, S., Herman, H., and Safai, S. 1980. "Thermal Expansion Study of Plasma-Sprayed Oxide Coatings." *Thin Solid Films* 73 (1): 43–52. doi:10.1016/0040-6090(80)90327-2.
- Rastegar, F., Craft, A.E. 1993. "Piston Ring Coatings for High Horsepower Diesel Engines." *Surface and Coatings Technology* 61 (1–3): 36–42.
- Rokni, M.R., Widener, C.A., Champagne, V.K., and Crawford, G.A.. 2015. "Microstructure and Mechanical Properties of Cold Sprayed 7075 Deposition during Non-Isothermal Annealing." *Surface and Coatings Technology* 276 (August): 305–15. doi:10.1016/j.surfcoat.2015.07.016.
- Rosen, B. Walter †, Hashin, Zvi ‡. 1970. "Effective Thermal Expansion Coefficients and Specific Heats of Composite Materials." *International Journal of Engineering Science* Volume 8 (Issue 2): 157–73. Safai, Saed, and Herbert Herman. 1977. "Microstructural Investigation of Plasma-Sprayed Aluminum Coatings." *Thin Solid Films* 45 (2): 295–307. doi:10.1016/0040-6090(77)90263-2.
- Sampath, S., Schulz, U., Jarligo, M.O., and Kuroda, S. 2012. "Processing Science of Advanced Thermal-Barrier Systems." *MRS Bulletin*, no. 37: 903–15.
- Sampath, S., and Herman, H.. 1996. "Rapid Solidification and Microstructure Development during Plasma Spray Deposition." *Journal of Thermal Spray Technology* 5 (4): 445–56. doi:10.1007/BF02645275.
- Sampath, S., Jiang, X. Y., Matejicek, J., Prchlik, L., Kulkarni, A., and Vaidya, A.. 2004. "Role of Thermal Spray Processing Method on the Microstructure, Residual Stress and Properties of Coatings: An Integrated Study of Ni-5 Wt. % Al Bond Coats." *Materials Science and Engineering A* 364 (1-2): 216–31. doi:10.1016/j.msea.2003.08.023.
- Sampath, S., 2010. "Thermal Spray Applications in Electronics and Sensors: Past, Present, and Future." *Journal of Thermal Spray Technology* 19 (5): 921–49. doi:10.1007/s11666-010-9475-2.
- Sampath, S., Dwivedi, G., Valarezo, A., and Choi, W.B. 2013. "Partnership for Accelerated Insertion of New Technology: Case Study for Thermal Spray Technology." *Integrating Materials and Manufacturing Innovation* 2 (1): 1. doi:10.1186/2193-9772-2-1.
- Scott, H. G. 1975. "Phase Relationships in the Zirconia-Yttria System." *Journal of Materials Science* 10 (9): 1527–35.
- Sharma, A., Gambino, Richard J., and Sampath, S. 2006. "Anisotropic Electrical Properties in

- Thermal Spray Metallic Coatings.” *Acta Materialia* 54 (1): 59–65. doi:10.1016/j.actamat.2005.08.029.
- Sharma, A., Gouldstone, A., Sampath, S., and Gambino, Richard J. 2006. “Anisotropic Electrical Conduction from Heterogeneous Oxidation States in Plasma Sprayed TiO₂ Coatings.” *Journal of Applied Physics* 100 (11): 114906. doi:10.1063/1.2382456.
- Shidu, S., Prakasf, S. 2006. “Nickel-Chromium Plasma Spray Coatings: A Way to Enhance Degradation Resistance of Boiler Tube Steels in Boiler Environment.” *Journal of Thermal Spray Technology* 15 (1): 131–40.
- Simons and Balluffi. 1960. “Measurements of Equilibrium Vacancy Concentrations in Aluminum.” *Phys. Rev.* 117 (1).
- Sprengel W., B. Oberdorfer, Steyskal, E.-M. and Würschum R.. 2012. “Dilatometry: A Powerful Tool for the Study of Defects in Ultrafine-Grained Metals.” *Journal of Materials Science* 47 (22): 7921–25. doi:10.1007/s10853-012-6460-9.
- Steyskal, W., Sprengel, B., Oberdorfer E. 2012. “Dilatometry : A Powerful Tool for the Study of Defects in Ultrafine-Grained Metals.” doi:10.1007/s10853-012-6460-9.
- Suzuki, M. 2000. “Structure and Properties of Plasma-Sprayed Zircon Coating.” *Thermal Spray: Surface Engineering via Applied Research* 9 (ASM International): 333–39.
- Taylor & Denman. 1974. "Thermal Expansion of Solids" *International Symposium of Thermal Expansion of Solids* New York, American Institute of Physics
- Taylor, T. A., and Walsh, P. N.. 2004. “Thermal Expansion of MCrAlY Alloys.” *Surface and Coatings Technology* 177-178: 24–31. doi:10.1016/j.surfcoat.2003.05.001.
- Taylor, T. A., and Walsh, P. N. 2004. “Dilatometer Studies of NiCrAlY Coatings.” *Surface and Coatings Technology* 188-189 (1-3 SPEC.ISS.): 41–48. doi:10.1016/j.surfcoat.2004.08.003.
- Thompson, R.J., and Hemker, K.J. 2010. “Thermal Expansion Measurements on Coating Materials by Digital Image Correlation.” Department of Mechanical Eng. Johns Hopkins University http://www.eyoungindustry.com/uploadfile/file/20151027/20151027192956_58463.pdf
- Tronche, A., Fauchais, P. 1987. “Hard Coatings (Cr₂O₃, WC□Co) Properties on Aluminium or Steel Substrates.” *Materials Science and Engineering* 92: 133–44. Tsipas S.A., Golosnoy I.O, Damani R., and Clyne T.W.. 2004. “The Effect of a High Thermal Gradient on Sintering and Stiffening in the Top Coat of a Thermal Barrier Coating System.” *Journal of Thermal Spray Technology* 13 (3): 370–76. doi:10.1361/10599630420380.
- Turner, Philip S. 1946. “Thermal-Expansion Stresses in Reinforced Plastics” *Journal of Research of the Nation Bureau of Standards* 37 (October): 239–50.
- Usmani, S., Sampath, S. 1999. “Time-Dependent Friction Response of Plasma-Sprayed Molybdenum” *Wear* 225-229: 1131–40. doi:10.1016/S0043-1648(98)00395-0.
- “Usmani, S., Sampath, S., Houck, D. and Lee, D. 1997. "Effect of Carbide Grain Size on the

- Sliding and Abrasive Wear Behavior of TS WC-Co Coatings.pdf.” *Tribology Transaction*, vol40, 3, 470-478.
- Vaidya, A., Srinivasan, V., Streibl, T., Friis, M., Chi, W. and Sampath, S. 2008. “Process Maps for Plasma Spraying of Yttria-Stabilized Zirconia: An Integrated Approach to Design, Optimization and Reliability.” *Materials Science and Engineering A* 497 (1-2): 239–53. doi:10.1016/j.msea.2008.07.058.
- Vaidya, A., Streibl, T., Li, L., Sampath, S., Kovarik, O. and R. Greenlaw. 2005. “An Integrated Study of Thermal Spray Process-Structure-Property Correlations: A Case Study for Plasma Sprayed Molybdenum Coatings.” *Materials Science and Engineering A* 403 (1-2): 191–204. doi:10.1016/j.msea.2005.04.056.
- Valarezo, A, Choi, W. B., Chi, W., Gouldstone, A. and Sampath, S 2007. “Process Maps of Ni-Cr Coatings by HVOF Spraying.” *Energy*, 954–59.
- Valarezo, A, J Japson, A Gouldstone, and S Sampath. n.d. “Residual Stress Development on Metallic Coatings by HVOF Spraying.”
- Valarezo, Alfredo, and Sanjay Sampath. 2011. “An Integrated Assessment of Process-Microstructure-Property Relationships for Thermal-Sprayed NiCr Coatings.” *Journal of Thermal Spray Technology* 20 (6): 1244–58. doi:10.1007/s11666-011-9665-6.
- Varis, T., Suhonen, T., Ghabchi, A., Valarezo, A., Sampath, S, Liu, X., and Hannula, S.-P. 2014. “Formation Mechanisms, Structure, and Properties of HVOF-Sprayed WC-CoCr Coatings: An Approach Toward Process Maps.” *Journal of Thermal Spray Technology* 23 (6): 1009–18. doi:10.1007/s11666-014-0110-5.
- Vassen Robert., Alexandra Stuke, Detlev Sto, and Forschungszentrum Ju. 2009. “Recent Developments in the Field of Thermal Barrier Coatings.” *Journal of Thermal Spray Technology* 18 (June): 181–86. doi:10.1007/s11666-009-9312-7.
- Wang and Tong. 2013. “A High Resolution DIC Technique for Measuring Small Thermal Expansion on Film Specimens.” *Optics and Lasers in Engineering* 51: 30–33.
- Wang, D. Berndt, C.C: 1991. “Anisotropic Thermal Expansion Behavior of Thermally Spray Coatings.” In *2nd Symposium Plasma Technik*. Vol. 53. doi:10.1017/CBO9781107415324.004.
- Williamson and Hall. 1953. “X-RAY LINE BROADENING FROM FILED ALUMINIUM AND WOLFRAM.” *Acta Matallurgica* 1.
- Williamson- Smallman. 1956. “Disclations Density in Some Anneales and Cold Worked Metals.” *Philisophical Magazine* 1.
- Wu Yuhong, Qu Meng, Giannuzzi Lucille, A., Sampath, S., and Gouldstone, A. 2007. “Focused Ion Beam Study of Ni5Al Single Splat Microstructure.” *Materials Research Society Symposium Proceedings* 983: 1–5. <http://www.scopus.com/inward/record.url?eid=2-s2.0-41549103883&partnerID=tZOTx3y1>.

- Yuuzou, Kawahara. 2007. "Application of High Temperature Corrosion-Resistant Materials and Coatings Under Severe Corrosive Environment in Waste-to-Energy Boilers." *Journal of Thermal Spray Technology* 16 (2): 202–13. doi: 10.1007/s11666-006-9012-5
- Zhang, Bo., Li, Xiaobo., and Li, Dan. 2013. "Assessment of Thermal Expansion Coefficient for Pure Metals." *Calphad* 43. Elsevier: 7–17. doi:10.1016/j.calphad.2013.08.006.